



## Durham E-Theses

---

### *ESCA applied to a study of some materials of geochemical interest*

Wilson, Rosemary

#### How to cite:

---

Wilson, Rosemary (1981) *ESCA applied to a study of some materials of geochemical interest*, Durham theses, Durham University. Available at Durham E-Theses Online: <http://etheses.dur.ac.uk/7837/>

#### Use policy

---

The full-text may be used and/or reproduced, and given to third parties in any format or medium, without prior permission or charge, for personal research or study, educational, or not-for-profit purposes provided that:

- a full bibliographic reference is made to the original source
- a [link](#) is made to the metadata record in Durham E-Theses
- the full-text is not changed in any way

The full-text must not be sold in any format or medium without the formal permission of the copyright holders.

Please consult the [full Durham E-Theses policy](#) for further details.

UNIVERSITY OF DURHAM

A thesis entitled

'ESCA APPLIED TO A STUDY OF SOME MATERIALS OF GEOCHEMICAL INTEREST'

Submitted by

Rosemary Wilson B.Sc. (Dunelm)

A candidate for the Degree of Master of Science

1 9 8 1

The copyright of this thesis rests with the author.  
No quotation from it should be published without  
his prior written consent and information derived  
from it should be acknowledged.



To Mum and Dad

## Acknowledgements

I would like to express my sincere gratitude to Professor David T. Clark for introducing me to the technique of ESCA and for guidance during this project. Valuable discussions with Dr J. Martin E. Quirke have provided a firm foundation on which the introductory sections of Chapter Two could be built.

This investigation was made possible through generous gifts of materials by Dr A.G. Douglas (University of Newcastle-upon-Tyne), Dr J.M. Hunt (Woods Hole Oceanographic Institution, Massachusetts, U.S.A.), and the American Gilsonite Company.

I am indebted to Mrs M. Cocks and Mr R. Coult (University of Durham), and to Dr M. West (University of Bristol) for performing the microanalytical work. The nmr spectra presented in this thesis are due to the expertise of Dr M. Murray (University of Bristol).

I am privileged to work in the company of a fine team of 'ESCA men'. In particular, I would like to thank Hugh Munro, Alan Harrison and Zaki AbRahaman for many helpful discussions and encouragement throughout.

I am grateful to Mrs Elizabeth Nevis for her assistance in preparing many of the figures in this thesis. Finally, may I extend my thanks to Mrs Ruth L. Reed for her great secretarial skill and patience in typing this manuscript.

Rosemary Wilson

Durham 1981

## Abstract

Electron spectroscopy for chemical applications (ESCA) has been used to study a series of samples of sedimentary organic matter comprising coal, kerogen and bitumen.

The elemental analysis data from the ESCA experiment is found to be in reasonable agreement with data obtained by conventional micro-analytical techniques. In addition, structural information derived from the ESCA analyses is presented.

The extent to which these geochemical materials undergo changes in functionality, as detected by ESCA, when subjected to nonequilibrium plasmas, excited principally in oxygen, has been investigated. Special attention has been paid to a study of the plasma oxidation of gilsonite, a naturally occurring bitumen, as a function of treatment time and plasma power.

Complementary to this investigation, a selection of polymer samples has also been treated under similar conditions.

## Contents

Page

Chapter One: <u>Electron Spectroscopy for Chemical Application (ESCA)</u>	
1.1	Introduction ... .. 1
1.2	Fundamental Electronic Processes Involved in ESCA ... .. 2
1.2.1	Photoionisation ... .. 2
1.2.2	Processes Accompanying Photoionisation ... .. 8
1.2.3	Electronic Relaxation ... .. 8
1.2.4	Shake-up and Shake-off Phenomena ... .. 9
1.2.5	Auger Emission and X-ray Fluorescence ... .. 12
1.3	Chemical Shifts ... .. 16
1.4	Fine Structure ... .. 22
1.4.1	Multiplet Splitting ... .. 22
1.4.2	Spin Orbit Splitting ... .. 23
1.4.3	Electrostatic Splitting ... .. 24
1.5	Sample Charging and Energy Referencing ... .. 26
1.6	Signal Intensities ... .. 29
1.7	Line Shape Analysis ... .. 35
1.8	ESCA Instrumentation ... .. 39
1.8.1	X-ray Source ... .. 40
1.8.2	Sample Analysis Chamber ... .. 42
1.8.3	Electron Energy Analyser ... .. 44
1.8.4	Electron Detection and Data Acquisition ... .. 45
1.9	Sample Handling ... .. 46
1.9.1	Solid Samples ... .. 46
1.9.2	Liquids ... .. 46
1.9.3	Gases ... .. 47
1.10	General Aspects of ESCA ... .. 48
1.11	Quantitative Analysis ... .. 52
Chapter Two: <u>An Evaluation of the Potential of ESCA in the Characterisation of Coal, Kerogen and Bitumen</u>	
2.1	Introduction ... .. 56
2.2	The Application of ESCA to Geochemistry ... .. 56
2.3	An Introduction to Organic Geochemistry ... .. 58

	<u>Page</u>
3.5 Modification of Polymer Surfaces by Oxygen Plasmas ... ..	120
3.5.1 Introduction ... ..	120
3.5.2 Experimental ... ..	124
3.5.2a Polymer Samples ... ..	124
3.5.2b Sample Preparation ... ..	126
3.5.2c Plasma Instrumentation ... ..	126
3.5.2d Plasma Configuration ... ..	128
3.5.2e Experimental Procedure ... ..	129
3.5.2f ESCA Instrumentation ... ..	130
3.5.3 Results and Discussion ... ..	130
3.5.3a Polyethylene, Polystyrene, Poly(ethylene terephthalate) and Bisphenol-A polycarbonate Polymer Films ... ..	131
3.5.3b Nylon 6,6, Polyphenylene sulphide, Bisphenol-A polysulphone and Ferrous sulphide ... ..	139
3.6 Modification of a Series of Geochemical Materials by Oxygen Plasma Treatments ... ..	146
3.6.1 Experimental ... ..	146
3.6.2 Results and Discussion ... ..	147
3.6.2a Plasma Treatment of Gilsonite ... ..	147
3.6.2b Oxygen Plasma Treatment of a Series of Coal, Kerogen and Bitumen Samples ... ..	156
3.7 Hydrogen Plasma Treatments of Gilsonite and Brown Coal ...	170
References ... ..	176

CHAPTER ONE

ELECTRON SPECTROSCOPY FOR CHEMICAL APPLICATIONS (ESCA)

## CHAPTER ONE

### Electron Spectroscopy for Chemical Applications (ESCA)

#### 1.1 Introduction

The ESCA experiment involves the measurement of binding energies of electrons ejected by interactions of a molecule with a monoenergetic beam of soft X-rays. In common with most other spectroscopic methods, X-ray photoelectron spectroscopy is a technique originally developed by physicists and is now extensively utilized in the fields of inorganic, organic and physical chemistry providing valuable information on structure, bonding and reactivity.<sup>1</sup>

Although independent investigations by De Broglie<sup>2,3</sup> and Robinson<sup>4-6</sup> into the photoelectric effect studied the X-ray induced electron emission from a variety of materials ranging from thin metal films to inorganic salts in the early part of the 20th century, only in the 1950s was the technique developed by Siegbahn and co-workers at the Institute of Physics, Uppsala University, Sweden.<sup>7,8</sup> Much of the pioneering work into high resolution X-ray photoelectron spectroscopy was carried out by Siegbahn, who christened the technique ESCA (Electron Spectroscopy for Chemical Analysis) which he later amended to Electron Spectroscopy for Chemical Applications. Siegbahn's two books 'ESCA Atomic, Molecular and Solid State Structure. Studied by Means of Electron Spectroscopy'<sup>9</sup> and 'ESCA Applied to Free Molecules'<sup>10</sup> provide extensive documentation of his early work.

The development of electron spectroscopy pre-Siegbahn is covered in a review by Jenkin, Leckey and Liesegang.<sup>11</sup>



The technique of ESCA is also known as:

- (1) X-ray Photoelectron Spectroscopy (XPS)
- (2) High Energy Photoelectron Spectroscopy (HEPS)
- (3) Induced Electron Emission Spectroscopy (IEES)
- (4) Photoelectron Spectroscopy of the Inner Shell (PESIS)

At this point it is worth mentioning that a multitude of approaches are available by which electrons, characteristic of the material from whence they originated, may be generated. These distinct techniques, based upon the analysis of electron energies following a collision between an impacting particle or photon and an atom, molecule or solid, may be classified under the generic term 'electron spectroscopy'. Types of electron spectroscopy are listed in Table 1.1. A detailed description of individual techniques is beyond the scope of this thesis; however the interested reader is referred to recent reviews by Baker and Brundle<sup>106</sup> and Rhodin and Gadzuk<sup>107</sup> and references therein.

## 1.2 Fundamental Electronic Processes Involved in ESCA

### 1.2.1 Photoionisation

Irradiation of a molecule with X-rays causes electrons with binding energies less than that of the exciting radiation to be photo-ejected.<sup>9</sup> X-ray sources in common use today are  $MgK\alpha_{1,2}$  and  $AlK\alpha_{1,2}$  with photon energies of 1253.7eV and 1486.6eV respectively. The electrons ejected may be either core or valence electrons (Figure 1.1) though the latter are usually studied using ultra-violet photoelectron spectroscopy (UPS)<sup>12</sup> with He(I) radiation (21.22eV), or He(II) radiation (40.8eV).

Table 1.1 Types of Electron Spectroscopy 106

<u>Name of technique</u>		<u>Basis of Technique</u>
Photoelectron spectroscopy (Ultraviolet excitation)	PES or UPS	Electrons ejected from materials by monoenergetic ultraviolet photons are energy analysed.
Photoelectron spectroscopy (X-ray excitation)	ESCA or XPS	Electrons ejected from materials by monoenergetic X-ray photons are energy analysed.
Auger electron spectroscopy	AES	Auger electrons ejected from materials following initial ionisation by electrons or photons (not necessarily monoenergetic) are energy analysed.
Ion neutralisation spectroscopy	INS	Auger electrons ejected from surfaces following impact of a noble gas ion are energy analysed.
Penning ionisation spectroscopy	PIS	Metastable atoms are used to eject electrons from materials. The electrons are then energy analysed.
Autoionisation electron spectroscopy		Similar to Auger electron spectroscopy. Electrons ejected in an auto-ionising decay of super-excited states are measured. Electron or photon impact can be used to produce the super-excited state.
Resonance electron capture ) Electron transmission spectroscopy )		The elastic scattering cross-section for electrons is measured as a function of the energy of the electron beam and the scattering angle.

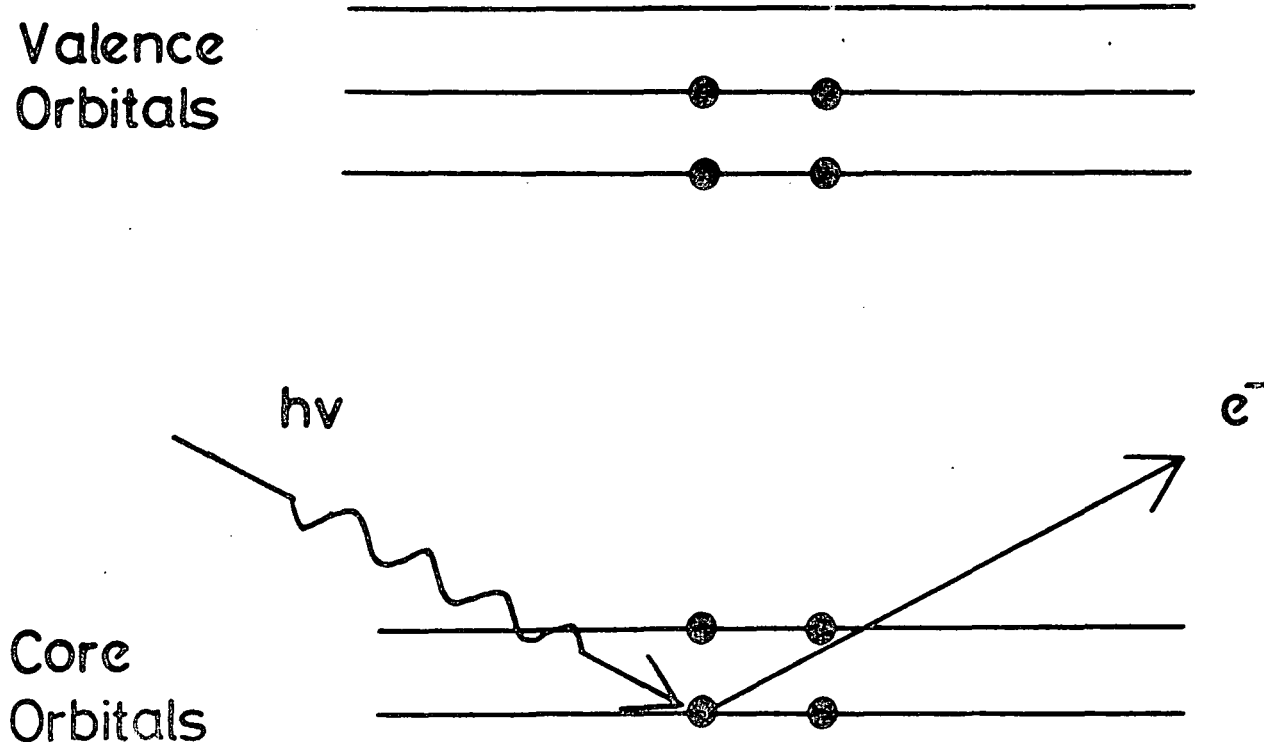


Figure 1.1 The photoionisation of a core level electron

It has been shown that the relative intensities of various peaks in the valence electron spectrum vary with differences in the incident excitation energy, not only between X-ray and U.V., but between X-ray photons of different energies.<sup>26</sup> These effects are attributed to differences in photoionisation cross-section involved in the various electron states in the valence band region. (The cross-section for photoionisation for a particular level is a measure of the probability of the level being ionised when irradiated by a photon of known energy, and is discussed more fully in Section 1.6.) Figure 1.2 demonstrates the striking difference between X-ray and U.V. valence band studies on carbon monoxide. The photon sources used are  $AlK\alpha_{1,2}$  (1486.6eV) and He(I) (21.2eV): note the difference in relative peak intensities between the two spectra.

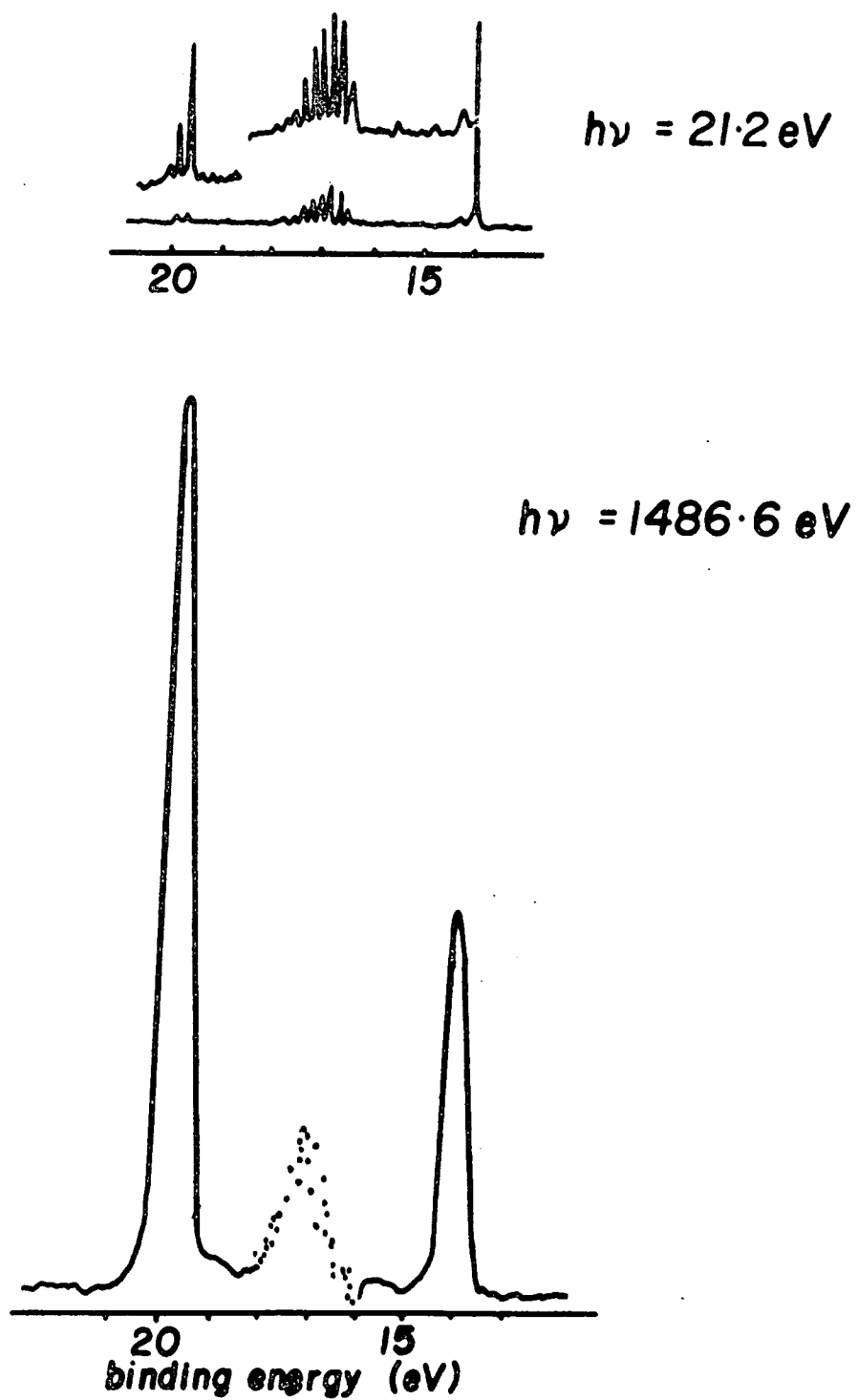


Figure 1.2 Valence band spectra of CO using  $\text{He(I)}$  and  $\text{AlK}\alpha_{1,2}$  photon sources

The photoemission process is complete in typically  $\sim 10^{-17}$  seconds.<sup>13</sup>

The total kinetic energy of an emitted photoelectron (K.E., which may include the contributions from the vibrational, rotational and translational motions, as well as electronic) is given by the equation 1.1

$$\text{K.E.} = h\nu - \text{B.E.} - E_r \quad (1.1)$$

where  $h\nu$  is the energy of the incident photon;  $h$  is Planck's constant and  $\nu$  is the frequency of the X-ray radiation. B.E. is the binding energy of the emitted electron which is defined as the positive energy required to remove an electron to infinity with zero kinetic energy, and  $E_r$  is the recoil energy of the atom. Siegbahn and co-workers<sup>9</sup> have shown that the recoil energy is usually negligible for light atoms when using typical X-ray sources, for example  $\text{MgK}\alpha_{1,2}$  and  $\text{AlK}\alpha_{1,2}$ . This is not the case however where high energy X-rays, for example  $\text{AgK}\alpha$  (22000eV) are employed, and recoil energies for light elements must be taken into account. Recent studies by Cederbaum and Domcke<sup>14</sup> show that these effects can lead to modifications of the vibrational band envelopes of light atoms and hence recoil energies for light elements must be considered. With the present resolution of typical ESCA spectra the excitations from the translational, vibrational and rotational motions are seldom observed to contribute to the final K.E. Therefore the equation for a free molecule reduces to equation 1.2

$$\text{K.E.} = h\nu - \text{B.E.} \quad (1.2)$$

It is important to understand the relationship that exists between the binding energies observed experimentally by ESCA for solids versus free molecules when compared with values calculated theoretically by *ab initio* and semi-empirical LCAO - MO - SCF treatments.

The most convenient reference level for a conducting sample is the Fermi level.<sup>15</sup> In a metal this level, sometimes referred to as the 'electron chemical potential', is defined as the highest occupied level at absolute zero.

The work function,  $\phi_s$ , for a solid is defined as the energy gap between the free electron (vacuum) level and the Fermi level in the solid, and is represented diagrammatically in Figure 1.3. The vacuum levels

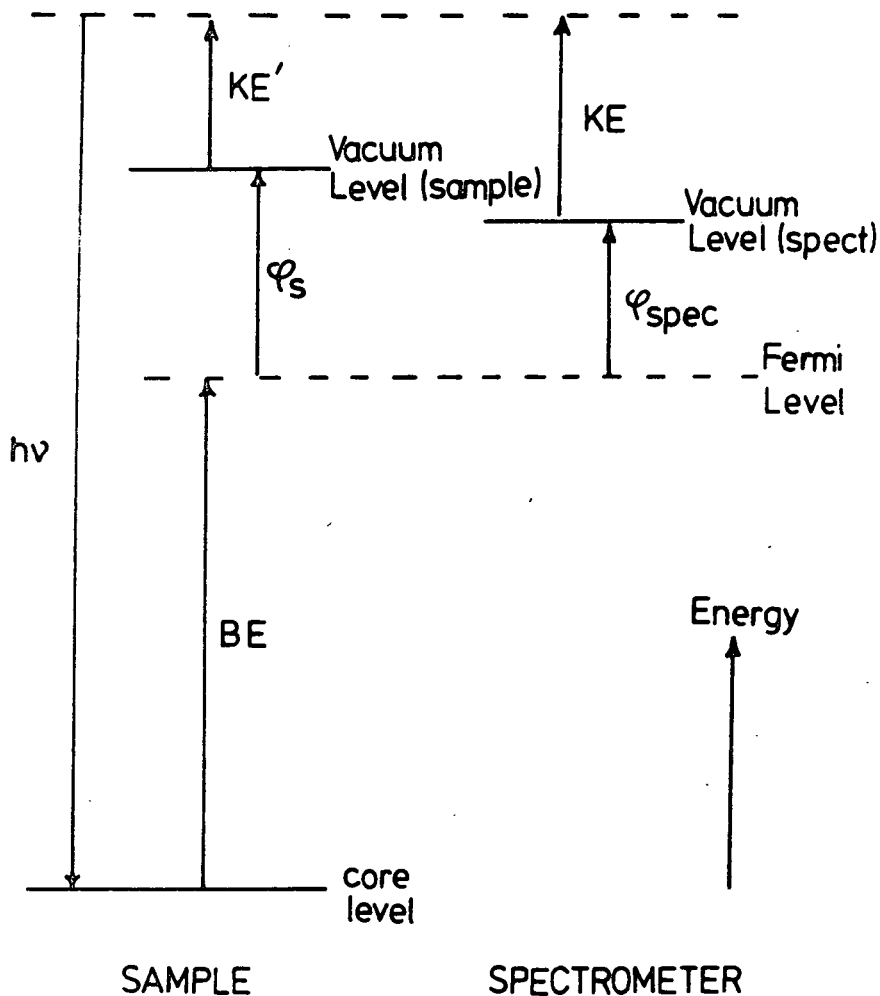


Figure 1.3 Relationship between vacuum level and Fermi level for a sample isolated from spectrometer

for the solid sample and the spectrometer may however be different and the electron will experience either a retarding or accelerating potential equal to  $\phi_s - \phi_{\text{spec}}$ , where  $\phi_{\text{spec}}$  is the work function of the spectrometer.<sup>6</sup>

In the ESCA experiment it is the kinetic energy of the electron when it enters the analyser that is measured, and taking zero binding energy to be the Fermi level of the sample, the following equation results

$$\text{B.E.} = h\nu - \text{K.E.} - \phi_{\text{spec.}} \quad (1.3)$$

The binding energy referred to the Fermi level does not depend on the work function of the sample but on that of the spectrometer and this represents a constant correction to all binding energies. Energy referencing and sample charging effects will be considered in Section 1.5.

### 1.2.2 Processes Accompanying Photoionisation

Several processes may accompany photoionisation and these may be divided into two main categories depending upon whether they are slow compared to the original photoionisation or occur within a similar time span. Electron relaxation, shake-up and shake-off occur within a similar time span and result in modification of the kinetic energy of the photoelectrons. Auger emission and X-ray fluorescence however are comparatively slow processes and cause little effect on the kinetic energy of the photoelectrons.

### 1.2.3 Electronic Relaxation

Accompanying the photoionisation process, which is complete within a time span of approximately  $10^{-17}$  seconds, there is a substantial electronic relaxation of the valence electrons.<sup>16-18</sup> It has been shown by theoretical and experimental studies that the relaxation energy is a

sensitive function of the electronic environment of a molecule<sup>19-23</sup> and hence is responsible for shifts in binding energies. Relaxation energies associated with core ionisations of first row elements have been found to be considerable<sup>23,24</sup> and are caused by the reorganisation of the valence electrons in response to the decreased shielding of the nuclear charge. This reorganisation changes the spatial distribution of the remaining electrons. The differences between relaxation energies for closely related molecules are small and therefore they cause only small changes in binding energies.

The theory of the chemical shift in core electron binding energies has received much attention<sup>18,26,27</sup>. Whereas the ionisation energies of core electrons in small molecules can be calculated by *ab initio* methods, this procedure is unrealistic when dealing with polyatomic molecules. It is then necessary to resort to approximate semi-empirical methods. These take many forms. The use of Koopmans' Theorem<sup>29</sup> in the calculation of binding energies does not account for electronic relaxation, whereas self-consistent field ( $\Delta$ SCF) calculations do take account of the relaxation energy (R.E.). This provides a method by which relaxation energies may be investigated, equation 1.4

$$\text{R.E.} = \text{B.E. (Koopmans)} - \text{B.E. } (\Delta\text{SCF}) \quad (1.4)$$

#### 1.2.4 Shake-up and Shake-off Phenomena

The removal of a core electron, which is almost completely shielding as far as the valence electrons are concerned, is accompanied by substantial reorganisation (relaxation) of the valence electrons in response to the effective increase in nuclear charge. This perturbation gives rise to a finite probability for photoionisation to be accompanied by simultaneous excitation of a valence electron from an occupied to an

unoccupied level (shake-up) or ionisation of a valence electron (shake-off) as shown in Figure 1.4. These relaxation processes result in excited

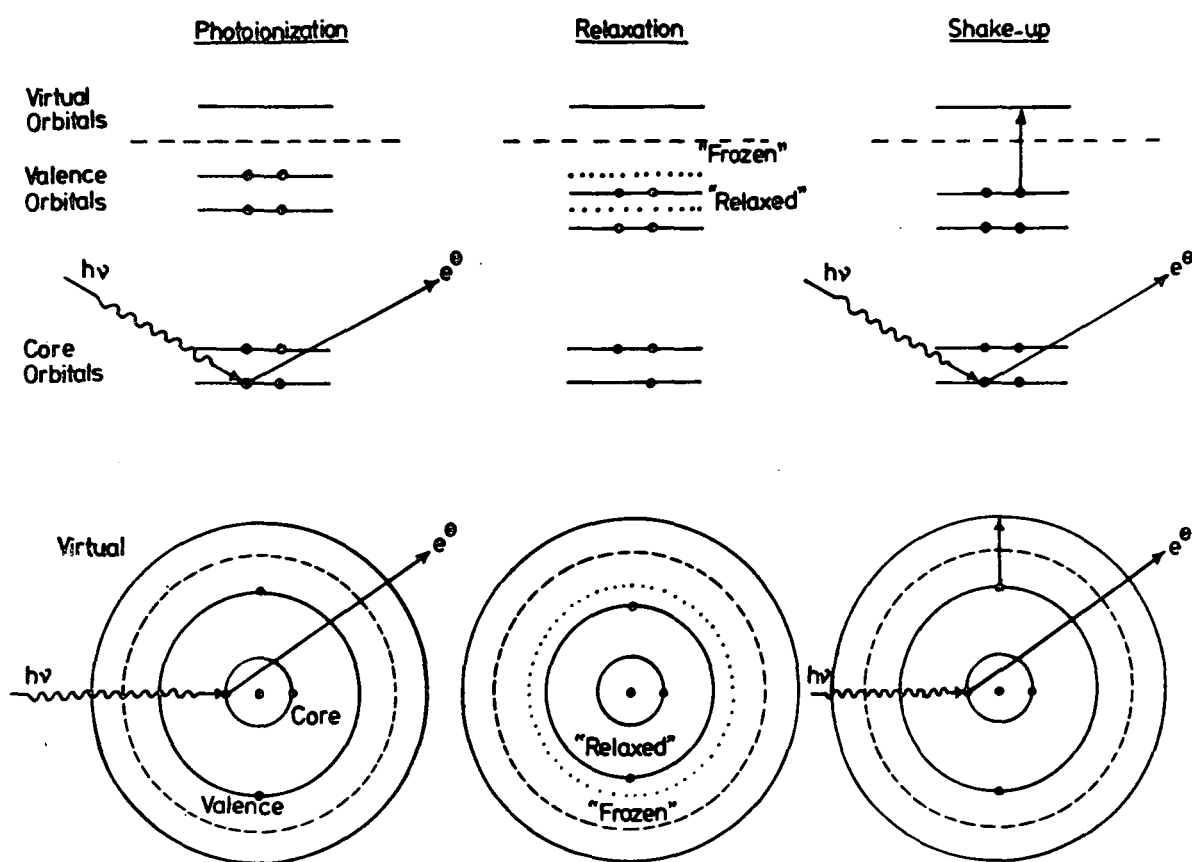


Figure 1.4 Photoionisation, shake-up and shake-off

states of the core ionised species. Since these phenomena take place on a similar time scale to photoionisation they result in a modification of the primary photoelectron signal producing satellite peaks occurring to the lower kinetic energy side of the main core signal. The shake-up process obeys monopole selection rules and may be viewed as an analogue of ultra-violet (U.V.) spectroscopy.

These processes have received much attention both from the experimental and theoretical standpoint. The theoretical relationship between shake-up and shake-off satellite intensities to the relaxation energy has been discussed by Manne and Åberg.<sup>30</sup> They showed that the weighted mean of the direct photoionisation, shake-up and shake-off peaks corresponds to the binding energy of the unrelaxed system (Figure 1.5).

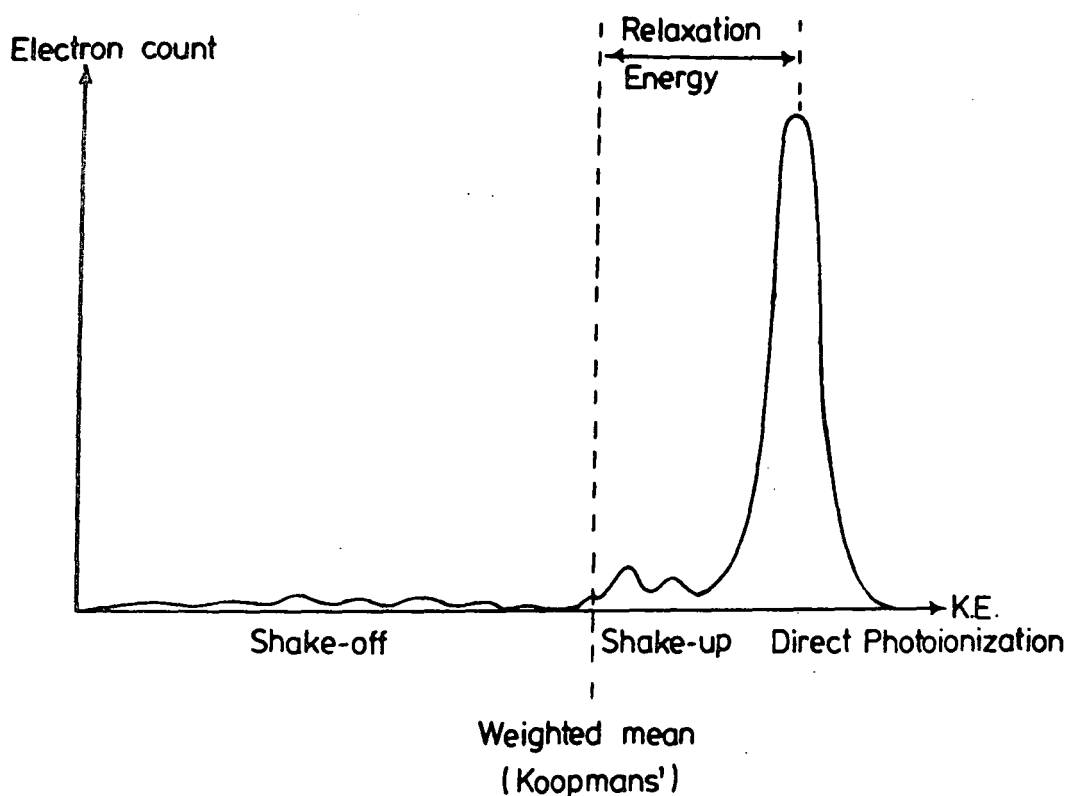


Figure 1.5 Relationship between relaxation energy, Koopmans' Theorem (mean) and the relative intensities of direct photoionisation, shake-up and shake-off

Shake-up and shake-off structure has been studied in a range of organic<sup>31,32</sup> and inorganic<sup>33,34</sup> materials, particular attention being paid to 'd' block elements.<sup>104</sup> The intensity of shake-up satellites varies from material to material, and the 3d spectra of the oxides  $\text{La}_2\text{O}_3$  and  $\text{CeO}_2$ , for example, show satellite structure of comparable intensity to the main photoelectron signals.<sup>35,36</sup> In such cases difficulty is encountered in distinguishing satellite and parent signals. Shake-up peaks are most difficult to identify the stronger they are and may be mistakenly interpreted in terms of a chemical shift effect.

The phenomenon of shake-up has proved to be of use in elucidating fine details of structure and bonding in polymer systems which are not directly attainable from the primary information levels in ESCA.<sup>37-39</sup>

Shake-up effects have been the subject of a recent review.<sup>40</sup>

### 1.2.5 Auger Emission and X-ray Fluorescence

There are two principal processes through which de-excitation of the hole produced in a core sub-shell normally decays, namely X-ray fluorescence<sup>41</sup> and Auger electron emission. Both these processes, which are shown schematically in Figure 1.6, are comparatively slow compared to photoionisation and so they have little effect on the kinetic energy of the original photoelectron.

The probability for each process is a function of the atomic number of the atom as shown in Figure 1.7, Auger emission predominating for lighter atoms<sup>8</sup> while X-ray fluorescence is more important for heavier elements.

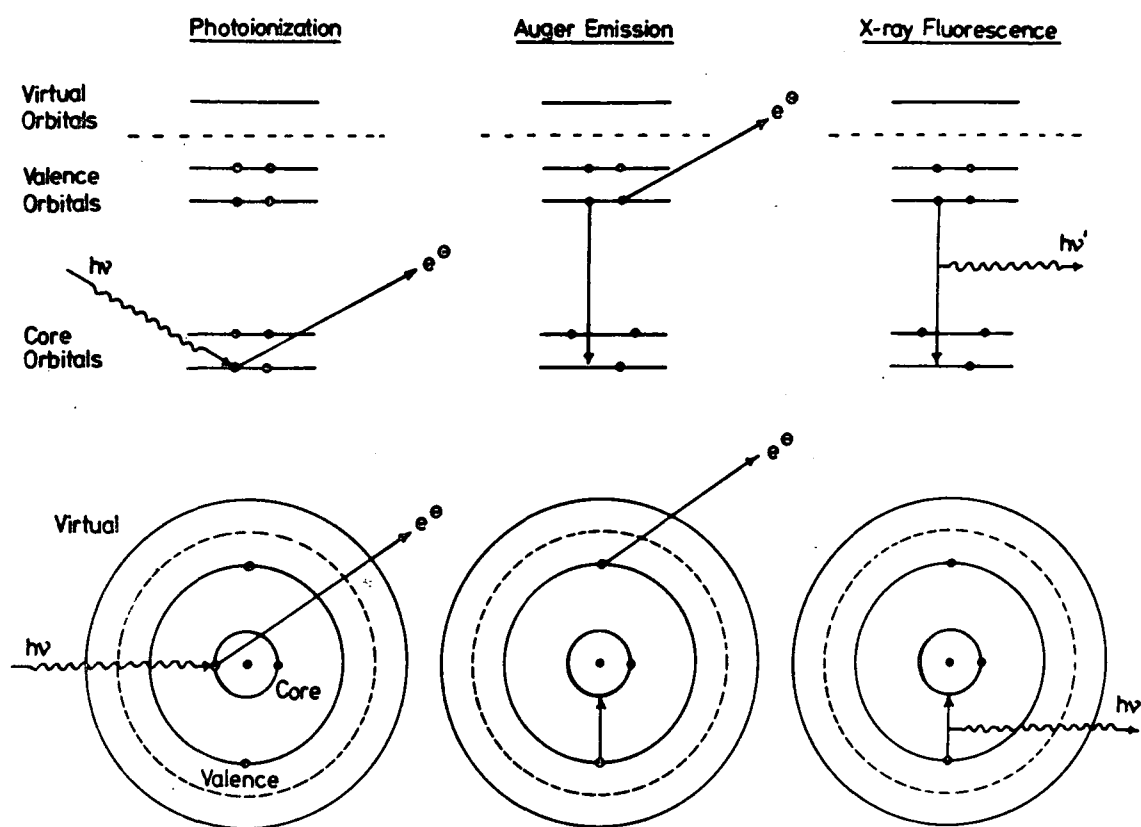


Figure 1.6 Photoionisation, Auger Emission and X-ray Fluorescence

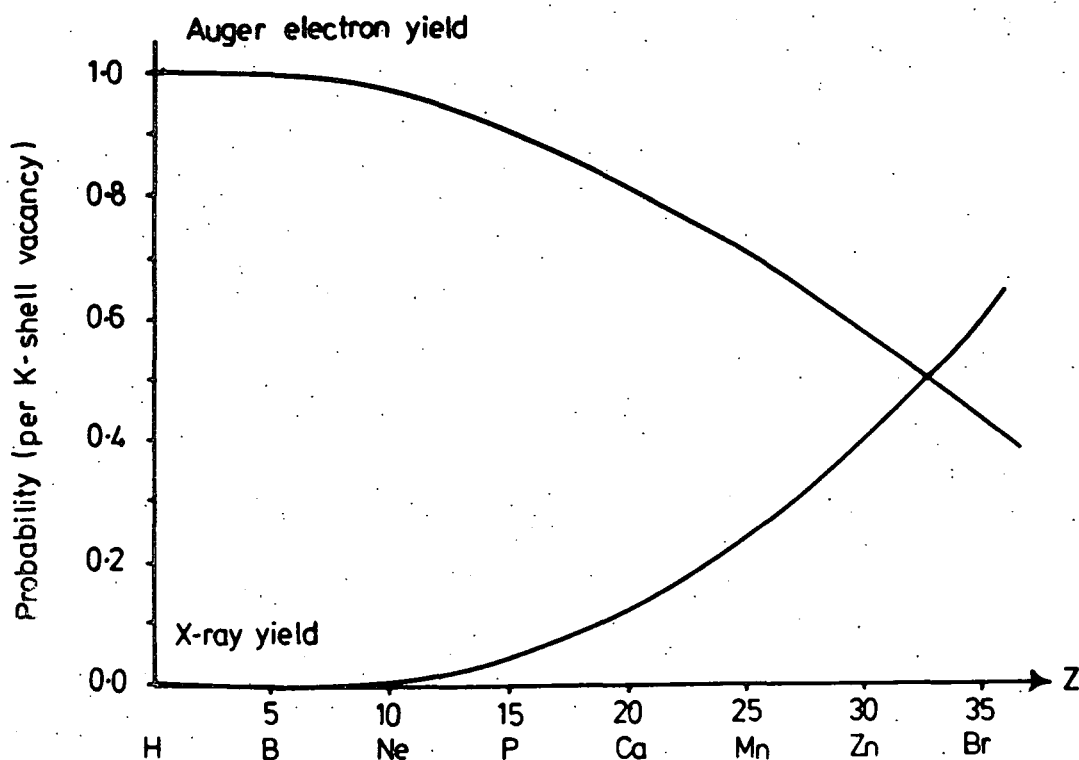


Figure 1.7 Efficiency of Auger and X-ray Fluorescence processes as a function of atomic number

Auger emission may be viewed as a two-step process in which the ejection of an electron from an inner shell by a photon is followed by an electron dropping down from a higher level to the vacancy in the inner shell with simultaneous emission of a second electron.<sup>42-47</sup> When the electron drops from a valence orbital, the Auger spectrum is related to the energies of both the valence and core orbitals. When the electron

drops from an inner orbital, a Coster-Kronig<sup>46</sup> transition, the Auger spectrum is related to the inner orbital transition. Such spectra are often very well resolved but unfortunately lead to broadening of the ESCA spectrum due to the very short lifetime of the process. For a Coster-Kronig process to occur, the difference in binding energies of the two inner shells must be sufficiently large to eject an electron from an orbital in the higher shell. These processes only occur in elements of atomic number <40.<sup>119</sup>

Auger Emission Spectroscopy (AES) is itself an important analytical technique in its own right and has found particular application to the study of the surfaces of metals and semiconductors. Commercial Auger spectrometers use an electron beam as the source of excitation radiation of typically 2 keV rather than X-ray photons. The technique is highly surface-sensitive since the sampling depth of the exciting electrons is only about five atomic layers<sup>48</sup> or  $\sim 1 \times 10^{-9}$  m. It should be noted that the flux dosage of the incident electron beam used in AES is approximately three orders of magnitude larger than a normal ESCA photon beam and radiation damage caused to organic material poses a severe problem.<sup>49,50</sup>

Due to the complexity of the Auger electron signal, chemical information is not so straightforwardly extracted as in ESCA. However, in the case of metal oxides, for example, the Auger chemical shift is much larger than the photoelectron chemical shift because of polarisation screening effects; the direction of the shift being such that the kinetic energy of Auger electrons from more polarisable salts is increased more than is the energy of the photoelectrons.

From the work of Shirley, Kowalczyk, Ley, McFeely and Pollak<sup>51-54</sup> in their studies of systems of Cu, Zn, Li and Na, and from the independent investigations by Wagner<sup>108</sup> and with co-worker Bilden<sup>25</sup>, a relationship

between shifts in Auger energy and the shifts in photoionisation peaks was derived.<sup>54</sup>

Wagner<sup>55</sup> has since developed the concept of the Auger Parameter, which is taken as the kinetic energy of the sharpest Auger line minus that of the most intense photoelectron peak, and is of considerable value to analytical chemists because it is a quantity independent of sample charging effects. Chemical state scatter plots<sup>56, 105</sup> on which photoelectron and Auger data are represented for a given element are likely to be of considerable importance in the use of ESCA for identification of chemical states.

### 1.3 Chemical Shifts

The core electrons of an atom are essentially localised and do not take part in bonding. Their energies are characteristic of the particular element and are sensitive to the electronic environment of the atom.<sup>1</sup> While the absolute binding energy of a given core level on a given atom will be characteristic of the element (Table 1.2), differences in electronic environment of a given atom in a molecule give rise to a small range of binding energies, 'chemical shifts', often representative of a particular structural feature; the classical illustration being the  $C_{1s}$  spectrum of ethyl trifluoroacetate shown in Figure 1.8. Shifts in core levels as a function of substituent for a wide range of polymers which have been investigated experimentally are shown in Table 1.3, and similar information exists for other core levels.<sup>105</sup> Such data taken in conjunction with relative cross-sections for photoionisation (to be covered in Section 1.6) from the relative core levels forms the basis for quantitative analysis by ESCA. This aspect will be treated in Section 1.11.

Table 1.2 Approximate core binding energies (eV)

	Li	Be	B	C	N	O	F	Ne
1s	55	111	188	284	399	532	686	867
	Na	Mg	Al	Si	P	S	Cl	Ar
1s	1072	1305	1560	1839	2149	2472	2823	3203
2s	63	89	118	149	189	229	270	320
2p <sub>1/2</sub>	31	52	74	100	136	165	202	247
2p <sub>3/2</sub>	31	52	73	99	135	164	200	245

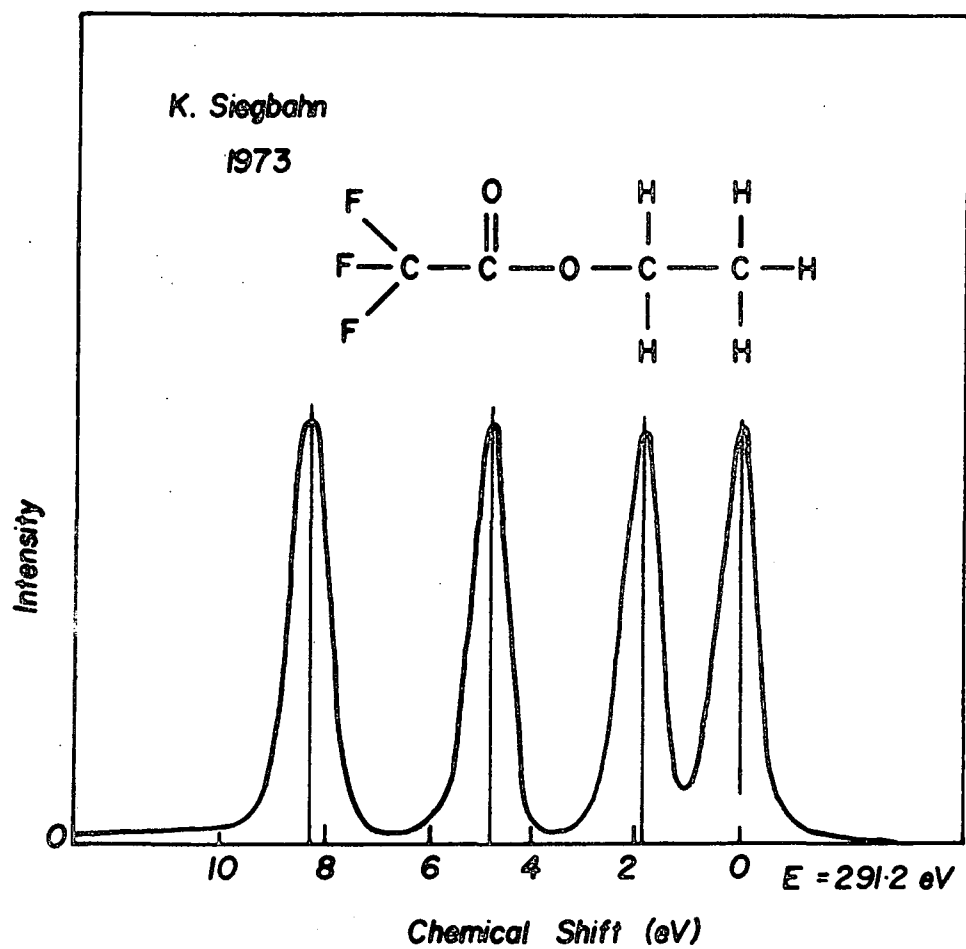


Figure 1.8  $C_{1s}$  spectrum of ethyl trifluoroacetate

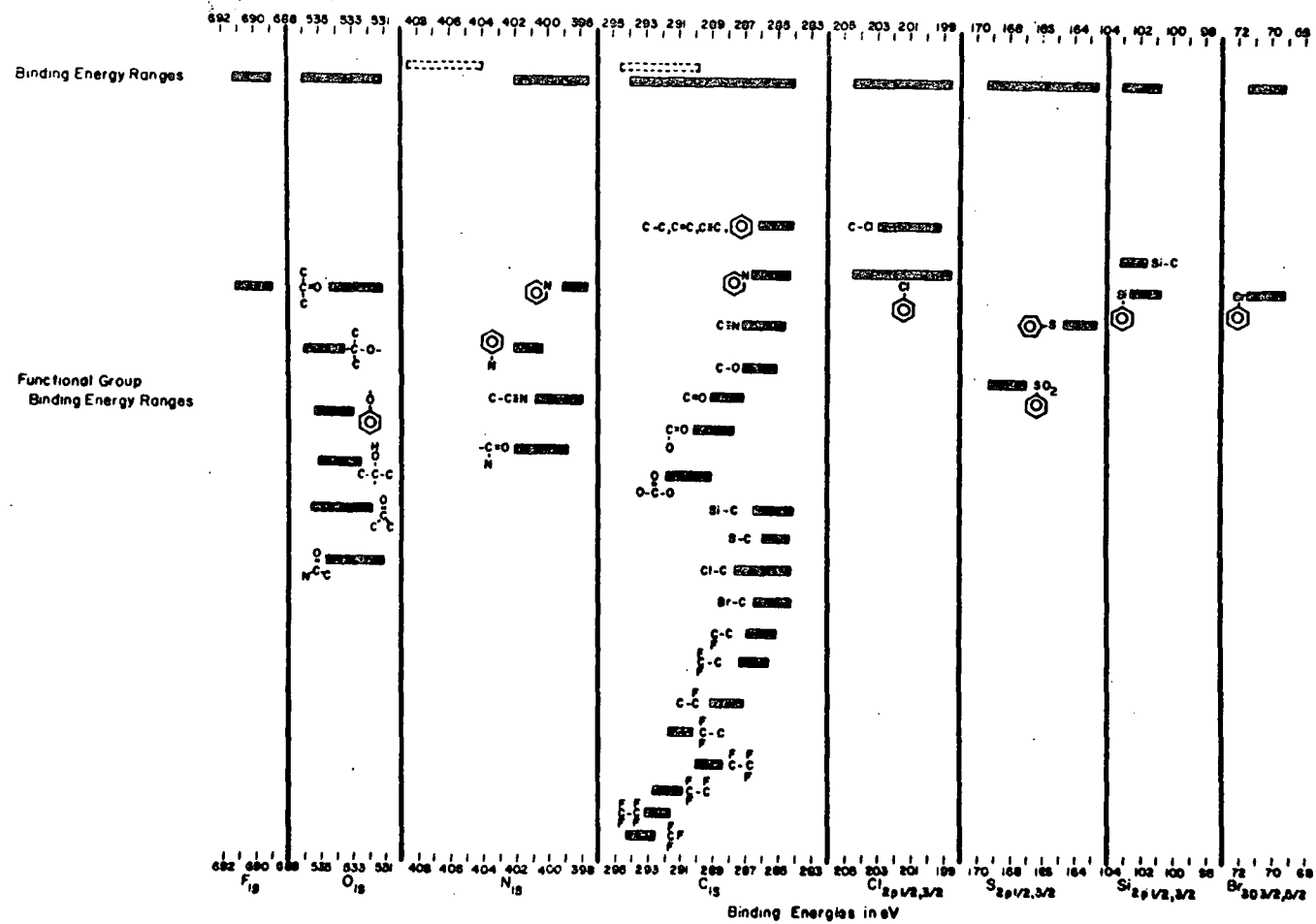


Table 1.3 Characteristic core level binding energies for various structural features in polymers.

When choosing a core level for study, the following factors are worthy of consideration:

- (1) The core level should have a high cross-section for photoionisation to give a high intensity spectrum.
- (2) The escape depth of the electrons should be taken into account (see Sections 1.6 and 1.11).
- (3) Levels should be chosen which are free from interference from other peaks in the same region of kinetic energy. This interference may be caused by either core level photoionisation peaks (e.g.  $Hg_{4f}/Si_{2p}$ ) or Auger electron signals. An example of the latter is given by Figure 1.9 which shows wide scan ESCA spectra for a polymer sample studied with both  $MgK\alpha_{1,2}$  and  $AlK\alpha_{1,2}$  radiation. The change in photon energy allows a ready identification to be made of the direct photoionisation peaks and those arising from Auger processes since the kinetic energy of the latter are independent of the way in which the initial hole is created. Thus the well-developed fluorine Auger spectrum is readily identified whilst the distinctive core-level spectra show that the material contains fluorine and carbon.
- (4) The line widths should be sufficiently narrow so as not to obscure subtle chemical shifts.
- (5) The peak should be well removed from high background signals, that is, there should be a high signal to noise ratio.

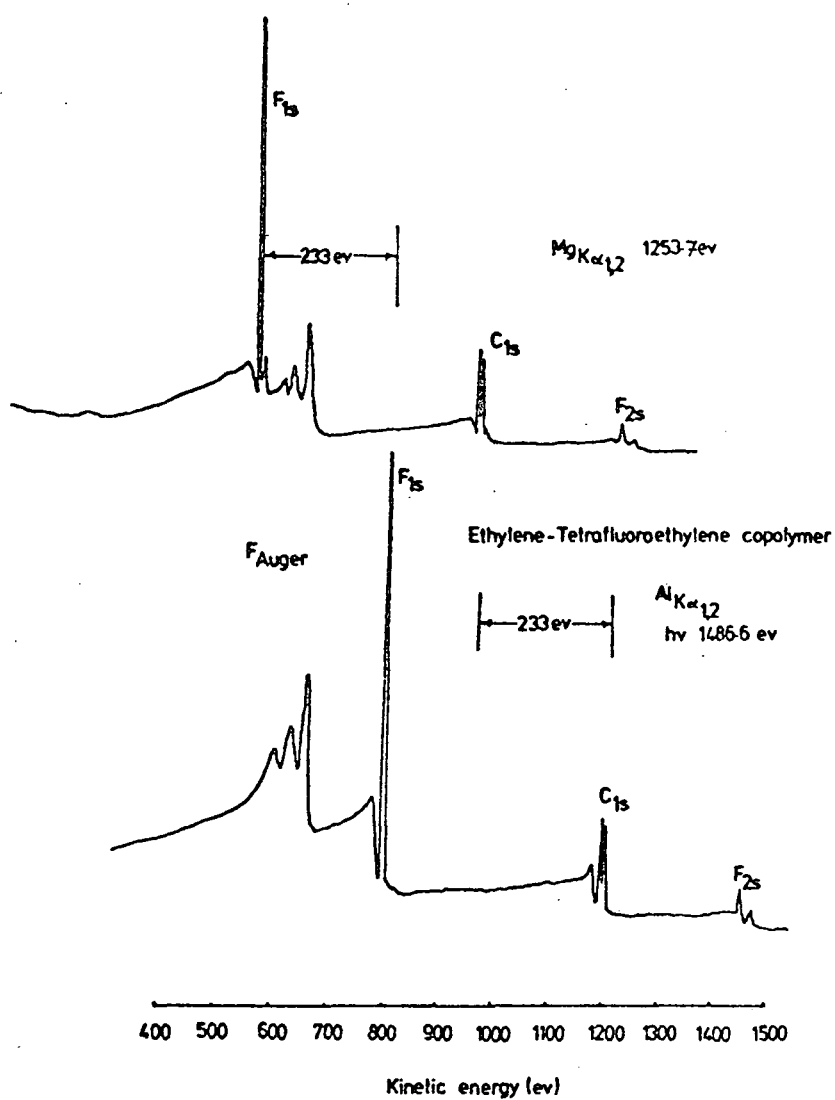


Figure 1.9 Wide-scan ESCA spectra for an ethylene-tetrafluoroethylene copolymer with  $MgK\alpha_{1,2}$  and  $AlK\alpha_{1,2}$  photon sources showing differentiation between photoionisation and Auger peaks.

Much attention has been paid to the theoretical interpretation of the chemical shift phenomenon observed experimentally. The following distinct but interrelated approaches have been used:

- (1) Koopmans' Theorem<sup>29</sup>
- (2) Core Hole Calculations<sup>58,59</sup> - linear combination of atomic orbitals - molecular orbital - self-consistent field method (LCAO MO SCF)
- (3) Equivalent Cores Model<sup>57</sup>
- (4) Charge Potential Model<sup>10</sup>
- (5) Quantum Mechanical Potential Model<sup>60-62</sup>
- (6) Many body formalism

An account of the physical processes involved in electron photoemission and their effects from a theoretical standpoint has been given by Fadley.<sup>63</sup>

#### 1.4 Fine Structure

##### 1.4.1 Multiplet Splitting

Multiplet splitting of core levels is the result of spin interaction between an unpaired electron resulting from the photoionisation process and other unpaired electrons present in the system. Examples can be found in the core level spectra of transition element compounds.<sup>64,65</sup> The theoretical interpretation of multiplet effects is relatively straightforward only for s-hole states and is based on Van Vlecks' vector coupling model.<sup>66</sup> The magnitude of the splitting provides information concerning the localisation or delocalisation of unpaired electrons in a compound, since the greater the localisation and spin densities on an atom the

greater will be the observed splitting. Multiplet splittings in photoelectron spectroscopy have been reviewed in some detail by Fadley.<sup>67</sup>

#### 1.4.2 Spin Orbit Splitting

When photoionisation occurs from an orbital which has an orbital quantum number ( $l$ ) greater than 1, i.e. from a p, d or f orbital, then coupling can occur between the spin ( $S$ ) and orbital angular momentum ( $L$ ) to yield a total momentum ( $J$ ). A doublet, which is usually well-resolved, is then observed in the spectrum instead of a single peak.<sup>9</sup> The relative intensities of the component peaks of the doublet are proportional to the ratio of the degeneracies of the states which is quantum mechanically defined as  $2J + 1$ . The relative intensities of the  $J$  states for s, p, d and f orbitals are shown in Table 1.4 and illustrated in Figure 1.10.

Table 1.4 J States for s, p, d and f orbitals

<u>Orbital</u>	<u>Orbital Quantum No.</u>	<u>Total Quantum No.</u>	<u>Intensity Ratio</u>
	$l$	$J = (l \pm S)$	$(2J+1) : (2J^l+1)$
s	0	$1/2$	singlet
p	1	$1/2, 3/2$	1 : 2
d	2	$3/2, 5/2$	2 : 3
f	3	$5/2, 7/2$	3 : 4

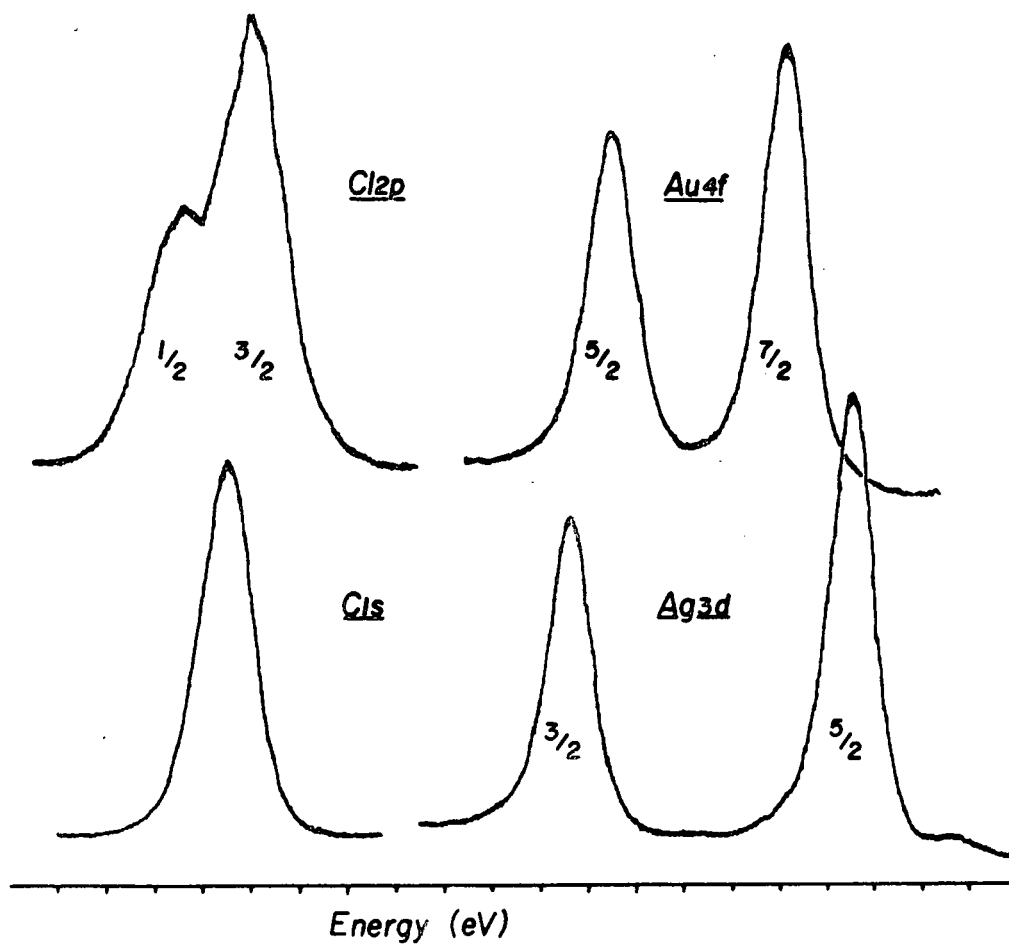


Figure 1.10 Spin-orbit splittings in  $Cl_{1s}$ ,  $Cl_{2p}$ ,  $Ag_{3d}$  and  $Au_{4f}$  core levels.

#### 1.4.3 Electrostatic Splitting<sup>68-70</sup>

This is caused by the differential interaction between the external electrostatic field and the spin states of the core level being investigated. It has been observed for a number of systems, for example,

the  $5p_{3/2}$  levels of uranium and thorium and in some compounds of gold. <sup>71,72</sup>

Correlation has been observed between electrostatic splitting and the quadrupole splittings obtained from Mössbauer spectroscopy, <sup>73</sup> which arise from the interaction of the nuclear quadrupole moment with an inhomogeneous electric field.

A summary of the type of splitting encountered in ESCA is given in Figure 1.11.

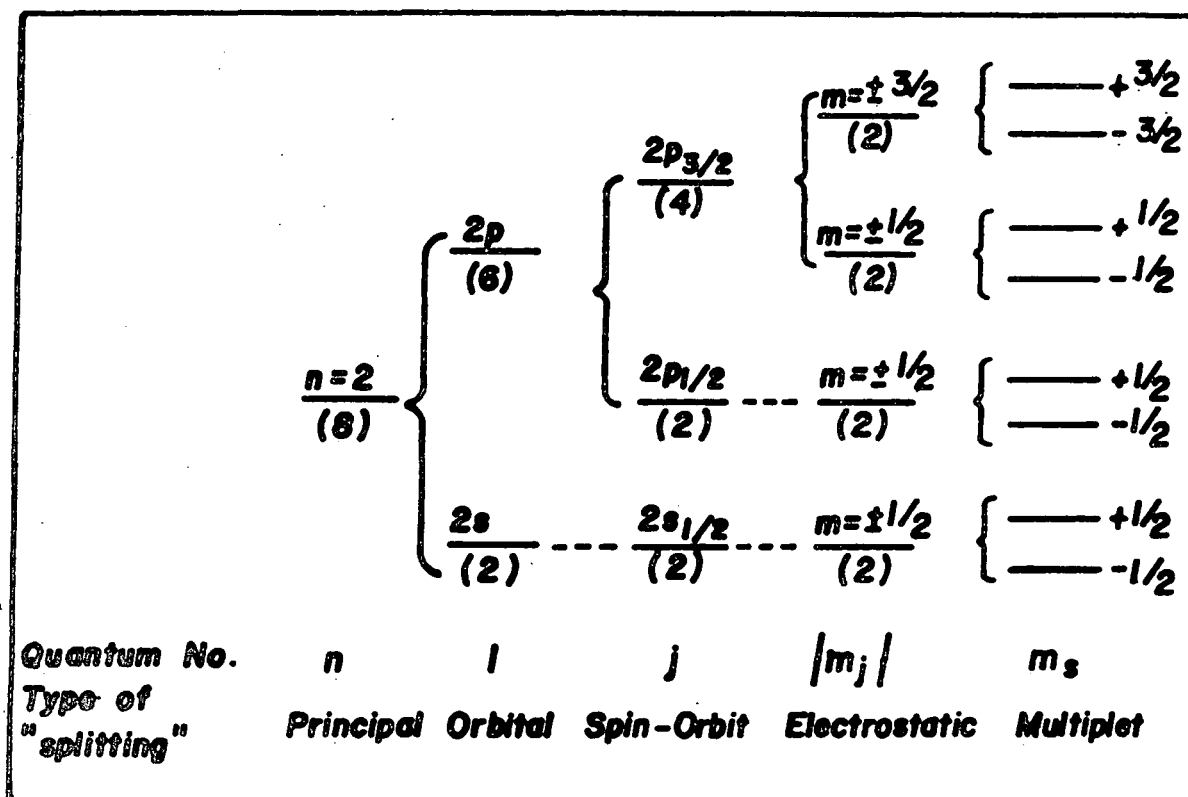


Figure 1.11 Schematic of the types of splitting encountered in ESCA

### 1.5 Sample Charging and Energy Referencing

As mentioned previously, for conducting samples, in electrical contact with the spectrometer, the Fermi level serves as a convenient level for energy referencing. However, with insulating samples or samples not in contact with the spectrometer, the Fermi level is not so well-defined and some calibration procedure must be adopted in order to correct for this.

The phenomenon of 'sample charging' associated with insulating samples arises from the inability of the sample to replace electrons at the surface from the surroundings in contact with the sample, either through conduction from the sample backing or by capture of stray electrons from the vacuum system.<sup>74-76</sup> This stray electron flux, which comprises slow electrons photoemitted from the sample, from photoelectrons generated by X-ray impact on the X-ray window and on the chamber walls, for example, has been shown to amount to 99% of the total photoemitted flux for an insulating sample.<sup>76</sup> Photoemitted electrons from the surface experience a net retardation and therefore larger binding energies are measured. All photoelectrons are affected by the same retardation voltage and are shifted in energy by the same amount.

For a sample with a uniformly distributed positive surface charge, the energy equation for a solid becomes:

$$\text{K.E.} = h\nu - \text{B.E.} - \phi_s - \Delta \quad (1.5)$$

where  $\Delta$  is the energy shift due to the positive sample charge.

A non-uniform distribution or non-equivalent positive potential ('differential sample charging') over the surface of the sample will lead to a broadening of the primary photoelectron peak. This is because the electrons from core levels of atoms of different charge will experience different retardation potentials at the surface.

One method by which charging may be detected is to vary the incident electron flux by means of an electron 'flood gun'.<sup>120</sup> Additional low energy electrons are released into the sample region: if the photoelectron peaks move to lower apparent binding energy, charging effects are present. Indeed, the use of such flood guns has found application in the study of the complex charging effects arising from conducting and insulating catalyst sites in industrial catalysts.<sup>121</sup>

The prime motivation for the use of electron flood guns is the very large sample charging for thick insulating samples in spectrometers employing monochromatic X-ray sources. The removal of bremsstrahlung as a source of secondary electrons can lead to shifts in kinetic energy scale in the hundred eV range and can be compensated by flooding the sample with low energy electrons. Samples can become negatively charged however, and the method needs great care to achieve an accuracy comparable with that of other methods.

An alternative source of low energy electrons is to illuminate the sample region with U.V. radiation from a low pressure, low power mercury lamp via a quartz viewing port in the source region of the spectrometer. Sufficient secondaries are generated from photoemission, from the metal surfaces of the sample analysis chamber, that sample charging is reduced to a low level.<sup>122</sup>

The most convenient method for overcoming the problems of sample charging connected with energy referencing employed in routine analyses is to use a suitable reference peak. A correction factor calculated from the observed kinetic energy of the photoelectrons corresponding to the reference peak is then used to find the binding energies of the other peaks. The two most commonly used calibration lines are the  $C_{1s}$  peak from  $(\underline{C}H_2)_n$  environments at 285.0 eV binding energy, either inherent in

the sample or arising from hydrocarbon contamination within the spectrometer, <sup>77-78</sup> and the  $Au_{4f\ 7/2}$  level at 84.0 eV, if the sample has been deposited on a gold substrate. <sup>1</sup>

A study by Clark, Dilks and Thomas <sup>123</sup> into the sample-charging phenomena arising in the ESCA experiment for a series of polymers has shown sample charging to be of importance as an information level in its own right. For samples studied as films or powders mounted insulated from the spectrometer probe and for gold under similar conditions, it has been shown that over a wide range of operating conditions, equilibrium charging shifts are characteristic of the sample and show a strong dependence on the theoretically calculated total photoionisation cross-sections. The surface sensitivity of the phenomenon has been demonstrated by monitoring changes in charging shifts as a function of hydrocarbon contamination, or in the case of thin films deposited on gold. The time-dependent behaviour of charging shifts for polymer films mounted directly in contact with the spectrometer was also reported. The utility of studying sample-charging shifts was demonstrated by reference to changes which occur upon surface modification of an ethylene-tetrafluoroethylene copolymer system in radio frequency plasmas excited in inert gases. Detailed ESCA analyses of both the core and valence spectra for the polymer system under similar reaction conditions have shown that the chemical changes which occur produce a surface which has a greatly reduced fluorine content. <sup>124-127</sup> The considerable difference existing between the charging characteristic of the fluorine containing copolymer and of a solely hydrocarbon based polymer such as polyethylene made it possible for the change in surface composition to be monitored by sample charging measurements.

## 1.6 Signal Intensities

The geometry employed in the ES200B spectrometer with a fixed arrangement of analyser and X-ray source is depicted in Figure 1.12.

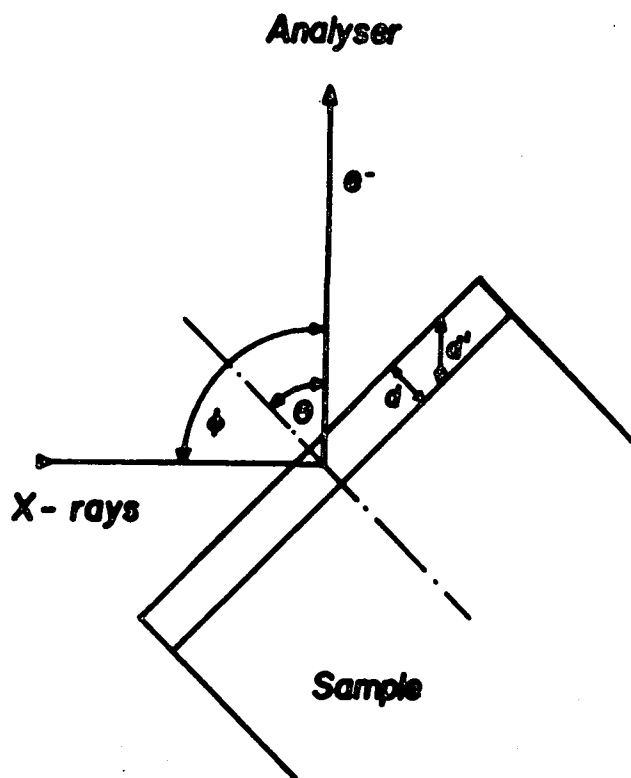


Figure 1.12 Schematic of the sample geometry relative to the X-ray gun and analyser.

$h\nu$  represents the incident photon beam and  $e^-$  is the fraction of photoemitted electrons entering the analyser,  $\theta$  is the angle between the X-ray source and the analyser entrance slit and  $\theta$  describes the angle of the sample in relation to the analyser. If the photoelectrons are emitted from a depth,  $d$ , of the sample, their true path length will be  $d^1$  where

$$d^1 = d \operatorname{cosec} \theta \quad (1.6)$$

Due to the short mean free paths of electrons (for K.E. > 50eV) in solids it is possible to enhance surface features with respect to bulk and subsurface by conducting experiments involving grazing exit of the photoemitted electrons which are analysed, that is with  $\theta$  approaching  $90^\circ$ . Angular dependence studies are only feasible on uniform flat surfaces (e.g. films or coatings) and is not applicable to samples with rough surface topography, such as is the case for powders.

For an infinitely thick homogeneous sample the intensity ( $I$ ) of the elastic (no energy loss) photoionisation peak corresponding to photoionisation from a core level  $i$  may be expressed as:

$$dI_i = F \alpha_i N_i k_i e^{-x/\lambda_i} dx \quad (1.7)$$

where:  $I_i$  is the intensity arising from core level  $i$ ,

$F$  is the exciting photon flux,

$d_i$  is the number of atoms per unit volume on which the core level  $i$  is localised,

$k_i$  is the spectrometer factor,

$\lambda_i$  is the electron mean free path.

On integration the equation 1.7 becomes:

$$I_i = \int_0^{\infty} F \alpha_i N_i k_i e^{-x/\lambda_i} dx \quad (1.8)$$

$$I_i = F \alpha_i N_i k_i \lambda_i \quad (1.9)$$

The parameters affecting the intensity of a given signal in ESCA are discussed more fully below.

The X-ray flux,  $F$ , is primarily dependent on the power applied to and the efficiency of the X-ray gun. However, the angle of incidence  $\emptyset$  of the X-rays and the analyser and  $\theta$  do have an effect on the intensity of the photoionisation peak.

The cross-section for photoionisation of core level  $i$ ,  $\alpha_i$ , is a parameter which describes the probability of the core level being ionised when irradiated by a photon of known energy<sup>81</sup> and includes only the fraction of the total number of electrons photoemitted within the angle of acceptance of the analyser focussing lens.  $\alpha_i$  is a function of the core level to which it relates and the energy of the incident photon. Values of  $\alpha_i$  may be calculated from the fundamental properties of the atom<sup>82</sup> or determined experimentally from gas phase ESCA experiments.<sup>10</sup> The geometry of the X-ray source with respect to the analyser entrance slit affects  $\alpha_i$  values, but for a particular spectrometer and using the same X-ray source and with a fixed value of  $\emptyset$  then  $\alpha_i$  is normally a constant. With  $MgK\alpha_{1,2}$  and  $AlK\alpha_{1,2}$  the cross-sections for photoionisation for core levels of most elements of the periodic table are within two orders of magnitude of that for the  $C_{1s}$  levels, therefore ESCA has a convenient sensitivity range for all elements. The cross-sections for core levels are normally considerably higher than those for valence levels.

The spectrometer factor,  $k_i$ , includes contributions due to detector efficiencies, analyser transmission characteristics which are both dependent on the kinetic energy of the core electrons being analysed, and geometric factors such as the solid angle of acceptance of the analyser.

The inelastic mean free path of photoemitted electrons (sometimes referred to as the escape depth)  $\lambda_i$ , is defined as the distance in the solid through which the electrons will travel before  $1/e$ th of them have not suffered energy loss through inelastic collisions. Both experimental<sup>83,84</sup> and theoretical<sup>85</sup> calculations of  $\lambda_i$  have been undertaken.  $\lambda_i$  is related to the kinetic energy of the photoionised electrons and ranges from  $\sim 4\text{\AA}$  for electrons of about 80eV K.E. to  $\sim 30\text{\AA}$  for electrons of about 1500 eV. This variation is presented graphically in Figure 1.13.

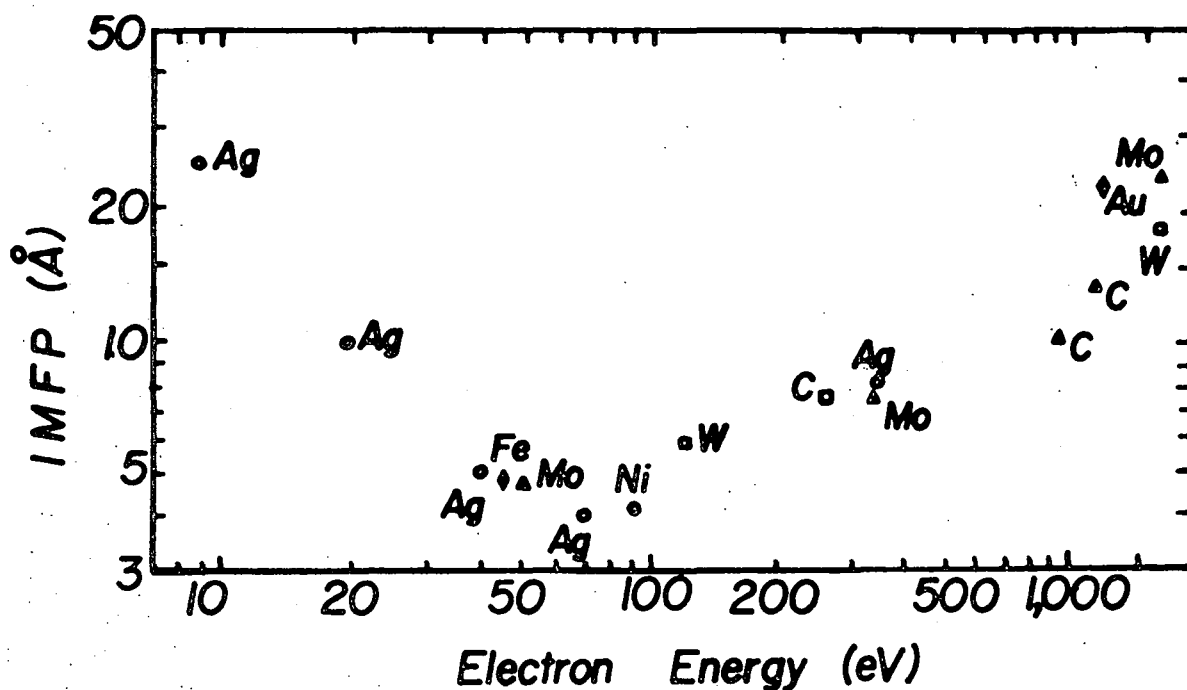


Figure 1.13 Mean free paths of photoemitted electrons.

The sampling depth (not to be confused with the electron mean free path) is defined as the depth from which 95% of the signal, arising from a given core level, derives and may be related to  $\lambda$  by

$$\text{Sampling depth} = -\lambda \ln 0.05 \quad (1.10)$$

$$\approx 3\lambda \quad (1.11)$$

As an example, for carbon 1s levels studied by a  $\text{MgK}\alpha_{1,2}$  X-ray source the kinetic energy of the photoelectrons is  $\sim 960\text{eV}$  and the mean free path of the electrons is  $\sim 15\text{\AA}$ . 50% of the signal seen by ESCA derives from the outermost  $10\text{\AA}$  of the sample and 95% from the top  $45\text{\AA}$ . This illustrates the high surface sensitivity of ESCA.

It has been noted that the sampling depth varies with  $\lambda$  and this effect is clearly illustrated by the high and low kinetic energy germanium peaks (Ge 3d 1222eV and Ge 2p 268eV) from a sample of germanium with a passive oxide surface, as shown in Figure 1.14.

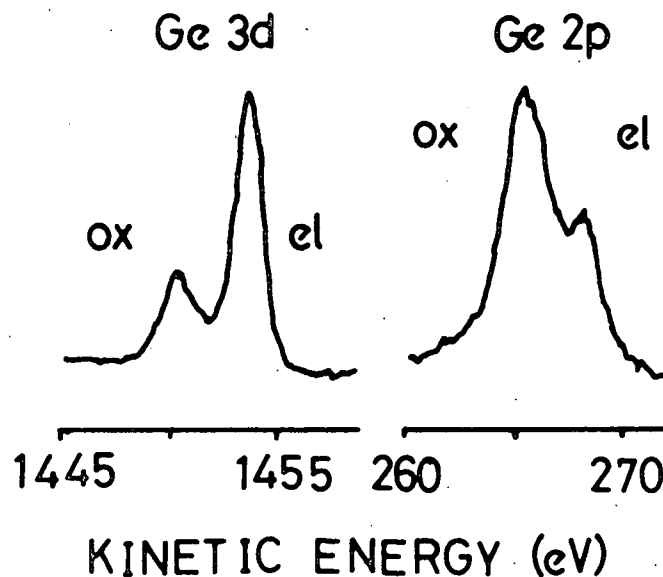


Figure 1.14 Ge core level spectra from Ge metal with a passive oxide overlayer, illustrating the greater sampling depth of the higher K.E. photoelectron.

In general, a departure from homogeneity within the sample region will be indicated by a marked deviation in the intensity ratio of widely spaced peaks (on the kinetic energy scale) from that obtained from homogeneous standards. The ratio of the intensities  $I_{\text{low}}/I_{\text{high}}$  for the high and low kinetic energy peaks provides an alternative method for analytical depth profiling. This may be used to monitor overlayer and modification effects; the intensity ratio tending to a minimum as the modification depth tends to  $3\lambda_{\text{high}}$ .

Although the number density  $N_i$  is not directly related to the density of the sample, it is generally the case that for similar materials the ESCA signal for a given core level will be more intense for the higher density material.<sup>78</sup> The most important consequence of  $N_i$  is that the relative signal intensities for core levels in a homogeneous sample are directly related to the overall stoichiometries of the atoms sampled. Thus for two core levels  $i$  and  $j$ ,

$$\frac{I_i}{I_j} = \frac{F\alpha_i N_i k_i \lambda_i}{F\alpha_j N_j k_j \lambda_j} \quad (1.12)$$

If  $i$  and  $j$  correspond to the same core level in differing chemical environments, then

$$k_i \alpha_i \lambda_i = k_j \alpha_j \lambda_j \text{ and } \frac{N_i}{N_j} = \frac{I_i}{I_j} .$$

If however  $i$  and  $j$  are different core levels then  $k_i \alpha_i \lambda_i \neq k_j \alpha_j \lambda_j$  and

$$\frac{N_i}{N_j} = \frac{I_i k_j \alpha_j \lambda_j}{I_j k_i \alpha_i \lambda_i} . \text{ The ratio } \frac{k_j \alpha_j \lambda_j}{k_i \alpha_i \lambda_i}$$

may be determined experimentally from standard samples of known stoichiometry containing  $i$  and  $j$ . Since  $k_i$  and  $k_j$  vary from one spectrometer to another as does  $(\sigma + \theta)$ , these ratios, known as sensitivity factors, must be determined for the particular spectrometer.<sup>86</sup>

Quantitative aspects of ESCA are to be discussed in Section 1.11.

## 1.7 Line Shape Analysis

The need for line shape analysis (deconvolution) arises when the chemical shift of a level is smaller than the linewidth of that level. The measured linewidths of component peaks for a core level may be expressed as

$$(\Delta E_m)^2 = (\Delta E_x)^2 + (\Delta E_s)^2 + (\Delta E_l)^2 + (\Delta E_{ss})^2 \quad (1.13)$$

$\Delta E_m$  is the measured width at half height, the so-called full width at half maximum (FWHM).

$\Delta E_x$  is the FWHM of the X-ray photon source. This is the dominant contributor to the observed line widths, typical values being 0.7 eV for  $MgK\alpha_{1,2}$  and 0.9 eV for  $AlK\alpha_{1,2}$ <sup>9</sup> and may be reduced using monochromatisation techniques.<sup>10</sup>

$\Delta E_s$  is the contribution due to spectrometer aberrations and is dependent on the emission energy and the choice of analyser slits.

$\Delta E_{ss}$  is the contribution due to solid state effects in the sample.

$\Delta E_l$  is the natural width of the core level under investigation and is related, via the uncertainty principle, to the lifetime of the core hole state. Small changes in line widths of the order of 0.1 eV have been found to be caused by chemical effects which have a small effect on the life time of the core hole state. This emphasises the need to estimate peak intensities by area and not by height.

The contribution to  $\Delta E_m$  from  $\Delta E_x$  for the commonly used photon sources (i.e. Mg and Al) are essentially Lorentzian line shapes. The characteristics for the energy distribution in  $MgK\alpha$  radiation are essentially comprised of four major component lines;  $\alpha_1$ ,  $\alpha_2$ ,  $\alpha_3$  and  $\alpha_4$ , the relative positions to the  $\alpha_1$  line are -0.33, +8.4 and +10.2 eV, with relative

intensities of 100, 50, 12.8 and 6.9.<sup>87</sup> The  $\alpha_3$  and  $\alpha_4$  lines are significantly removed from the  $\alpha_1$  and  $\alpha_2$  lines and manifest themselves as satellite peaks to the high kinetic energy side of the intense primary photoionisation signal in the ESCA spectrum. A similar situation is true for AlK $\alpha$  radiation.<sup>87</sup>

The contribution to  $\Delta E_m$  from  $\Delta E_s$  is considered to be Gaussian, whereas that from  $\Delta E_l$  is Lorentzian.

The convolution of these line shapes produces a hybrid shape with a Gaussian distribution dominating the overall line shape and with Lorentzian character in the tails. The use of pure Gaussian shapes introduces only small errors into the line shape analysis.<sup>10</sup>

Deconvolution procedures may be grouped into two main categories:

- (1) Deconvolution by mathematical methods which have been reviewed by Carley and Joyner.<sup>88</sup>
- (2) Curve fitting by simulation, either in analogue or digital fashion.

Figure 1.15 is an example of a complex spectrum which has been deconvoluted using this approach into its individual components with area ratios shown.

For the work in this thesis, deconvolution was performed by analogue simulation using a Du Pont 310 curve resolver (and the accuracy is of the order of a few percent). On this instrument, the binding energy, line width and peak height are controlled by the operator as is also the line shape, though this is usually set for a Gaussian form. The underlying philosophy in such a technique is outlined in Table 1.5. When dealing with complex line shapes, a detailed knowledge of prototype systems becomes increasingly more important.



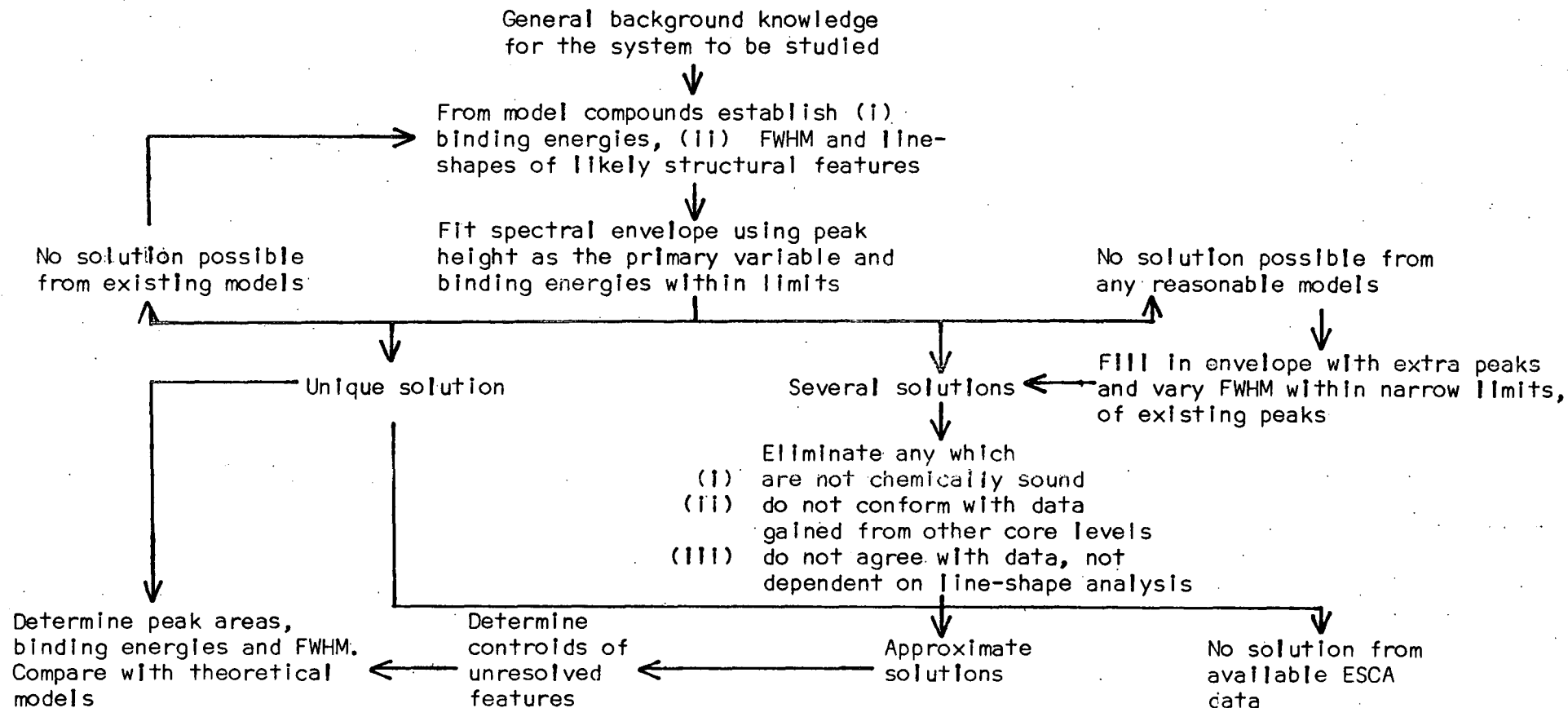


Table 1.5 Line-shape analysis by curve fitting; schematic of logic procedure.<sup>1</sup>

## 1.8 ESCA Instrumentation

Instrumentation used in the ESCA experiment may be conveniently considered in four parts:

- (1) X-ray source,
- (2) Sample chamber,
- (3) Electron energy analyser,
- (4) Electron detection.

Most of the work in this thesis was carried out using an A.E.I. ES200B spectrometer; a custom-designed Kratos ES300 spectrometer was also used for some of the work described in Chapter Two.

A schematic of the basic experimental set-up is given in Figure 1.16.

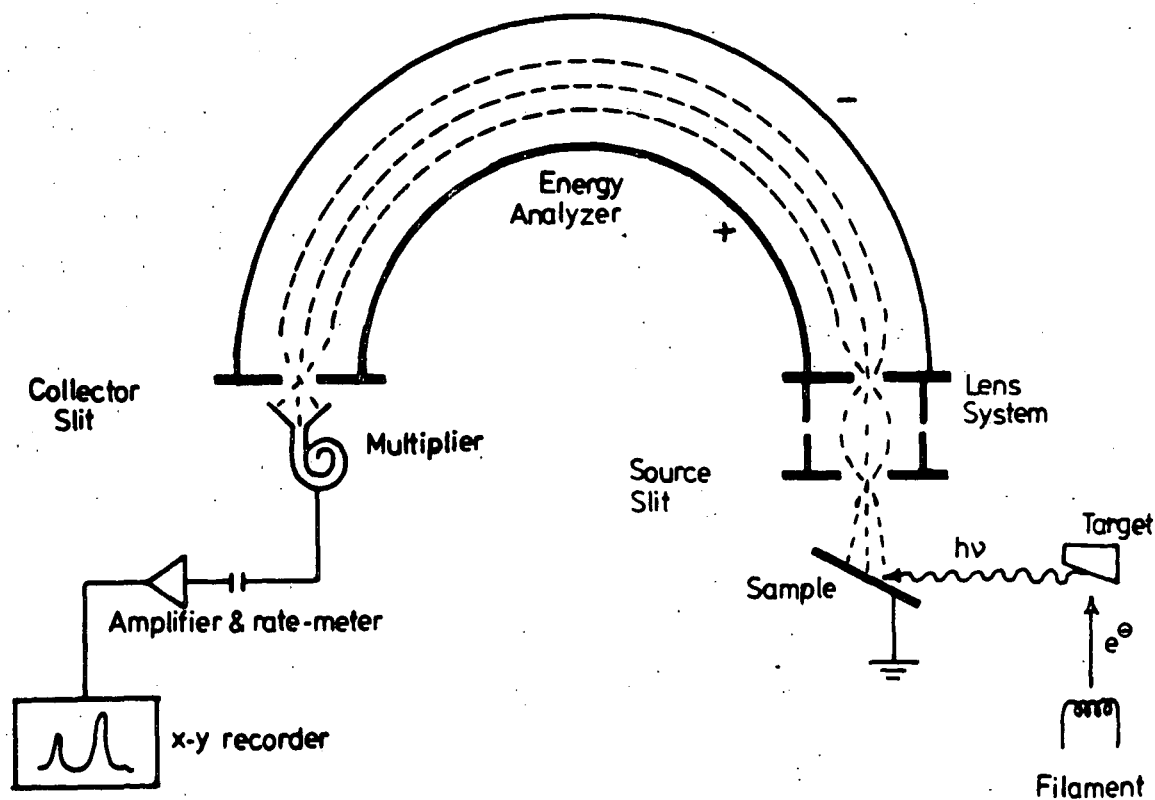


Figure 1.16. Schematic of the ESCA Instrumentation

### 1.8.1 X-ray source

The X-ray beam is commonly produced by the bombardment of a target (or anode) with high energy electrons. A typical, non-monochromatic X-ray spectrum is shown in Figure 1.17, which illustrates the appearance of

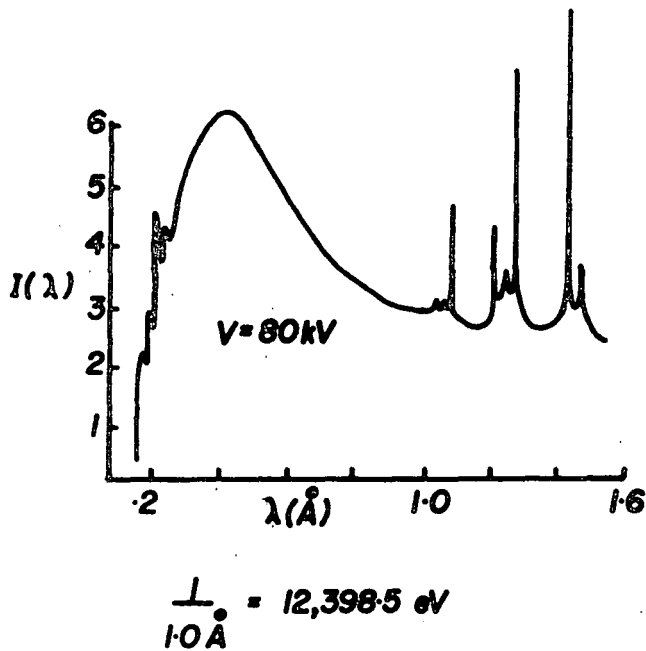


Figure 1.17 X-ray spectrum of a tungsten anode

emission lines, characteristic of the anode material superimposed on a continuous spectrum (Bremsstrahlung).<sup>89</sup> The continuum's shape depends only on the energy of the incident electrons on the anode, and not on the nature of the anode material.

Soft X-ray sources are most commonly employed in ESCA, for example, the MgK $\alpha$  ( $h\nu = 1253.7$  eV) and AlK $\alpha$  ( $h\nu = 1486.6$  eV) lines; only very occasional use being made of harder X-rays such as CuK $\alpha_1$  ( $h\nu = 8048$  eV) and CrK $\alpha_1$  ( $h\nu = 5415$  eV). Other sources intermediate in energy are SiK $\alpha$  (1739.5 eV)<sup>90</sup> and TiK $\alpha$  X-rays (4510 eV) and it is likely that these harder X-ray sources will be employed in future Auger work.<sup>91,92</sup>

The ES200B spectrometer has a Marconi Elliott GX5 high voltage supply unit with integrally variable voltage, 0-60 kV and current, 0-80 mA. The X-ray source comprises an unmonochromatised magnesium anode of Henke design<sup>93</sup> with hidden filament; this reduces risks of contamination of the target by evaporated tungsten from the electron gun filament. Normal source operating conditions are 12 kV and 15 mA. The X-ray flux is of the order of 0.1 millirad s<sup>-1</sup>,<sup>94</sup> which causes little or no radiation damage to the majority of systems. The target is isolated from the sample chamber by a thin aluminium window (~ 0.003" thick) to prevent interference due to electrons from the filament. The risk of scattered electrons exciting X-radiation from the aluminium window is reduced by operating the filament at near ground potential (+ 10V) and the anode at high positive voltage. Aluminium impurity, sometimes found in magnesium targets, is known to cause satellites due to AlK $\alpha$  excitation of the sample under investigation. These satellites, which have intensities a few percent of the primary peaks, particularly affect attempts to detect peaks from elements present in trace amounts.

The ES300 spectrometer is equipped with a dual-anode<sup>95</sup> with magnesium and titanium targets and a monochromatised AlK $\alpha_{1,2}$  X-ray source, their usual operating conditions being (9 kV, 8 mA), (13.5 kV, 18 mA) and (15 kV, 35 mA) respectively. The monochromator for the AlK $\alpha_{1,2}$  uses slit filtering<sup>19</sup> and diffraction from the (10 0) plane of quartz<sup>10</sup> at the Bragg angle of 78.3°. Other monochromators may use dispersion compensation or 'fine focussing' systems.<sup>96</sup>

The titanium anode probes further into the surface yielding data on bulk composition.<sup>97</sup> The typical sampling depth using the titanium target is  $\sim 200 \text{ \AA}$ , compared with a sampling depth in the region of  $50 \text{ \AA}$  when a magnesium X-ray source is employed. Hence analytical depth profiling at three levels is available at the flick of a switch.

An idealised photon source for photoelectron spectroscopy would be a monochromatised source of continuously tunable energy and high intensity. Synchrotron radiation<sup>98</sup> has been developed since the 1960s and facilities for its use are becoming available.<sup>99</sup> The phenomenon results naturally from the centripetal acceleration of charged particles moving at relativistic velocities inside an accelerator: storage ring systems are also in use. The tunable polarised source so produced is capable of supplying exciting photons in the ultrasoft X-ray region. The use of synchrotron radiation sources would enable the study of, for example, the variation of the cross-section behaviour of different core levels as a function of photon energy.

### 1.8.2 Sample Analysis Chamber

Figure 1.18 is a drawing of the ES200B spectrometer equipped with monochromator showing the relative positions of the sample, X-ray sources and analyser.

The source chamber has several access ports for sample introduction and treatments. Sample entry is via fast-entry insertion locks allowing for rapid sample turn round and angular dependent studies. Purpose-built reaction chambers may be attached onto the source chamber via an insertion lock and this provides facilities for 'in situ' treatment of samples.

Typical operating pressures for the ES200B are  $< 10^{-7}$  torr for samples of low volatility and a pressure in the  $10^{-9}$  torr range is obtainable

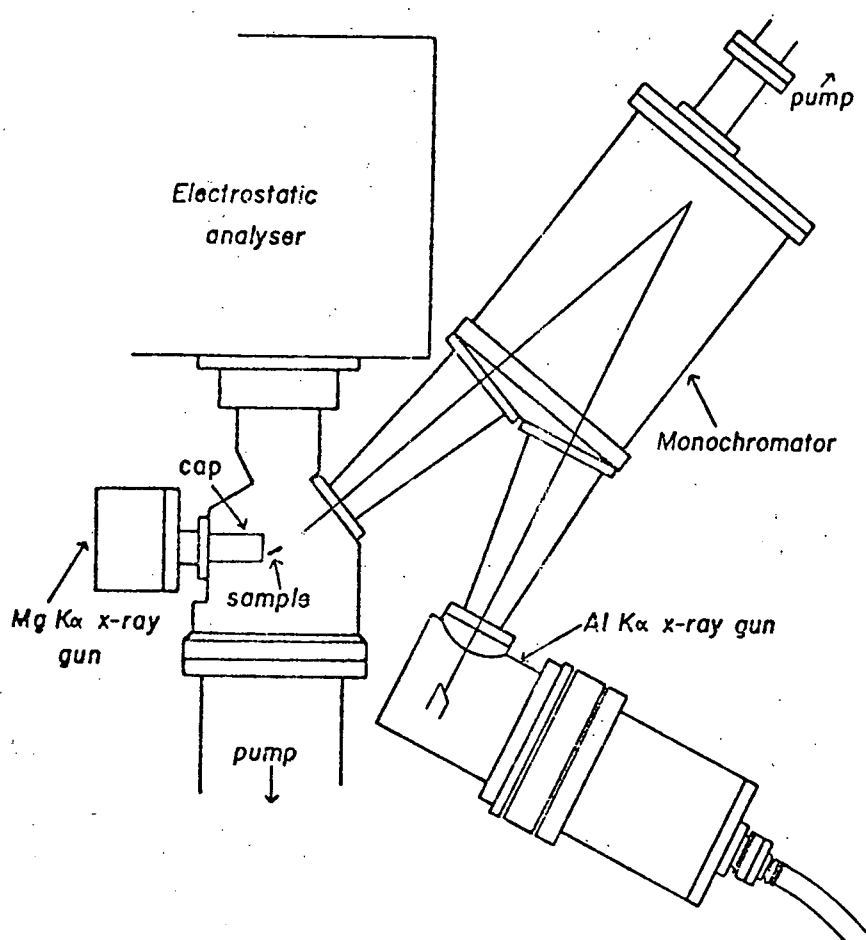


Figure 1.18 General layout of the A.E.I. ES200B spectrometer

after baking. These pressures are achieved using cold-trapped diffusion pumps backed by rotary pumps.

The ES300, which has a specially designed preparation chamber attached permanently to the sample analysis chamber to cater for the needs of the polymer research interests of the laboratory, has separately pumped

analyser and source regions. Pumping for the source region of the spectrometer is by means of an Alcatel 450  $\text{ls}^{-1}$  air-bearing, air-turbine turbomolecular pump, whilst the analyser is pumped by a 120  $\text{ls}^{-1}$  pump of the same design. The base pressure for normal operating conditions is  $\sim 8 \times 10^{-9}$  torr.

### 1.8.3 Electron Energy Analyser

The ES200B has a hemispherical double focussing analyser based on the principle described by Purcell<sup>100</sup> which is screened from external magnetic interference by means of mu-metal shields.

The resolution of the analyser,  $\Delta E/E$ , where  $E$  is the energy of the electrons, should be  $\sim 1$  in  $10^4$  for ESCA studies and is related to the mean radius of the hemispheres ( $R$ ), and the combined width of the source and collector slits ( $W$ ) by the equation 1.14 :

$$\Delta E/E = \frac{R}{W} \quad (1.14)$$

The resolution may be improved by:

- (1) Reducing the slit width, which reduces the signal intensity,
- (2) Increasing the radius of the hemisphere, thereby increasing engineering costs and pumping requirements,
- (3) Retarding the electrons before entry into the analyser.

In practice a compromise is made on the slit widths to obtain sufficient signal intensity and on the size of the hemisphere so as to prevent mechanical distortion and keep costs down. The ES200B uses a retarding lens to slow the electrons down before entry into the analyser and cuts down on the resolution requirements of the analyser.<sup>101</sup>

This lens assembly also serves to remove the sample region from the analyser and hence more flexible sample handling can be employed.

Focussing of the electrons at the detector slit may take place by either of two methods:

- (1) Scanning the retarding potential applied to the lens and keeping a constant potential between the hemispheres, or
- (2) Scanning the retarding potential and the potential between the analyser hemisphere simultaneously maintaining a constant ratio between the two.

The first method of fixed analyser transmission (FAT) has greater sensitivity at low kinetic energies (<500 eV) and the second, fixed retardation ratio (FRR) has greater sensitivity at higher electron kinetic energies. The FRR mode is employed in this work.

#### 1.8.4 Electron detection and data acquisition

Electrons of pre-selected energy pass from the analyser into an electron multiplier via the collector slit. The output from the multiplier undergoes amplification and is fed into a data handling system. ESCA spectra may then be generated in two ways:

- (1) The continuous scan, where the electrostatic field is increased from the starting kinetic energy continuously, a ratemeter monitoring the signal from the amplifier. In this way a graph of electron count rate versus the kinetic energy of the electrons may be recorded on an X-Y plotter.
- (2) The step scan, where the field is increased by preset increments (typically 0.1 eV) and at each increment (a) counts may be measured for a fixed length of time or (b) a fixed number of counts may be timed. The data so obtained is stored in a

multichannel analyser. Many scans can be accumulated to average random fluctuations in background thereby enhancing signal to noise ratios.

It should be borne in mind that where data acquisition is a lengthy procedure (greater than say 1 hour) sample changes, such as hydrocarbon build-up or sample charging effects, may lead to erroneous spectra.

## 1.9 Sample Handling

### 1.9.1 Solid Samples

Solids may be mounted onto the spectrometer probe tip using double-sided adhesive insulating tape. Here sample charging effects will occur and a more satisfactory technique involves depositing a thin layer of the sample onto a gold substrate as a film by evaporation from a suitable solvent, or sublimation, for example. Small strips and wires may be held in a chuck and powdered samples may be mounted by pressing into a metal gauze or piece of soft metal foil such as lead or indium.

A typical probe has facilities for temperature dependence studies, heating being achieved by means of conduction from a thermostatically controlled resistance heater. Cooling is carried out by pumping liquid nitrogen through the probe, thus enabling solids which are slightly volatile to be studied. More volatile solids are usually sublimed from a capillary tube, which may be heated, onto a cooled probe tip.

### 1.9.2 Liquids

Although the technique of ESCA may be applied to the analysis of solids, liquids and gases, the development of liquid studies is still in its infancy. <sup>118</sup> The only technique that is at present viable on

commercially available instruments involves the injection of the liquid into a heatable ( $25^{\circ}\text{C}$  to  $150^{\circ}\text{C}$ ) evacuated reservoir shaft followed by diffusion of the vapour through a metrosil leak and subsequent condensation onto a cooled gold plate on the tip of the sample probe. The sample surface is continually renewed and contamination and radiation damage effects are thereby reduced.

Two techniques for studying liquids and solutions have been developed by Siegbahn where samples are studied as submillimeter beams<sup>102</sup> or as a film on a wire passing through the X-ray beam parallel to the analyser entrance slit.<sup>89</sup>

### 1.9.3 Gases

Gases may be studied either in condensed phase using a cooled probe or in the gaseous phase for which purpose gas cells have been developed. Studies using molecules in the gas phase have the following advantages:<sup>19</sup>

- (1) No inherent broadening of the levels due to solid state effects.
- (2) Problems of sample charging are removed.
- (3) Increased signal to background ratio.
- (4) Radiation damage, if it occurs, is of no importance unless the sample is recirculated.
- (5) By mixing with standard gases, peaks may be readily calibrated.
- (6) Inelastic losses and shake-up or shake-off processes may be distinguished by varying the sample pressure.
- (7) Direct comparison with theoretical calculations is simplified.

## 1.10 General Aspects of ESCA

ESCA is an extremely powerful tool with wide-ranging applicability.

The principal advantages of the technique may be summarised as follows:

- (1) The sample may be solid, liquid or gas and sample sizes are small e.g. in favourable case 1mg solid,  $0.1\mu\text{l}$  liquid and  $0.5\text{cm}^3$  of a gas at STP.
- (2) The high sensitivity of the technique is such that a fraction of a monolayer coverage may be detected.
- (3) The process is virtually non-destructive, since the X-ray flux is small ( $0.1\text{ millirad sec}^{-1}$ ). This is especially advantageous over Auger spectroscopy where the electron beam produces many surface changes, particularly in polymeric systems where cross-linking and degradation can occur.
- (4) The technique is independent of the spin properties of the nucleus and can be used to study any element of the periodic table with the exception of hydrogen and helium. These are the only elements for which the core levels are also the valence levels.
- (5) Materials may be studied 'in situ' in their working environments with a minimum of preparation.
- (6) The technique provides a large number of information levels from a single experiment and these are listed in Table 1.6.
- (7) ESCA has a higher sensitivity than many other analytical techniques, as shown in Table 1.7.
- (8) The data is often complementary to that obtained by other techniques and has unique capabilities centred to the development of a number of important fields.

- (9) For solids, ESCA has the capability of differentiating the surface from subsurface and bulk phenomena, allowing analytical depth profiling.
- (10) The information relates directly to bonding and molecular structure and applies to both inner and valence orbitals of the molecule. This enables a thorough analysis of electronic structure of the system to be made.
- (11) The information levels are such that 'ab initio' investigations are possible and the theoretical basis is well understood, resulting in considerable interest to theoreticians.

The following aspects should also receive consideration:

- (1) The overall costs are quite high, being comparable to Fourier Transform I.R., laser Raman and conventional Mass Spectrometers, and considerably more expensive than standard I.R. equipment.
- (2) The vacuum system associated with ESCA instrumentation means that routine sample handling requires provision of vacuum interlocks and also implies that it is not possible to switch the spectrometer on to routinely investigate a sample.
- (3) Although ESCA has the capability of studying solids, liquids and gases, it is only for solids and gases that the requisite instrumentation is routinely available.

Whilst the technique has excellent depth resolution (in the range of  $\sim 100 \text{ \AA}$ ), the spatial resolution is poor and an area of  $0.3 \text{ cm}^2$  is normally sampled.

- (5) If the surface differs from the bulk, then it is not possible to say anything about the bulk structure by means of ESCA without sectioning the sample.

- (6) With conventional unmonochromatised X-ray sources and slitted designs, two features are of importance in studying thick samples, namely sample charging and the polychromatic nature of the X-ray source. The former, arising from a distribution of positive charge over the sample surface under the conditions of X-ray bombardment can be a severe problem for thick insulating samples and needs careful consideration. The latter leads to a relatively poor signal to background ratio; however this has been alleviated considerably by the development of efficient monochromatisation schemes and multiple collector assemblies.
- (7) To take full advantage of the technique often requires a relatively high level of theoretical competence. However, it must be emphasised that the technique has capability for exploitation at many levels, for example from routine trouble shooting problems where only a straightforward comparison is required, to investigations of a phenomena at a fundamental level.

It is the composite nature of the large range of available information levels which endows ESCA with such wide ranging capabilities and this hierarchy of information levels is set out in Table 1.6.

Table 1.6 The Hierarchy of Information Levels available in ESCA

- (1) Absolute binding energies, relative peak intensities, shifts in binding energies. Elemental mapping for solids, analytical depth profiling, identification of structural features, etc. Short-range effects directly, longer-range indirectly.
- (2) Shake-up - shake-off satellites. Monopole excited states; energy separation with respect to direct photoionisation peaks and relative intensities of components of 'singlet and triplet' origin. Short and longer range effects directly (Analogue of U.V.).
- (3) Multiplet effects. For paramagnetic systems, spin state, distribution of unpaired electrons (Analogue of e.s.r.).
- (4) Valence energy levels, longer range effects directly.
- (5) Angular dependent studies. For solids with fixed arrangement of analyser and X-ray source, varying take-off angle between sample and analyser provides means of differentiating surface from subsurface and bulk effects. For gases with variable angle between analyser and X-ray source, angular dependence of cross-sections, asymmetry parameter  $\beta^{103}$ , symmetries of levels.

A comparison of analytical techniques is shown in Table 1.7.

Table 1.7 Sensitivities of Various Analytical Techniques

<u>Bulk Techniques</u>	<u>Minimum Detectable Quantity (g)</u>
Infrared absorption	$10^{-6}$
Atomic absorption	$10^{-9}$ - $10^{-2}$
Vapour phase chromatography	$10^{-3}$ - $10^{-7}$
High pressure liquid chromatography	$10^{-6}$ - $10^{-9}$
Mass spectroscopy	$10^{-9}$ - $10^{-15}$

Surface Techniques

ESCA	$10^{-10}$
Neutron activation analysis	$10^{-12}$
Ion scattering spectrometry	$10^{-15}$
X-ray fluorescence	$10^{-7}$
Auger emission spectroscopy	$10^{-14}$
Secondary ion mass spectrometry	$10^{-13}$

1.11 Quantitative Analysis

Having presented an outline of the nature of the processes involved in the ESCA experiment together with instrumentation details with particular reference to the qualitative viewpoint, for a thorough appreciation of the data which is to follow in subsequent chapters of this thesis, it is necessary to highlight certain aspects of the procedures used in deriving elemental analytical information at the quantitative level.

As mentioned previously, the first information level available from the ESCA experiment includes the relative intensities of the photo-ionisation peaks within a spectrum. These may be used in conjunction with

a knowledge of certain other factors, which will be expanded upon in the following discussion, to yield a quantitative analysis.

In order that ESCA, essentially a surface sensitive technique, may be applied successfully to problems of quantitative elemental analysis, it is of prime importance that the outermost monolayers of the sample under investigation be representative of the bulk composition of the material as a whole. Knowledge of the degree of homogeneity of the material sampled is therefore important.

A common situation of vertical inhomogeneity is caused by the presence of a layer of surface contamination. The depth of material sampled ( $\sim 3\lambda$ , where  $\lambda$  is the inelastic mean free path of the photoelectron) depends on the core level studied since  $\lambda$  is a function of the kinetic energy. A contamination layer therefore leads to errors in quantitative analysis especially when peaks of widely different kinetic energy are used.

For homogeneous samples, elemental analysis is as follows. The area of the most intense core level peak of each element, together with associated structure (shake-up for example) where this can be assigned, is measured. These figures are divided by the appropriate sensitivity factors, derived using compounds of known stoichiometry to yield atomic ratios.

Tables of relative elemental sensitivities have been formulated from experimental work using model compounds by a number of research workers,<sup>108-110</sup> and are unaffected by chemical environment.<sup>116</sup> These results which are reported in the literature refer to instruments used in the FAT mode of electron detection and are not strictly applicable to raw data obtained from FRR type instrumentation. Theoretical calculations of photoionisation cross-sections have been performed<sup>81-2, 109, 111-2</sup> and the methods employed form the subject of a review by Huang and Rabalis.<sup>113</sup>

Discrepancies between results obtained using theoretical cross-sections and experimentally derived sensitivity factors stem from the assumption that X-ray photoionisation in solids should be essentially an atomic process. In some cases the processes accompanying core ionisation which detract from the main photoionisation peak may be difficult to assess experimentally.

Crystallinity effects have been found to be important when dealing with materials containing inorganic solids. (This is an aspect of considerable significance in relation to the findings presented in Chapters Two and Three of this thesis pertaining to a selection of geochemically important materials.) The solid state matrix phenomenon was first noted by Wagner<sup>108</sup> in his study of a variety of sodium and fluorine containing compounds. Swingle,<sup>111</sup> Wyatt and co-workers,<sup>114</sup> and Ng and Hercules<sup>115</sup> have studied the effect on relative peak intensities of matrix effects, especially for ionic compounds. Nearest neighbour inelastic scattering effects in certain systems appear to play an important role, causing a variation of escape probability with change in chemical composition.<sup>115</sup>

Evans, Adams and Thomas, in their studies aimed at the development of ESCA as a quantitative surface analytical technique, have reported a means of probing the surface structure and composition of layered silicate minerals using X-ray photoelectron diffraction, together with energy-dispersive X-ray (K-emission) analyses and X-ray diffraction and extensive chemical analyses.<sup>128</sup> X-ray photoelectron diffraction patterns were obtained from monocrystalline mineral flakes cleaved 'in situ'; a set of spectra being produced at 5° increments of take-off angle. The diffraction of the outgoing photoelectrons by the atoms surrounding the emitting site allows differentiation between equivalent, near-equivalent, and non-equivalent sites occupied by two or more elements either in one single crystal or in crystals of closely similar

structure. This is found to apply even when the element(s) concerned comprise only a small fraction of the crystal and when the sub-lattice lacks both long and short range order.

Despite these factors, reproducible, quantitative, instrument-independent ESCA analyses to within 10% are possible provided that the necessary calibration procedures for voltage scales and intensity response are followed. 117

CHAPTER TWO

AN EVALUATION OF THE POTENTIAL OF ESCA IN THE CHARACTERISATION  
OF COAL, KEROGEN AND BITUMEN

## CHAPTER TWO

### AN EVALUATION OF THE POTENTIAL OF ESCA IN THE CHARACTERISATION OF COAL, KEROGEN AND BITUMEN

#### 2.1 Introduction

In the previous chapter a survey of the essential features of ESCA was presented. To date ESCA has found application in numerous far-reaching areas, its inherent surface-sensitivity serving as the prime impetus behind its utilisation.

The work which forms the subject of this chapter concerns the ESCA analysis of a series of materials of interest to the organic geochemist. The elemental analysis data from the ESCA experiment are compared with data obtained by conventional microanalytical techniques. In addition, structural information derived from the ESCA analyses is presented.

#### 2.2 The application of ESCA to geochemistry

Surprisingly little work has been published relating to ESCA applied to geochemical problems. Two recent reviews focussing on the fields of mineralogy<sup>189</sup> and coal science<sup>190</sup> give an overall account of previous studies. Detailed investigations into the surface structure and composition of silicate minerals<sup>128, 191</sup> and their cation exchange reactions<sup>192</sup> have been made by Evans and coworkers.

Three aspects of coal science and analysis have been the subjects of ESCA investigations and each will be presented in the following discussion.

The problems associated with the routine estimation of oxygen in coal will be treated in more detail in Section 2.3.3a of this chapter. Coal scientists and technologists would welcome the development of rapid

direct methods for the analyses for oxygen and organic sulphur. To this end a series of coal and mineral samples have been analysed using ESCA and the data compared with microanalysis results.<sup>193</sup> Although the ESCA carbon and total sulphur determinations were found to be in reasonable agreement with the associated ultimate chemical analyses, correlation in the case of oxygen was poor.

Two salient features of this work should be noted. Firstly, no allowance was made for the presence of oxygen bound in other components such as minerals: a photoelectron signal characteristic of silicon was reported for some specimens. Secondly, the relative intensities of the core electron envelopes were monitored as a function of peak height rather than overall area (Section 1.7).

Coal often contains significant quantities of sulphur which is recognised as existing in three forms:<sup>94</sup> inorganic sulphates, iron pyrites ( $\text{FeS}_2$ ), and organic sulphur compounds. Quantitative analysis of the organic sulphur component is calculated by subtracting the sum of the sulphate and pyritic sulphur from the total sulphur. The 'by difference' method is particularly susceptible to systematic errors and direct techniques are far more attractive.

The extent of research into the analysis of the sulphur constituents of coal reflects not only the academic interest in the subject, but also the technological importance of the sulphur moieties both with respect to the process of combustion itself and to environmental pollution control.<sup>195</sup> Coal cleaning methods are normally capable of removing completely only pyrite; some organically bonded sulphur is found to remain after treatment.<sup>197</sup> The similar surface chemical characteristics of coal and its associated pyrite complicates their separation by cleaning methods which utilise surface property differences, such as flotation or selective

agglomeration. Oxidation of the iron pyrite in coal, prior to cleaning, is known to change the surface characteristics of the pyrite and so improve the efficiency of the separation processes.<sup>195</sup> The ability of ESCA to monitor changes in surface chemistry, together with the wide range of chemical shifts associated with the  $S_{2p}$  photoionisation level,<sup>197-199</sup> acted as the driving force behind ESCA studies of sulphur in coal. The results of the individual studies, which are well documented elsewhere,<sup>190</sup> illustrate the potential of ESCA in the realms of coal oxidation phenomena.<sup>190, 195</sup> However, attempts to measure the proportion of organic sulphur directly from the  $S_{2p}$  core level envelope has proved less rewarding than was first anticipated owing to the overlap of the bulk of the organic sulphur signal with the pyrite peak.<sup>193,200</sup> For meaningful comparison of peak positions on the binding energy scale from spectrum to spectrum, the need for energy referencing to allow for sample charging effects (especially manifest in spectra of insulating samples, see Section 1.5) cannot be over-emphasized.

Other ESCA studies have focussed on coal carbonisation,<sup>200</sup> analysis of coal ash<sup>201</sup> and airborne particulates.<sup>190</sup> Very little work has been performed concerning elements other than sulphur in coal.<sup>190, 200</sup>

### 2.3 An Introduction to organic geochemistry

Before presenting a detailed account of the experimental procedures and findings used in this chapter, it is useful to indicate the relationship existing between the material-types under consideration here, namely coal, kerogen and bitumen from the organic geochemist's viewpoint.

Organic geochemistry, at the molecular level, was pioneered by Treibs. In 1934, he isolated and partially identified metalloporphyrins from a variety of crude oils and shales, and initiated studies which encompassed research into the fate and distribution of carbon compounds

in contemporary environments and in Recent and ancient sediments. <sup>202</sup>

The rapid development of this field reflects, for example, its growing appreciation by scientists and technologists, concerned with exploration and exploitation of new potential sources of fossil fuels. Such a wealth of documentation has evolved around the formation and occurrence of these organic materials that it would be foolhardy to attempt to furnish a thorough analysis of the literature: instead, the interested reader is referred elsewhere. <sup>205-7, 255-6</sup>

As in any interdisciplinary subject, a common system of nomenclature and classification is essential in the development of unambiguous communication and hence the furtherance of knowledge. This in itself is not an easy task as is witnessed by Breger <sup>203</sup> and Durand <sup>204</sup> and reflects the complexity of the sedimentary organic matter. This also indicates the diversity of the interpretations of the transformation processes in sediments, especially as concerns petroleum formation.

### 2.3.1 Sedimentary organic matter

The evolution of sedimentary organic matter is a very complex procedure during which living material undergoes decomposition and the fraction preserved, along with various other organic materials which are introduced, is incorporated in sediment over geological time. The organic matter can be derived from organisms living in the sedimentation basin. <sup>204</sup> The nature of the resulting material will depend on the type of precursor (plant or animal), the environment (marine or terrestrial) of the source bed and the biological and geological processes (bacterial action, burial, compaction and geothermal heating) to which the sediment has been subjected.

It should come as no surprise from consideration of the previous discussion that, owing to the very nature of these organic substances, precise definitions which are universally accepted for coal, kerogen and bitumen are hard to come by. Hunt <sup>205</sup> describes *coal* as 'A readily combustible rock containing more than 50 percent by weight, and more than 70 percent by volume, of organic material formed from the compaction or induration of variously altered plant remains.' In this thesis, the word *kerogen* will be used in reference to the solvent unextractable portion of organic matter in sediments, as opposed to the soluble fraction called *bitumen*. <sup>204</sup>

Both coal and kerogen, the main precursor material to petroleum, originate predominantly from organisms of the plant kingdom. They are both subjected to the same geological processes during their formation. There are however some important differences. <sup>206</sup> Coal is found at its site of deposition (the same is true for kerogen) as a solid and relatively pure massive organic substance: kerogen is finely dispersed and intimately mixed with the mineral matrix in petroleum source beds. Most coals are remnants of terrestrial higher plants, whereas the kerogen of petroleum source beds is generally dominated by aquatic lower plants and bacteria. Most acknowledged petroleum source beds were deposited in marine environments and most coals formed under non-marine conditions.

### 2.3.2 The formation and classification of coal

The development of the practically unaltered plant material from peat <sup>209</sup> through the stages of the different brown coals (lignite), sub-bituminous and bituminous coals to anthracite and meta-anthracites is known variously as coalification, metamorphism or carbonification. <sup>207</sup> A measure of the extent to which the organic material has matured is given by its *rank*. The change in rank of a coal is determined by depth of

burial, pressure and temperature; these are interrelated through geothermal gradients.<sup>208</sup> Classification of coals according to their rank can be achieved by consideration of optical, chemical or physical properties. The American Society for Testing and Materials has issued a standard specification relevant to this topic (ASTM D388) and is described by Francis and Peters.<sup>210</sup> Chemical changes which occur during coalification include condensation, polymerisation, aromatisation, and loss of oxygen-, nitrogen- and sulphur-containing functional groups linked to the molecular structure of coal.

Although chemical identification of functional groups and general information on the carbon skeleton are established, the structural examples given in the literature<sup>206</sup> represent the general framework of the coal structure. Coal is not a homogeneous substance but consists of various constituents. These components are revealed under the microscope and may be differentiated by their morphology. Macerals, as they were termed by Stopes,<sup>211</sup> are analogous to the minerals of inorganic rocks but differ in having less uniform chemical composition and physical properties. All macerals have the suffix 'inite', and are classified in three groups:

- 1) Vitrinite, originating from wood or bark and is the most abundant maceral group;
- 2) Exinite (or lipinite), formed from the remains of spores, resins, algae and cuticles;
- 3) Inertinite, named for its relatively inert behaviour on coking, and comes from the same type of plant components as vitrinite, although this material was strongly affected by oxygen during the early stages of coalification.

Since macerals are derived from different types of materials and were sometimes subjected to different conditions before burial, they were affected to different degrees by the conditions that form coal. As rank increases, differences in the properties of macerals tend to become minimized, particularly in the anthracite range.

The essential differences between the maceral groups are perhaps best displayed on the van Krevelen diagram<sup>254</sup> (Figure 2.1). This diagram

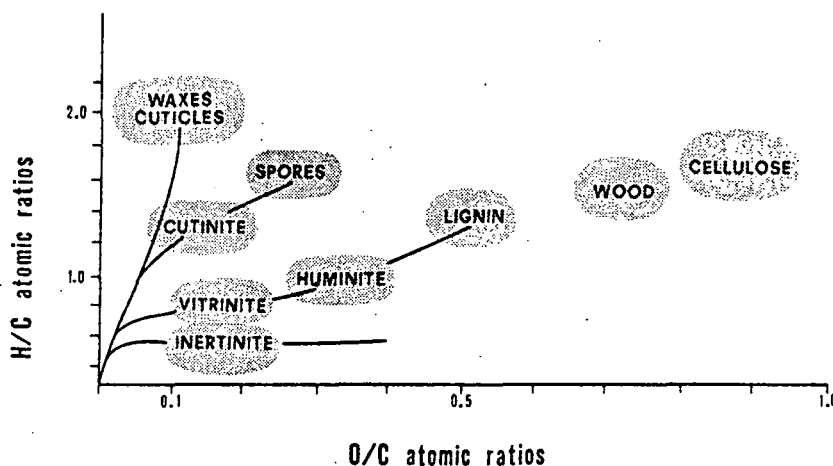


Figure 2.1 Selected plant and coal materials and their respective position in the van Krevelen diagram.<sup>206</sup>

Incorporates information on the three most abundant elements in coal (carbon, hydrogen and oxygen) and shows the coalification trends of the various plant components.<sup>206</sup> The chemical evolution pathways of kerogen may be unfolded by such representation (Section 2.3.3b).

A further distinction is made between coal types according to their origin and mode of formation. Humic coals form from plant cell and wall material deposited at the site where the plants grew under oxidising (or aerobic) conditions and their evolution proceeds via the stages of peat formation through to anthracite. They contain 'woody' tissue and in lower rank coals. This material is represented by the 'huminite' maceral type; in bituminous and anthracite coals by the vitrinite group of macerals.

The other coal type, the sapropelic coals, are relatively rare and are not stratified in contrast to humic coal. Sapropelic coals form from spores, pollen and algae deposited in relatively fine-grained organic muds in quiet shallow water environments, such as ponds, lakes and lagoons, under oxygen-deficient, reducing (or anaerobic) conditions. Both transported (or allochthonous) organic and mineral matter and local (or autochthonous) organic matter constitute the 'Ingredients' of sapropelic coals, of which there are essentially two basic types as recognised under a microscope. Boghead coals, also called torbanites, contain larger amounts of algal remains whereas cannel coals are characterised by higher concentrations of spores.

### 2.3.3 The nature of kerogen

Kerogen, the solvent unextractable portion of organic matter in sediments, is by far the most abundant form of organic carbon on Earth.<sup>231</sup> Depending on its origin, and its stage of maturation, kerogen can make up to 90 - 95% of the organic matter of a sediment.<sup>232</sup> Kerogen, by virtue of its insolubility, is of particular interest to the organic geochemist. Being insoluble, kerogen is obviously less prone to migration and less sensitive to contamination than extractable materials. Therefore, kerogen is the most reliable form of indigenous organic matter in sediments.<sup>233</sup>

Much effort has been devoted to the characterisation and structural elucidation of kerogen with the aim of aiding a better understanding of:

- 1) The source of the precursor organic material.
- 2) The environmental conditions of deposition.
- 3) The type of evolution and maturation processes.
- 4) The gas and oil potential of kerogen and the source rock potential of the sediment.

The book edited by Durand<sup>234</sup> reviews thoroughly the advances which have been made over recent years in the study of kerogen.

Since kerogen is insoluble and generally occurs finely disseminated in fine grained sedimentary rocks, isolation free from the inorganic material is a difficult process.<sup>†</sup> Similarly, attempts to determine the precise nature of the substance have proved impossible, owing to its insolubility. A variety of different techniques have been applied to the study of kerogen.

The classification of kerogens according to the degree of thermal maturation and kerogen type, has been made by:<sup>205</sup>

---

†

Both physical processes involving flotation, ultrasonic, electromagnetic and electrostatic methods, and chemical techniques, whereby the kerogen is isolated by making the mineral phase soluble while keeping modifications in the chemical composition of the organic material as small as possible, have been employed. The latter approach commonly involves the use of hydrochloric acid and hydrofluoric acid: some changes in the chemical nature of the kerogen are known to occur. 235-6, 238

- 1) palynologists, from the microscopic examination of mineral-free organic residues in transmitted light;
- 2) coal petrographers, from the microscopic examination of polished rock surfaces in reflected light;
- 3) petroleum geochemists, from the changes in the elemental composition of kerogen with maturation.

All these methods give little detailed structural data. It is the latter approach, involving classification according to the chemical composition of the kerogen as determined by microanalytical techniques, which is the most directly relevant in connection with the work to be presented here.

### 2.3.3a Elemental Analysis

The elemental analysis of kerogens, which forms the subject of a recent review by Durand and Monin,<sup>228</sup> has shown itself to be a simple method capable of establishing a classification of kerogens according to their ability to generate oil and gas in depth. There are however certain points which have to be borne in mind: †

---

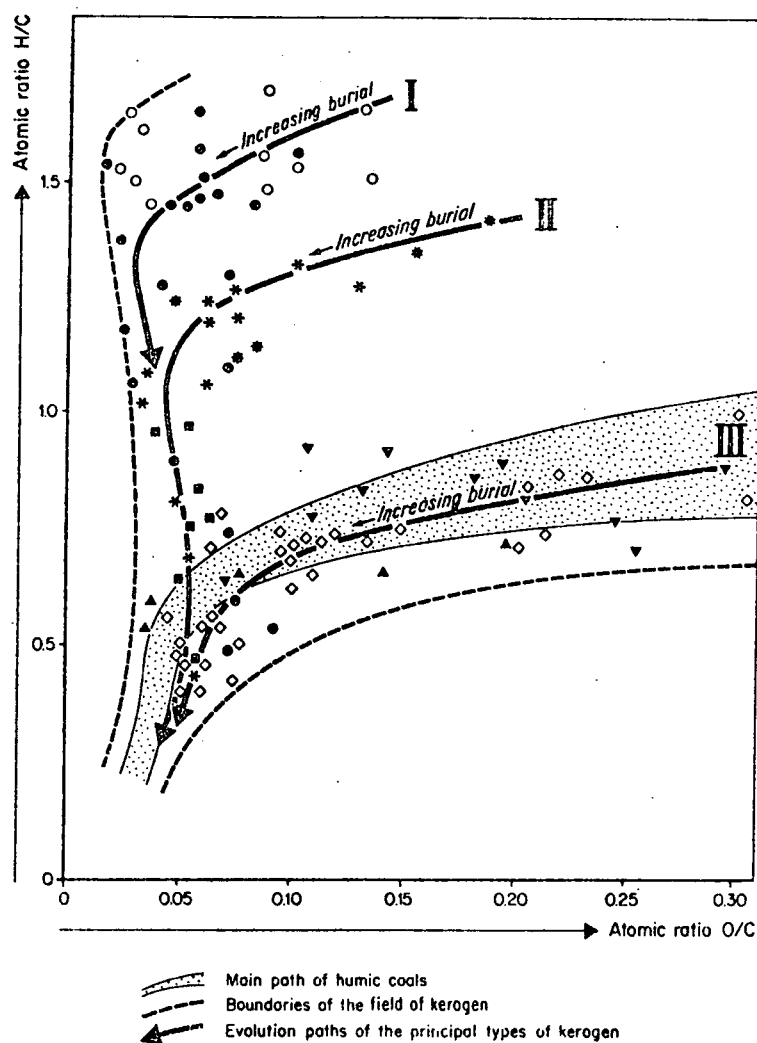
† These problems are akin to those faced by coal technologists. Analysis of coal and coke is divided into two areas, namely proximate and ultimate or chemical analyses. 194, 208  
Proximate analysis includes the determination by prescribed methods of moisture, volatile matter, fixed carbon and ash. The utility of such analyses depends upon the basis on which they are reported. Four common bases are used: as-received, dry, dry ash free (daf), and dry mineral matter free (dmmf).

- 1) Kerogens may contain water.
- 2) They are heterogeneous.
- 3) Their transformation into gaseous products through combustion or pyrolysis may be incomplete.
- 4) They contain residual minerals, mainly pyrite.

The precise determination of oxygen content in kerogens is difficult.<sup>228</sup> In particular, oxygen determinations, as calculated by difference, after measurement of carbon, hydrogen, nitrogen and sulphur, have proved unreliable, especially for kerogens with high ash contents. Improvements in microanalytical methods, derived from the Unterzaucher's method<sup>237</sup> whereby the oxygen component is converted to carbon monoxide for analysis, have been developed and it is hoped that one of the major problems has been overcome. However, authors continue to give oxygen contents by difference despite the inadequate meaning of this calculation. Discrepancies in microanalytical data between laboratories, especially in the case of oxygen measurements, may be significant. Reproducibility of results, even from the same laboratory, can be poor. These factors, coupled with the inherent nature of the materials, allude to the fact that it is difficult to use the values found in the literature for comparative purposes.

### 2.3.3b Kerogen classification

Representation of microanalytical data of the major elemental constituents of kerogen (carbon, hydrogen and oxygen) on a van Krevelen diagram (Figure 2.2) provides the most suitable form by which elemental analysis results may be processed.<sup>228</sup> When the elemental composition of a kerogen is plotted on such a diagram, it is found to fall into one of three distinct bands,<sup>205-6</sup> as was the case for the various types of



Type	Age and /or formation	Basin, country	
I	Green River shales (Paleocene - Eocene)	Uinta, Utah, U.S.A.	●
	Algal kerogens (Botryococcus, etc...), Various oil shales		○
II	Lower Toarcian shales	Paris, France, W. Germany	*
	Silurian shales	Sahara, Algeria and Libya	■
	Various oil shales		*
III	Upper Cretaceous	Douala, Cameroon	◇
	Lower Mannville shales	Alberta, Canada	▲
	Lower Mannville shales	Alberta, Canada	▼

Figure 2.2 Principal types and evolution paths of kerogen <sup>206</sup>

coals or coal macerals. Kerogens taken at various depths from the same formation normally group along the same evolution path. <sup>252</sup> Those kerogens of closely related environments of deposition will also fall along the same evolution path. The different curves start with different H/C ratios according to the nature of the original organic material and conditions of deposition. The curves come close together for kerogen samples from deeply buried sites as the kerogen approaches 100% carbon.

The three main kerogen types which seem to account for most existing kerogens are mentioned in the following discussion. More detailed descriptions are to be found in the literature. 205-6, 228, 252

Type-I kerogen contains many aliphatic chains, with few aromatic nuclei. The H/C ratio is originally high, and the potential for oil and gas generation is also high. This type of kerogen is either mainly derived from algal lipids or from organic matter enriched in lipids by microbial activity.

Type-II kerogen contains more aromatic and naphthenic rings. The H/C ratio and the oil and gas potential are lower than observed for Type-I kerogen but still very important. Type-II kerogen is usually related to marine organic matter deposited in a reducing environment, with medium to high sulphur content.

Type-III kerogen contains mostly condensed polyaromatics and oxygenated functional groups, with minor aliphatic chains. The H/C ratio is low, and oil potential is only moderate, although this kerogen may still generate abundant gas at greater depths. The O/C ratio is comparatively higher than in the other two types of kerogen. The organic matter is mostly derived from terrestrial higher plants.

### 2.3.3c Structure determination

Two basic strategies have been adopted in the structural elucidation of kerogens. Chemical degradation has been used to obtain structural information on kerogens by cleaving the material into smaller fragments, usually for analysis by gas chromatography (GC) and for mass spectroscopy (MS). Typical procedures include oxidation, ozonolysis, reduction and other cleavage with boron tribromide. Vitorovic has produced an overview of the chemical methods which have been employed. 239

All these degradation methods have disadvantages. The degradation reactions are either specific, resulting in low overall yields, or non-specific, leaving uncertainty as to whether the products truly reflect the structure of the original kerogen.

The other approach concerns the spectrometric investigation of the entire kerogen. Studies have concentrated on pyrolysis-gas chromatography/mass spectrometry (Py-GC/MS),<sup>233, 243</sup> electron spin resonance<sup>242</sup> and nuclear magnetic resonance ( $^1\text{H}$  and  $^{13}\text{C}$  nmr).<sup>244-9</sup> Both electron and X-ray diffraction have been used to probe the kerogen lattice.<sup>206, 253</sup> Py-GC/MS has proved valuable for the characterisation of volatile components from kerogen. However, Van de Meent<sup>233</sup> et al have shown that the yield of such products is low (~ 10%). ESR provides information on the paramagnetic components of kerogen.

Both  $^1\text{H}$  and  $^{13}\text{C}$  nmr are of limited value owing to poor resolution of nuclei in similar chemical environments.<sup>244, 246</sup> However, it is possible to distinguish between aliphatic and aromatic components. The poor spectral resolution and sensitivity problems associated with solid state nmr studies are likely to be overcome with the development of an emerging technique, known as cross-polarization with magic-angle spinning.<sup>249</sup> Although this technique is still in the early stages of development, it already has been applied to coals and oil shales.<sup>248</sup> The major advantages are that measurements are made directly and non-destructively; virtually no sample preparation is required.

Infrared spectroscopy has been used in the study of a variety of coals, kerogens and humic substances.<sup>251</sup> The spectra so obtained show a limited number of rather broad bands; moreover all these carbonaceous solids essentially give the same bands. 'Fingerprint' analysis of the solid is therefore impossible; but, upon consideration of individual band intensities, infrared spectroscopy can provide a semi-quantitative

functional analysis of the complex solid, examined as a whole. Painter and Coleman<sup>251</sup> have described the use of Fourier transform infrared difference spectroscopy as a means for analysing the mineral matter in coal.

## 2.4 Experimental

### 2.4.1 Samples

The specimens which form the subject of this investigation include torbanite, Kimmeridge kerogen, vitrinite and brown coal, kindly donated by Dr A.G. Douglas, University of Newcastle-upon-Tyne, a natural bitumen in the form of a commercial sample of a gilsonite 'select' from the American Gilsonite Company and a series of gilsonites including a sample of weathered gilsonite, gratefully received from Dr J.M. Hunt, Woods Hole Oceanographic Institution, Woods Hole, Massachusetts, U.S.A. Discussion of individual materials will be presented in the results section of this chapter.

The samples were prepared for analysis by grinding a portion of the material to a fine powder using a pestle and mortar, thereby unveiling a fresh, previously unexposed surface for analysis. In this way any features characteristic of vertical inhomogeneities, caused by oxidation phenomena or migration of constituents to the surface, for example, would be minimised. The freshly powdered samples were examined in their as received form and were not subjected to any other treatment prior to analysis.

### 2.4.2 Instrumentation

#### 2.4.2a ESCA analysis

The freshly powdered sample was mounted on a spectrometer probe-tip by means of double-sided adhesive Scotch insulating tape. The sample

was pressed onto the tape with the aid of a metal spatula and the excess that had not adhered was tapped off. The ESCA experiment is such that monolayer coverage of the adhesive tape by the sample is all that is required in order to produce a spectrum representative of the sample under investigation. An excess can lead to contamination of the sample chamber of the spectrometer and its associated vacuum system.

Two types of adhesive tape have been used in this work; Scotch tape containing a silicon-based adhesive, and a silicon-free Scotch tape. Before embarking on the main part of this project, ESCA spectra of both varieties of tape have been run and are shown in Figure 2.3. Comparison

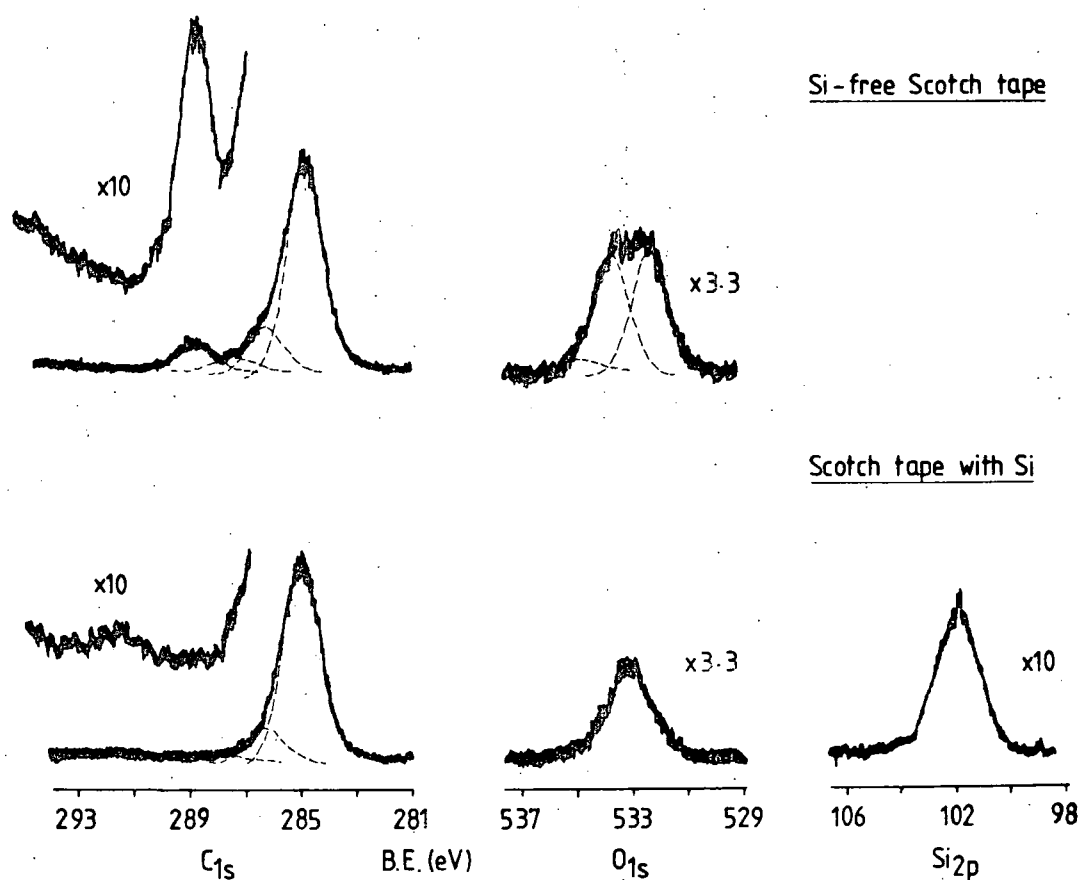


Figure 2.3 ESCA core level spectra of Scotch tape

of these spectra with those obtained from the powder samples, prepared as previously described, verify that in the latter spectra the Scotch tape is not detected by ESCA, and the photoionisation signal is characteristic of the sample alone.

Most of the ESCA spectra were recorded on an A.E.I. ES 200B spectrometer with an  $\text{MgK}\alpha_{1,2}$  X-ray source operated at 12kV and 15mA and with a base pressure of  $\sim 5 \times 10^{-8}$  torr. A custom-designed Kratos ES 300 spectrometer, equipped with a magnesium/titanium dual anode was also used: the chosen operating conditions were 13kV, 11mA for the magnesium anode, and 13.5kV, 18mA for the titanium anode. Under the experimental conditions employed for the magnesium anode, the gold  $4f_{7/2}$  level (at 84eV binding energy) used for calibration purposes, had an FWHM of  $\sim 1.2\text{eV}$ .

A complete ESCA analysis took in the region of 2-3 hours to complete; the core level spectra of the elements carbon, oxygen, nitrogen and sulphur were recorded in typically one hour, depending on the intensity of the respective photoionisation signals. Radiation damage to the sample from long-term exposure to the X-ray beam was not evident.

Deconvolution and area ratios were determined using a Dupont 310 analogue curve-resolver as described in Section 1.7. The resulting analyses and stoichiometric data thereby obtained were found to be spectrometer independent.

#### 2.4.2b Elemental Analysis

Elemental analysis for carbon, hydrogen and nitrogen was carried out, in Durham, using a Perkin Elmer CHN 240 elemental analyser. Analysis for sulphur was based on the modified oxygen flask combustion method described by Budesinsky.<sup>258</sup> Atomic absorption was employed to monitor the levels of nickel, vanadium and tin in the samples of gilsonite 'select',

before and after oxygen plasma treatment (Section 3.6). In each case the volatile components were removed in a flame before the sample was dissolved in dilute nitric acid ready for analysis.

#### 2.4.2c Infrared analysis

The infrared spectra were recorded on a Perkin Elmer 457 grating infrared spectrophotometer. The materials were prepared for analysis in the form of pressed KBr discs. Figure 2.4 shows the infrared spectra of the respective samples. The difficulties encountered when studying coals and kerogens by infrared spectroscopy have been noted in Section 2.3.3c. The character of the spectra presented here equates well with that of spectra found in the literature. 204,206,256-7

#### 2.4.2d Nuclear magnetic resonance analysis

Proton ( $^1\text{H}$ ) and  $^{13}\text{C}$  nuclear magnetic resonance (nmr) spectroscopy was employed to investigate the aromatic nature of gilsonite 'select' and weathered gilsonite.  $^1\text{H}$  and  $^{13}\text{C}$  nmr spectra were obtained using a JEOL FX-200 spectrometer in the Fourier transform mode, and chemical shifts referenced, in parts per million on the  $\sigma$  scale, from internal tetramethyl silane ( $\text{Me}_4\text{Si}$ ).  $^{13}\text{C}$  nmr spectra were obtained using the technique of gated decoupling, in order to obtain meaningful integrations. The gilsonite samples were dissolved in  $\text{CDCl}_3$  prior to analysis.

### 2.5 Results and Discussion

Each material is described in turn and the corresponding information derived from the ESCA experiment is presented.

Gilsonite, a naturally occurring bitumen found in the Uinta Basin, Utah, USA, has been the subject of extensive investigations into its chemical constitution, employing both ESCA and elemental analysis as the principal

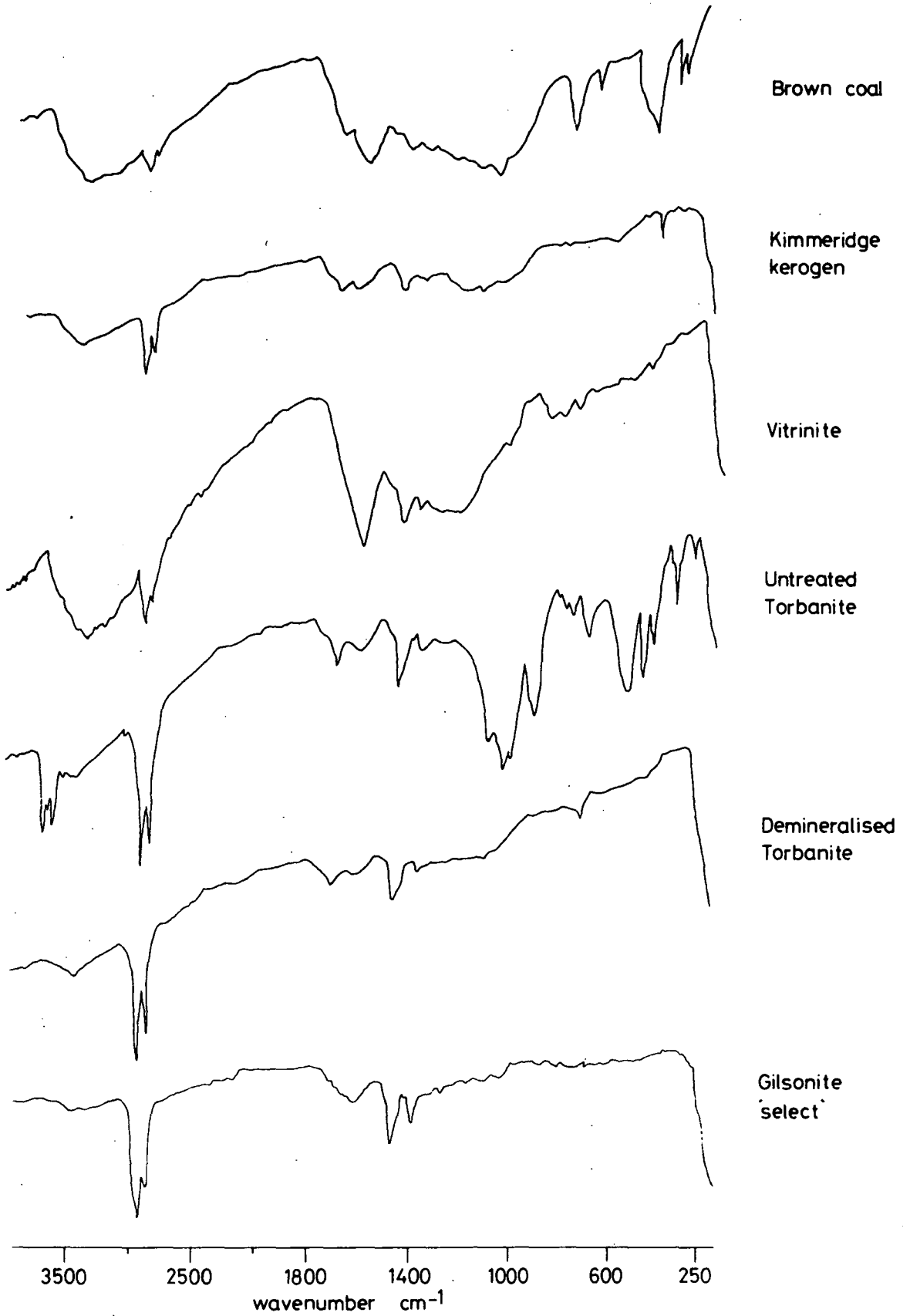


Figure 2.4 Infrared spectra of the geochemical samples

analytical probes. This material has a fascinating history and the application of a novel technique such as ESCA to the study of gilsonite has the potential of offering an interesting research project in its own right. The work on gilsonite reported here also provides a firm basis on which the scope of ESCA in the analysis of geochemical materials may be evaluated.

## 2.5.1 Gilsonite

### 2.5.1a Introduction

The Uinta Basin of northeastern Utah, USA, is noted for many deposits of native bitumens that occur in lacustrine and fluvial sedimentary rocks of early Tertiary age.<sup>218</sup> Although many natural hydrocarbons have been described in the Uinta Basin, there are only four distinctly different types.<sup>219</sup> These are ozocerite, albertite, gilsonite and wurtzilite. A system of classification of these natural bitumens and coals is presented by Hunt,<sup>205</sup> after the terminology of Abraham.<sup>220</sup> Under this regime, gilsonite is classified as an asphaltite, a solid, insoluble in carbon disulphide and fusible only with difficulty. Estimates of the amount of bitumens in the Uinta Basin vary from 25 to 50 million tons. Independent predictions,<sup>221</sup> by Abraham, and Hunt, indicating that this quantity represents only a small fraction (1%) of the total organic matter in the nearby rocks, in the light of the present energy-deficient economy, has encouraged further research.

Gilsonite manifests itself in the form of veins and crack-filling deposits, widely distributed over the 9000 square mile area of the Uinta Basin. The location of these veins is related to the structure and geological history associated with the Eocene sediments of the basin.<sup>219,222</sup> Vein formation is probably due to gilsonite entering the vein openings as a heavy immature liquid and then solidifying and hardening over geological time as the

formation was uplifted and exposed.<sup>205</sup> A noteworthy feature of the mode of occurrence of gilsonite lies in the fact that gilsonite is found in vertical and nearly parallel veins, ranging in depths of up to 1200 feet and in widths from a few inches up to 22 feet,<sup>223</sup> and several miles in length.

The physical and chemical characteristics are variable from one part of a vein to another and from vein to vein. The rock walls against some gilsonite veins may be impregnated with gilsonite for a distance up to about 2 feet from the vein, with no clear line of demarcation between impregnated and non-impregnated rock. The homogeneous gilsonite in the interior of a vein will have different chemical and physical characteristics from the material close to the walls. For commercial purposes therefore, gilsonite from the interior of the vein is classified as 'selects' and that from the margins as 'seconds'.<sup>218</sup>

Two of the largest deposits are the Cowboy Vein in the Bonanza Group, and the Rainbow Vein. These are estimated to contain a total of  $16 \times 10^6$  tons of asphalt.<sup>224</sup> An index map of the Uinta Basin, showing the relative positions of the principal bitumen deposits, is displayed in the paper by Cross and Wood:<sup>221</sup> whilst Figure 2.5 maps out the main sites of gilsonite veins.

Gilsonite 'veinlets' or 'roots' can be traced downward to their apparent source in the oil shales of the Parachute creek member of the Green River Formation.<sup>218</sup>

Possibly the earliest account relating to gilsonite in the literature is dated 1866; W.P. Blake in 1885 gave these hydrocarbon deposits the mineralogical name, 'Uintaite'. The term 'gilsonite' commemorates Samuel Gilson who pioneered the commercial use of the substance in the 1880s.<sup>218</sup> Today, the American Gilsonite Company processes in the region of 170,000 tons

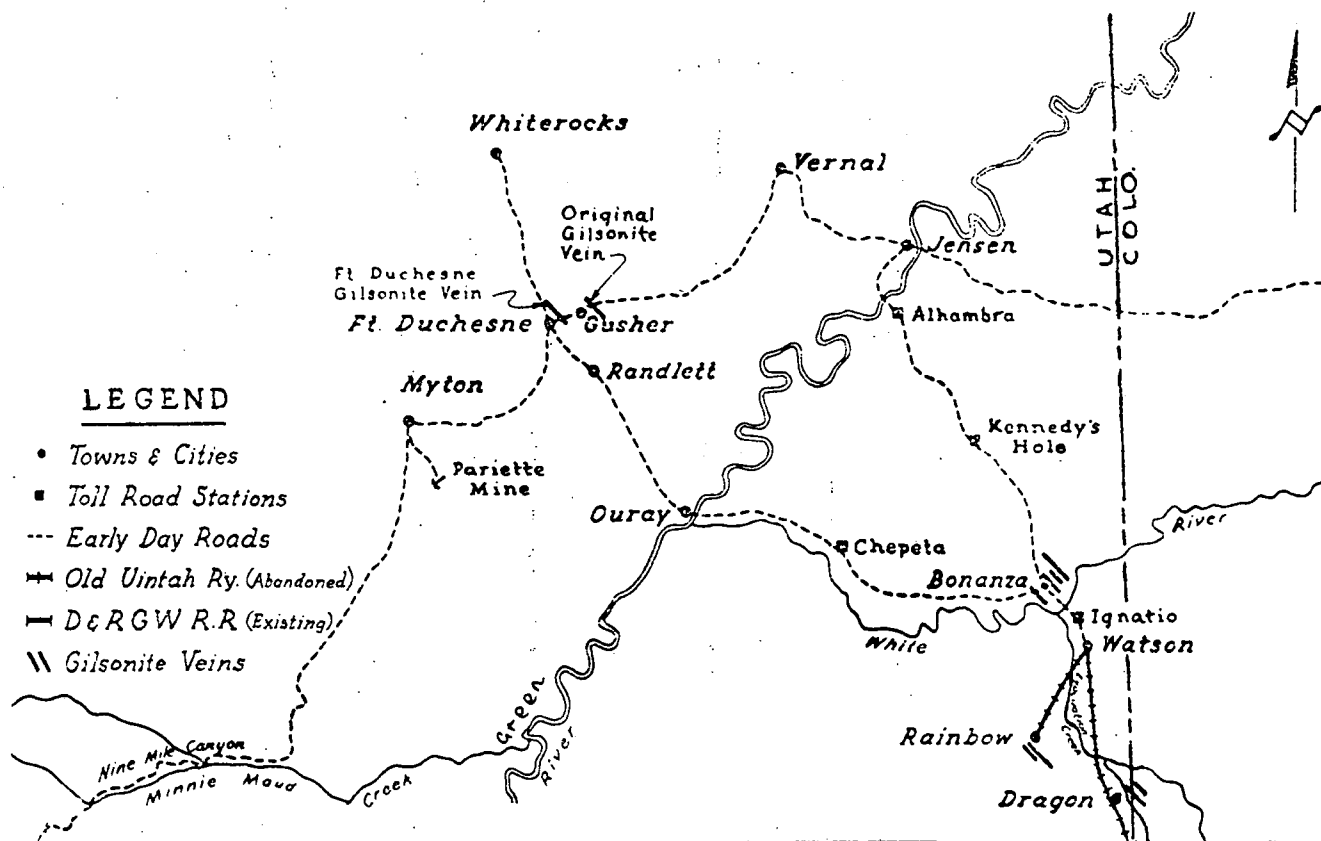


Figure 2.5 Location of principal gilsonite veins <sup>225</sup>

of product annually for use in the oil drilling, foundry, building board and explosives industries, in addition to the use by the car, ink, paint and varnish industries. A descriptive account of the development of gilsonite refining is given by Kretchman. <sup>225</sup>

In order that an appreciation of the factors governing the occurrence of the natural bitumens of the Uinta Basin may be realised, studies have been undertaken to reveal the chemical and physical composition and properties of the materials. The analytical techniques available at the time of the earlier work were mainly infrared analysis, liquid chromatography, refractive index, and elemental analysis. More recently, gas chromatography coupled with mass spectroscopy have been applied, yielding fingerprint traces

of the hydrocarbon constituents <sup>226</sup> and analysis for constituent carboxylic acids. <sup>227</sup> A summary of the physical, chemical and geological characteristics of gilsonite is given by Cross and Wood. <sup>221</sup>

The low atomic H/C ratio of 1.42 establishes the aromatic character of gilsonite and this is borne out by, for example, mass spectrometry and infrared analysis of the fraction soluble in carbon disulphide. Gilsonite is described <sup>218</sup> as being predominantly aromatic, containing condensed ring aromatic structures in the high molecular weight asphaltene<sup>†</sup> fraction and simpler dinaphthyl structures in the oil constituents and resins. \* Microscope photometry and X-ray diffractometry have been used to study the arrangement of the aromatic layer structures in gilsonite and the changes which occur on carbonisation. <sup>259</sup> Douglas and Grantham <sup>226</sup> have reported values for the percentage of saturated hydrocarbons in gilsonite which fall in the range 0.86 - 2.2% based on column chromatographic work. Elemental analysis shows gilsonite to contain oxygen and to have the highest nitrogen content of the Uinta Basin bitumens: the sulphur level is low.

Analysis for trace metals in the natural bitumens of the Uinta Basin has been performed on the residue after dry ashing of the materials. <sup>218</sup> The ash, which accounts for 0.1% of the original gilsonite, was found to be relatively high in nickel, with traces of other metals. Nickel is known to be present in gilsonite in the form of metalloporphyrin complexes. <sup>260</sup> Indeed, Quirke and co-workers, have studied the chemistry of the porphyrins inherent in gilsonite. <sup>261-2</sup>

---

<sup>†</sup> Asphaltenes are aliphatic constituents of crude oil that are soluble in carbon disulphide but insoluble in petroleum ether or n-pentane.

\* Petroleum resins are the fraction of residuum that is insoluble in liquid propane but insoluble in n-pentane.

Naturally occurring porphyrins act as biological markers. The geochemical importance of porphyrins relates to the fact that their carbon structures can be traced back, through geological time and the stages of evolution of the material in which they are incorporated, to the original living organisms. These porphyrins are usually found as metal complexes (most commonly nickel and vanadium as vanadyl,  $VO^{2+}$ ), but free porphyrins also occur. <sup>260</sup>

The weathering of seeps or seams exposed to the atmosphere is an important factor in the evaluation of the relationship of a surface seep to possible petroleum accumulations. <sup>205</sup> With this in mind, a series of gilsonite samples, taken from the surface and at depth from the same vein, were analysed for their carbon, oxygen, nitrogen and sulphur contents. <sup>222</sup> It was found that the more weathered samples had less hydrogen, and more oxygen; the nitrogen and sulphur content of these samples showed no change over the entire range. This data indicates that the alteration of solid gilsonite is a result of the formation of stable oxygenated compounds, rather than of increased polymerisation.

#### 2.5.1b Results and discussion

In total, six different gilsonite samples were analysed using ESCA and microanalysis. A sample of a commercial gilsonite 'select', supplied by the American Gilsonite Company, was used for the main part of the investigation and for the plasma treatments in Chapter Three. Details of the other gilsonite samples supplied by Dr J.M. Hunt are as follows:

- 1) Chepeta Vein gilsonite
- 2) Soft gilsonite, Cowboy Vein
- 3) Hard gilsonite, Neal Vein, south of Rainbow
- 4) Hard gilsonite
- 5) Weathered gilsonite, Gusher Vein.

The locations of the various gilsonite veins are indicated in Figure 2.5.

The ESCA wide scan spectrum (from 100 to 1253.7eV kinetic energy) of gilsonite 'select' shows a very strong  $C_{1s}$  peak and weaker signals from the  $N_{1s}$  and  $O_{1s}$  regions. The relative intensities of the core level signals for the elements carbon, oxygen, nitrogen and sulphur, together with details of the  $C_{1s}$  envelope deconvolution, are listed in Table 2.1. The corresponding information for the other materials included in this study is also presented.

A more detailed investigation of the carbon photoionisation peak (Figure 3.20) reveals the predominant hydrocarbon nature of gilsonite as is evident by the major component of the  $C_{1s}$  envelope at 285eV binding energy. This peak accounts for ~ 88% of the total carbon signal. A slight shoulder to the higher binding energy side of the main hydrocarbon peak at 286.3eV is characteristic of carbon singly bonded to oxygen or  $C-N$  environments. Evidence for such functionalities is given by the presence of a low intensity  $N_{1s}$  and  $O_{1s}$  peaks at binding energies characteristic of carbon-nitrogen and carbon-oxygen functionalities in organic environments. The broad nature of the  $N_{1s}$  signal which is centred at 400.0eV binding energy is indicative of there being several carbon bonded to nitrogen environments, including aliphatic and aromatic amines and heterocyclic nitrogen functionalities such as pyrrolic nitrogen. No evidence was found for the presence of oxidised nitrogen species such as nitrate ester linkages which would occur to higher binding energy of the amine type  $N_{1s}$  peak, in the 407eV region. These observations are entirely reasonable in view of the high protein content of the original organic matter from which gilsonite has evolved, and the significant porphyrin content of gilsonite. <sup>263</sup>

The low level oxygen content manifests itself in the form of a weak signal (~ 3% of the intensity of the total  $C_{1s}$  envelope), at a binding energy of 534.1eV. Analysis of the  $C_{1s}$  envelope reveals a low level of

Table 2.1 Relative area intensities of core electron signals, total C<sub>1s</sub> area taken as 100 units, figures in brackets indicate binding energies (eV)

		<u>C</u> - H	<u>C</u> - O	> <u>C</u> = O	<u>C</u> - O	O - <u>C</u> - O	$\pi \rightarrow \pi^*$	O <sub>1s</sub>	N <sub>1s</sub>	S <sub>2p</sub>
			(286.3)		(288.5)	(290.1)		(534.1)	(400.0)	(163.6)
Gilsonite		88.1	10.6	-	0.9	0.4		2.9	3.4	0.32
Weathered Gilsonite			(286.3)	(287.9)	(289.1)	(290.5)		(533.0)	(399.5)	*
		83.3	13.3	1.7	0.8	0.8		6.3	3.5	0.64
Untreated Torbanite	(283.5)		(286.3)	(287.6)	(289.4)	(290.0)	(292.0)	(534.1)	(401.2)	
	6.5	46.7	34.6	10.3	4.2	1.4	0.9	162.6	1.5	-
Demineralised Torbanite			(286.3)	(287.9)	(289.4)	(290.1)		(533.7)	(400.5)	*
		69.9	19.6	5.6	3.5	1.4		11.4	2.1	0.7
Kimmeridge Kerogen			(286.3)	(287.5)	(288.8)	(290.2)		(532.8)	(400.5)	
		76.8	16.2	4.0	2.0	1		16.1	3.1	9.4 <sup>†</sup>
Vitrinite			(286.4)	(288.0)	(289.1)	(290.2)	(291.6)	(533.2)	(399.9)	(164.4)
		69.0	20.7	5.1	0.7	2.1	1.4	19.8	3.0	0.8
Brown Coal	(283.5)		(286.2)	(287.6)	(288.9)	(290.0)	(291.6)	(533.3)	(400.6)	
	5.9	52.5	23.8	9.9	4.0	3.0	1.0	46.5	1.5	-

\* denotes a broad band

† doublet structure

carboxyl and carbonate carbon functionalities at binding energies 288.5eV and 290.1eV respectively. Grantham and Douglas have also identified a low level of carboxylic acid esters by chromatographic techniques.<sup>226</sup> Comparison of the peak at 286.3eV binding energy under the carbon envelope with the integrated  $C_{1s}/O_{1s}$  intensity data suggests that the carbon singly bonded to oxygen corresponds almost exclusively to ether linkages, rather than free hydroxyl groups.

The spectrum of gilsonite recorded using the Ti  $K\alpha$  X-ray source of the ES 300 spectrometer, which probes more deeply into the sample, shows there to be a higher concentration of oxygen in the bulk than in the surface regions sampled with Mg  $K\alpha_{1,2}$  X-radiation. The respective C : O stoichiometries are 100 : 3 and 100 : 1.7.

Gilsonite is found to be low in sulphur, as expected, the sulphur functionalities detected giving rise to a peak at 163.4eV in the ESCA spectrum. This is representative of organic sulphur functionalities including sulphide and heterocyclic sulphur compounds such as thiophenes.<sup>105</sup>

Very low intensity peaks were also observed corresponding to silicon, aluminium and chlorine present in trace amounts (<0.3% of total  $C_{1s}$  intensity) and at binding energies of 102.9eV, 75.7eV and 199.1eV respectively. Both the silicon and aluminium are present in the form of their oxides and arise from the mineral material inherent in the gilsonite material: the chlorine is present as chloride. These mineral oxides will contribute to the oxygen photoelectron signal to a small extent.

No photoionisation signals relating to either nickel or vanadium were discernable. It should be noted that in the case of nickel, the most intense peak which arises from the Ni  $2p_{3/2}$  core level would occur towards the low kinetic energy end of the ESCA<sup>2</sup> spectrum (at ~ 400eV kinetic energy).<sup>105</sup> In this region the instrumental sensitivity, when operating in the FRR mode, is low (Section 1.8.3). Microanalysis detects nickel at

the 0.02 wt % level; vanadium, if present, amounts to less than 0.01%, whilst the tin content is estimated at less than 0.1%.

The analysis for tin was prompted by the observation of a 2 : 3 doublet of 8.6eV separation at 496.1eV and 487.5eV in the ESCA spectrum. These peaks correspond to signals from the  $3d_{3/2}$  and  $3d_{5/2}$  levels of tin, <sup>105</sup> although the origin of such a component in gilsonite is uncertain. The intensity of the total signal is small, of the order of <1% of the total  $C_{1s}$  envelope.

The apparent absence of shake-up satellite structure, occurring to the high binding energy side of the main  $C-H$  peak under the carbon envelope and arising from  $\pi \rightarrow \pi^*$  excitations accompanying core ionisation in conjugated systems, is unexpected, since gilsonite is reported to be predominantly aromatic. <sup>218</sup> The shake-up structure is characteristic of the higher occupied and low unoccupied valence orbitals. A number of organic systems has been investigated in Durham with particular reference to shake-up structure and include a study of condensed aromatic and polymer systems. <sup>270</sup> The exact structure and intensity of the shake-up peak is found to vary according to the material. It is possible therefore that the shake-up structure associated with the aromatic networks in gilsonite are present in the  $C_{1s}$  spectrum as a very broad band which is not clearly visible even upon magnification.

The aromatic component in gilsonite was however illustrated by  $^1H$  and  $^{13}C$  nmr and the pertinent spectra for both the gilsonite 'select' and the weathered gilsonite sample from the Gusher Vein are presented in Figures 2.6 and 2.7. Whilst interpretation of the types of environment present, as detected by  $^{13}C$  nmr, is difficult due to the proximity of nmr peaks arising from different structural features, <sup>246</sup> signals from aliphatic and aromatic constituents are discernible. A similar situation is true for  $^1H$  nmr spectra. Integration of the aromatic and aliphatic bands in

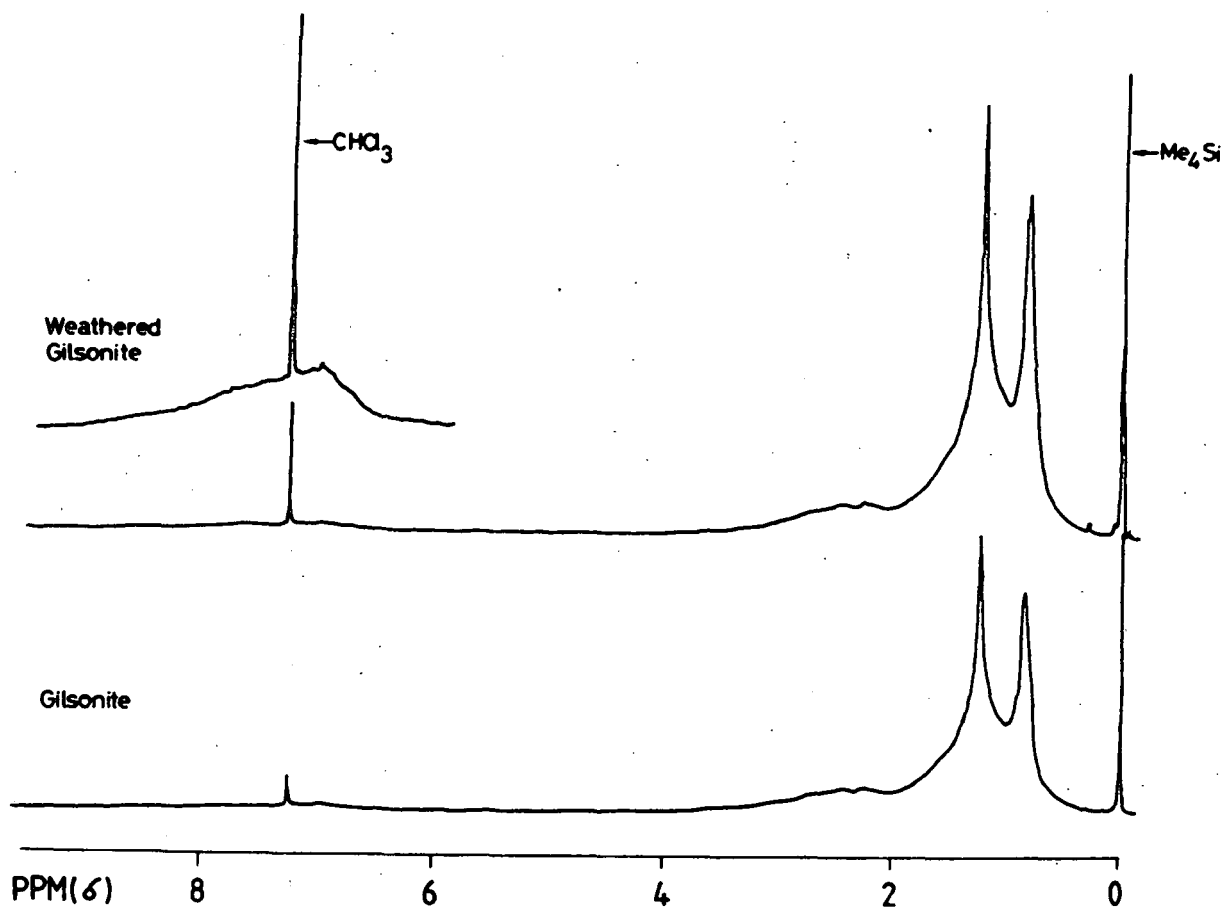


Figure 2.6 Proton nmr spectra of gilsonite 'select' and weathered gilsonite from Gusher Vein

the <sup>13</sup>C nmr spectrum of gilsonite 'select' gives the ratio of aromatic to aliphatic carbon as being 1 : 4.

The infrared spectrum of the gilsonite solid ran in the form of a KBr disc and showed little obvious signs of aromaticity (Figure 2.4).

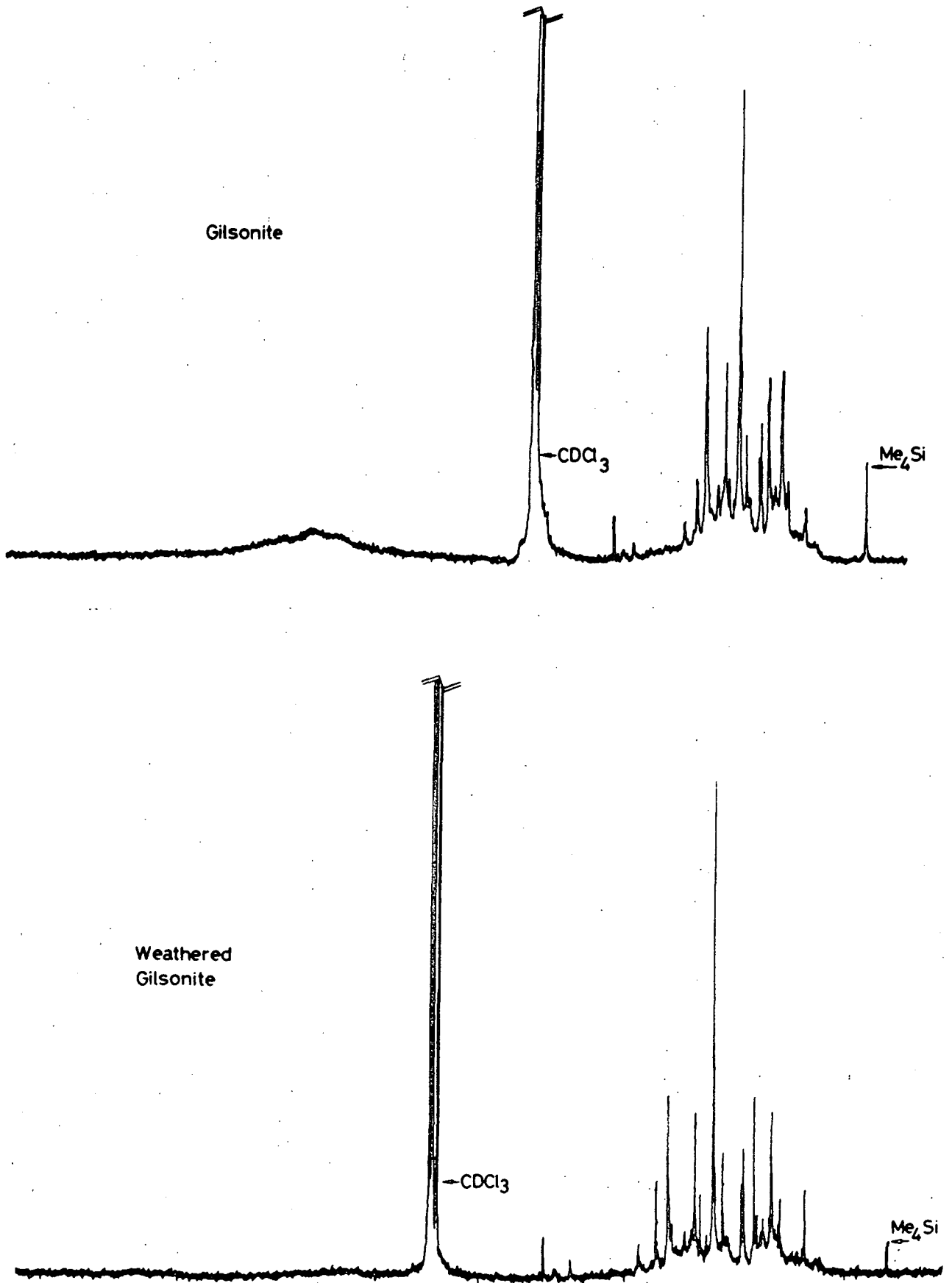


Figure 2.7  $^{13}\text{C}$  nmr spectra of gilsonite 'select' and weathered gilsonite

The spectrum is dominated by strong C-H stretch in the  $2900-3000\text{cm}^{-1}$  and corresponding asymmetric bending of methylene and methyl groups at  $1455\text{cm}^{-1}$  and methyl symmetric bending vibration near  $1375\text{cm}^{-1}$ . A broad OH stretching band around  $3400\text{cm}^{-1}$  is also present which may in part be due to moisture content; whilst the bending mode will contribute to the band at  $1630\text{cm}^{-1}$ . The broad nature of the band around  $1630\text{cm}^{-1}$  may be due to C=O stretching of carbonyl (aldehyde, ketone) and/or carboxyl (acid, ester) groups producing a shoulder in the region of  $1710\text{cm}^{-1}$ .

A feature common to all coals and kerogens of a certain degree of evolution is a series of three absorption bands at  $870$ ,  $820$  and  $750\text{cm}^{-1}$ , of roughly equal intensity, owing to out of plane deformation vibrations of aromatic CH groups.<sup>250</sup> These bands are also visible in the gilsonite spectrum. In fact, although the stretching band of the aromatic CH groups is expected between  $3000$  and  $3100\text{cm}^{-1}$ , it is much weaker than the out of plane deformation band, and is only observed as a distinct band in the spectra of coals.<sup>250</sup>

### 2.5.1c Comparison of elemental analytical data

Consideration of the relative intensities of the individual photoionisation peaks for the elements carbon, nitrogen, oxygen and sulphur allows elemental stoichiometric data to be acquired and hence an insight into the overall elemental composition to be ascertained. Figures relating to the elemental composition (expressed as weight per cent) and stoichiometry of gilsonite 'select' as revealed by the ESCA spectra, recorded using both the ES 200 and ES 300 instrumentation, are compared with values derived from conventional microanalytical techniques in Table 2.2. In addition, data obtained for the samples of gilsonite from named veins are presented. It is important to note that ESCA is unable to yield information relating to hydrogen within a specimen; in all cases the values for hydrogen analysis

Table 2.2 Elemental analyses and overall stoichiometric data for a series of gilsonite samples

	Elemental analyses (wt %)					Overall stoichiometry				
	C	H	N	O	S	C	H	N	O	S
Gilsonite 'select'	(84.25)	(12.38)	(2.84)	-	(0.61)	(100)	(176.3)	(2.89)	-	(0.27)
ES200	82.57	-	2.75	1.99	0.38	100	-	2.86	1.74	0.17
ES300	82.13	-	2.47	2.46	0.55	100	-	2.58	2.25	0.25
Chepeta Vein	(82.98)	(11.09)	(2.38)	(3.05)	0.50	(100)	(160.4)	(2.46)	(2.76)	(0.23)
	22.23	-	1.72	4.5	0.46	100	-	1.79	4.10	0.21
Cowboy Vein	(83.24)	(11.21)	(1.00)	(3.7)	(0.85)	(100)	(161.6)	(1.03)	(3.33)	(0.38)
	82.59	-	1.42	3.94	0.84	100	-	1.47	3.58	0.38
Neal Vein	(83.09)	(11.11)	(1.93)	(3.35)	(0.52)	(100)	(160.5)	(1.99)	(3.02)	(0.23)
	80.31	-	2.99	5.67	-	100	-	3.19	5.30	-
Hard Gilsonite*	(81.39)	(11.07)	(2.47)	(4.53)	(0.54)	(100)	(163.2)	(2.60)	(4.17)	(0.25)
	79.01	-	3.75	5.59	0.58	100	-	4.07	5.31	0.27
Gusher Vein	(86.02)	(11.29)	(2.23)	-	(0.49)	(100)	(157.5)	(2.22)	-	(0.21)
(Weathered Gilsonite)	81.10	-	2.78	4.09	0.74	100	-	2.94	3.78	0.34

\* Details relating to the precise origin of this sample are not available.

N.B. ESCA results were obtained using the ES200 instrumentation unless otherwise specified.  
Microanalytical results in brackets.

were those obtained from microanalysis. The microanalytical determination of oxygen was by difference.

The reproducibility of conventional elemental analysis for the elements carbon, hydrogen and nitrogen was investigated and the relevant figures are listed in Table 2.3. Examination of these figures shows that the ESCA analyses are in reasonable agreement with the microanalytical determinations. Furthermore, such a relationship is found to hold for the other materials examined in this chapter (Table 2.4). The inadequacies of the by difference determination for oxygen are clearly obvious.

#### 2.5.1d Weathered Gilsonite

Special mention should be made of the ESCA data for the sample of weathered gilsonite from Gusher Vein. Measurement of relative intensities of the photoionisation peaks shows that the weathered sample has increased in oxygen content by a factor of two compared with a sample of gilsonite 'select', whilst the nitrogen content for both materials is approximately equal. This is in agreement with the findings of Hunt.<sup>222</sup> ESCA indicates that the sulphur level in the weathered sample is higher, although this may well be spurious in view of the low sulphur content of gilsonites in general. In fact, a wide scan spectrum of weathered gilsonite detects a rise in the level of silicon present and a more detailed scan reveals an  $Si_{2p}$  peak at 101.6eV binding energy corresponding to silicate silicon. In spite of the fact that the silicate component contributes to the oxygen signal, there is still evidence for oxidation of the organic carbon from deconvolution of the  $C_{1s}$  envelope. Curve resolution shows an increased carbon singly bonded to oxygen peak and development of carbonyl functionalities as a peak at 287.9eV binding energy.

Table 2.3 Microanalysis of gilsonite 'select'

	C	H	N	S*	O
Durham	82.68	12.72	3.51	(0.62)	0.48
	83.35	12.61	2.45	(0.59)	0.98
	82.51	13.26	2.84		0.78
	84.20	12.20	3.06		0.54
	84.18	12.75	2.80		-0.34
	83.98	12.92	2.58		-0.09
	84.08	12.61	2.72		-0.02
	83.10	12.47	2.60		1.22
	84.90	13.10	2.73		-1.34
	84.65	12.63	2.56		-0.45
	(85.32	11.71	3.02		-0.66
	(				
	(85.06	12.00	3.20		-0.87
Bristol	86.16	11.09	2.88		-0.74
	85.34	11.22	2.81		0.02
Mean	84.25	12.38	2.84	(0.61)	
Standard Deviation	1.07	0.66	0.28		

\* Sulphur analysis performed on two samples only.  
Averaged value included in calculation of oxygen by difference.

† Measurements recorded prior to refurbishing of elemental analyser instrumentation.

Table 2.4 Elemental analyses and overall stoichiometric data

	<u>Elemental analysis (wt %)</u>					<u>Overall stoichiometry</u>				
	C	H	N	O	S	C	H	N	O	S
Untreated Torbanite	(56.02) 39.80	(7.86) -	(1.55) 0.58	(34.06) 51.76	(0.51) -	(100) 100	(168.4) -	(2.37) 1.26	(45.60) 97.56	(0.34) -
Demineralised Torbanite	(81.87) 79.13	(11.25) -	(1.41) 1.62	(4.64) 7.22	(0.83) 0.78	(100) 100	(164.90) -	(1.48) 1.76	(4.25) 6.84	(0.38) 0.37
Kimmeridge Kerogen	(57.09) 72.46	(6.37) -	(1.85) 2.20	(23.49) 9.33	(11.2) 9.63	(100) 100	(133.89) -	(2.78) 2.60	(30.86) 9.66	(7.34) 4.98
Vitrinite	(74.0) 79.06	(5.2) -	(1.6) 2.32	(18.6) 12.52	(0.64) 0.89	(100) 100	(84.32) -	(1.85) 2.52	(18.85) 11.88	(0.32) 0.42
Brown Coal	(47.7) 69.41	(3.74) -	(0.61) 1.02	(47.53) 25.83	(0.42) -	(100) 100	(94.09) -	(1.10) 1.26	(74.73) 27.9	(0.33) -

N.B. ES200 spectrometer used for all ESCA measurements.  
Mineral components not taken into consideration.

Microanalytical results in brackets.  
No residual ash detected upon combustion.

## 2.5.2 Torbanite

### 2.5.2a Introduction

A sample of Scottish torbanite from Bathgate, Lothian, was included in this study. Torbanite or boghead coal, as it is also known, is a sapropelic coal which contains alginite and micrinite macerals.<sup>268</sup> Formed in small freshwater lakes from sediments rich in algal remains which were laid down during the Carboniferous Age, Scottish torbanite contains defined organic remnants, clearly recognisable under a microscope.<sup>207</sup> This organic debris comprises algae, spores, pollen and vegetal tissues and usually amounts to a minor part of the organic matter with a range of a few percent of the total kerogen. However, in certain rare types of rocks, like torbanite, this type of constituent occurs in great quantities.<sup>206</sup> The characteristic constituent of torbanite kerogen is alginite and is finely dispersed within a clay mineral matrix.<sup>207</sup>

Chemically all algae are distinguished by relatively high contents of fatty and proteinaceous substances.<sup>207</sup> Robinson<sup>235</sup> reports that Australian torbanite of the Permian geologic age contained about 74 percent material resistant to oxidation by alkaline permanganate, which is indicative of the presence of considerable fatty remains. Alginite from Scottish torbanite has the lowest aromaticity of all bituminous coal minerals. This is reflected in the high H/C ratio in the region of 1.5.<sup>205</sup> The number of polyaromatic nuclei and heteroatomic bonds is low, compared with the other types of organic matter. The small amount of oxygen present (the O/C ratio is generally <0.1) exists mainly in the form of ester linkages.<sup>206</sup> When plotted on a van Krevelen diagram, torbanite kerogen is found to lie on the evolution path of Type-I kerogen.

### 2.5.2b Results and discussion

ESCA analyses were performed on both the untreated 'raw' torbanite and the torbanite kerogen isolated from its mineral matrix by wet chemical demineralisation techniques. The striking differences in the photoionisation spectra of the isolated kerogen and the raw material demonstrates the ability of ESCA to detect the mineral phase. The wide scan spectrum of the untreated torbanite shows prominent signals from the silicon and aluminium constituents of the clay mineral matrix. A more detailed investigation of the individual  $\text{Si}_{2p}$  (104.1eV) and  $\text{Al}_{2p}$  (75.7eV) peaks reveals their respective intensities to amount to 38% and 23% of the total  $\text{C}_{1s}$  band intensity.

Clay minerals are rich in oxygen; for example, the kaolinite group of clays has an elemental stoichiometry of  $\text{Al}_4 \text{Si}_4 \text{O}_{10} (\text{OH})_8$ . The presence of such an inorganic mineral phase accounts for the unexpectedly intense ESCA oxygen signal in the untreated torbanite. (The carbon to oxygen atomic ratio corresponds to 100 : 98.)

Also uncharacteristic of the pure torbanite kerogen is the apparent surfeit of carbon/oxygen functionalities discernible under the rather broad  $\text{C}_{1s}$  envelope (Table 2.1). These functionalities, which include  $\underline{\text{C}}-\text{O}$ , carbonyl, carboxyl and carbonate moieties, are likely to originate from other organic carbon compounds within the material as a whole. A low level signal (~ 1% of the total  $\text{C}_{1s}$  envelope) at 295.2eV binding energy is characteristic of the potassium component of the clay.

The ESCA spectrum of the demineralised sample shows that the silicon and aluminium components have been almost entirely eliminated.<sup>†</sup> For example, the  $Al_{2p}$  level is found to have shrunk to 2% of its intensity in the untreated material. There is also a marked drop in oxygen concentration, as is evident from the  $O_{1s}$  core level photoionisation peak. Comparison of the overall intensities of the  $C_{1s}$  and  $O_{1s}$  peaks lead to a carbon to oxygen atomic ratio of 100 : 6.8, a finding which is consistent with elemental analyses reported in the literature.<sup>206</sup>

The overall FWHM of the  $C_{1s}$  envelope of the demineralised torbanite sample is significantly less than that of the raw material, the respective values being 2.0eV and 2.9eV. Deconvolution of the  $C_{1s}$  envelope of the demineralised sample and relative area analysis of the resulting component peaks show that the chemical nature of the carbon constituent is predominantly hydrocarbon-like. Of the other components present, the peak at 286.3eV corresponding to carbon singly bonded to either oxygen or nitrogen is the most intense; whereas those indicative of  $>\underline{C} = O$ ,  $\underline{C} = \overset{O}{\parallel} - O$  and  $O - \overset{O}{\parallel} - O$  functionalities are comparatively minor. The low level  $K_{2p}$  peak at 295.2eV binding energy of the untreated sample is no longer observable.

Nitrogen is detectable in the spectra of the untreated and demineralised torbanite samples, the latter sample showing a more intense signal. The binding energies at which these peaks occur correspond to nitrogen bound in the form of amine.

---

<sup>†</sup> Infrared spectroscopy is a technique which may be used to monitor procedures for kerogen isolation.<sup>238</sup> Indeed, infrared spectra of the torbanite sample before demineralisation shows strong absorption in the region of  $1100\text{cm}^{-1}$ , characteristic of silicates (Figure 2.4). Also prominent in the spectrum are the sharp bands at  $\sim 3600\text{cm}^{-1}$  which arise from OH groups in the mineral phase. These bands are not present in the spectrum of the isolated kerogen.

The demineralised torbanite also shows a low level of sulphur, as a very broad, weak  $S_{2p}$  band present in the spectrum at less than 1% of the total  $C_{1s}$  peak intensity. No sulphur could be detected in the raw torbanite.

The elemental composition of the torbanite kerogen as determined by ESCA is  $C_{100} N_{1.8} O_{6.8} S_{0.4}$  which compares most favourably with the value of  $C_{100} H_{164.9} N_{1.5} O_{4.3} S_{0.4}$  derived from microanalysis.

### 2.5.3 Kimmeridge Kerogen

As an example of a Type-II kerogen, the kerogen concentrate from the bituminous shale of Kimmeridge Bay, Dorset, was subjected to examination by ESCA. Type-II kerogen is usually related to marine sediments where autochthonous organic matter has been deposited in a reducing environment. In dispersed state, Type-II kerogens are the source material of a great number of oil or gas fields. <sup>206</sup>

The details of nitrogen and oxygen photoionisation peak intensities and carbon envelope deconvolution are presented in Table 2.1. The most striking feature of the ESCA spectrum lies in the prominence of the sulphur core level signal which amounts to over 9% of the intensity of the  $C_{1s}$  envelope. This corresponds to a carbon to sulphur ratio of 100 : 5, compared with a microanalytical ratio of 100 : 7.3. The percentage of sulphur in Kimmeridge kerogen is far higher than that found in the organic precursors to the kerogen. <sup>271</sup>

The  $S_{2p}$  envelope (Figure 3.26) consists of two distinct components centred at binding energies of 163.9eV and 169.0eV, the respective intensities being in a ratio of 77 : 53. Although unequivocal assignment of a particular species to each component cannot be made, a study of model systems is helpful when analysing spectra of materials of unknown composition. For example,

the spectra of ferrous sulphide, polyphenylene sulphide and bisphenol-A polysulphone have been run and are shown in Figures 3.17 - 9. Inorganic sulphide, as in  $\text{FeS}_2$ , is found at a binding energy of  $\sim 162\text{eV}$ , whereas the polyphenylene sulphide organic sulphide peak occurs at  $\sim 163\text{eV}$ : the  $\text{S}_{2p}$

$$\begin{array}{c} \text{O} \\ || \\ \text{S} \\ || \\ \text{O} \end{array}$$

sulphone ( - S - ) peak of bisphenol-A polysulphone is centred at 168eV

binding energy. This information, together with the tables available in the literature,<sup>105,190</sup> leads to the assignment of the  $\text{S}_{2p}$  component peak at 169eV as being due to oxidised sulphur species, whilst the peak to lower binding energy comprises sulphur bound in organic sulphur environments. It should be noted that although a low intensity iron peak ( $\text{Fe}_{3p}$  54.6eV) is detectable, it is unlikely that there is a significant contribution to the 163.9eV  $\text{S}_{2p}$  component by inorganic sulphide in the form of  $\text{FeS}_2$ .

#### 2.5.4 Vitrinite

##### 2.5.4a Introduction

Vitrinite is a coal maceral type comprising the remains of woody and humic components which is the most abundant maceral of humic coals. Vitrinite is the dominant constituent of the bright, black and lustrous bands that characterise hard coals. The maceral occurs in two forms:<sup>207</sup> telinite which shows the cell structure of wood or bark, and collinite derived from the cell filling. Vitrinite particles are found in about 80% of the clays and sands of sedimentary basins.<sup>205</sup>

Atomic H/C and O/C ratios for vitrinite samples will vary according to their degree of coalification.<sup>268</sup> When represented on a van Krevelen diagram, the evolution track followed by the vitrinite maceral group is found to correspond to the Type-III kerogen pathway.<sup>206</sup> This is

reasonable, since both vitrinite and Type-III kerogen are rich in terrestrial plant material.

The aromaticity of vitrinite varies with rank, and has been measured by such diverse techniques as X-ray diffraction, optical and spectroscopic examination and chemical studies.<sup>207</sup> Vitrinites typically contain about 70% aromatic carbon atoms in hard brown coals and over 90% in anthracites. The oxygen content of vitrinite decreases progressively with increasing rank as the oxygen functionalities are split from the periphery of the aromatic cluster network.<sup>206</sup> Accompanying this process there is a loss of methyl groups, and condensation of the aromatic ring clusters as the coal structure approaches that of anthracite.

Both the nitrogen and sulphur content of vitrinite show little change with increasing rank, the respective values lying in the ranges 1.15 - 1.35% and 0.4 - 0.6%.<sup>207</sup> Nitrogen is assumed to occur in heterocyclic ring systems. Various forms of organic sulphur such as thiophenol, sulphide, disulphide and heterocyclic, have been distinguished with 70% of the organic sulphur probably occurring in heterocyclic aromatic ring structures.<sup>269</sup>

#### 2.5.4b Results and discussion

A sample of vitrinite extracted from the hard bituminous coal from the Nottingham coal field, Babbington, was used in this investigation. The ESCA spectrum of vitrinite indicates the presence of carbon, oxygen, nitrogen and sulphur, together with a very low level of silicon ( $Si_{2p}$ , 103.5eV), aluminium ( $Al_{2p}$ , 76.5eV) and chlorine ( $Cl_{2p}$ , 198.7eV), the intensity of the latter signals not exceeding 1% of the total carbon envelope intensity. Also detected in the ESCA spectrum were two low intensity peaks (amounting in total to ~ 1% of the  $C_{1s}$  envelope area) occurring at 495.7eV and 486.7eV on the binding energy scale, the areas of the peaks being in the ratio of 1 : 2.6.

The nature of these signals is uncertain; however, the photoionisation lines from the  $3d_{3/2}$  and  $3d_{5/2}$  levels of tin are known to occur in this region, with an intensity ratio of 2 : 3.<sup>105</sup>

The elemental composition of vitrinite, as determined by ESCA, is revealed as being 79.1% C, 12.5% O, 2.3% N and 0.9% S, as compared with microanalytical figures of 74.0% C, 5.2% H, 18.6% O, 1.6% N and 0.6% S. This information establishes that the vitrinite originates from hard bituminous coal rather than a coal of a higher rank.<sup>207</sup> The H/C and O/C atomic ratios, obtained from ESCA C and O values and the microanalytical result for hydrogen, are 0.78 and 0.12 respectively. When recorded on a van Krevelen diagram, this result is found to fall on the coalification pathway of bituminous coal as depicted by Hunt.<sup>205</sup>

Curve resolution of the  $C_{1s}$  envelope shows the existence of

$\overset{0}{\text{C}} - \overset{0}{\text{O}}$ ,  $\overset{||}{\text{C}} = \overset{||}{\text{O}}$ ,  $\overset{||}{\text{C}} - \overset{||}{\text{O}}$  and  $\overset{||}{\text{O}} - \overset{||}{\text{C}} - \overset{||}{\text{O}}$  environments, which manifest themselves as peaks to the higher binding energy side of the prominent  $\overset{||}{\text{C}} - \text{H}$  photoelectron signal. A low intensity signal at 291.4eV is indicative of  $\pi \rightarrow \pi^*$  shake-up transitions from conjugated systems.

The  $O_{1s}$  and  $N_{1s}$  signals are broad, which implies that each element is present in more than one chemical environment within the sample. The weak intensity  $S_{2p}$  peak centred at 164.4eV is characteristic of organic sulphide-type sulphur linkages. To the higher binding energy side of this  $S_{2p}$  peak there is evidence for a low level of oxidised sulphur in the form of a shoulder at 168.9eV.

### 2.5.5 Brown coal

Brown coal falls into the category of a humic coal which is in the early stages of coalification. The formation of brown coal proceeds via the humification of lignin in peats to give humitinite.<sup>207</sup> This stage

is followed by gelification which leads to vitrinite formation. Hence brown coal and vitrinite fall on the same evolution pathway and therefore it is of value to compare and contrast these two materials in this work, especially with respect to the type and relative abundance of oxygen functionality as detected by ESCA.

The brown coal studied here is of the Miocene Age and originates from Indonesia.

From a knowledge of the chemical changes which occur during the maturation of brown coal to bituminous coal,<sup>268</sup> the level of oxygen functionalisation in the younger brown coal would be expected to be greater than has been established for vitrinite. This is indeed found to be the case, not only from consideration of the ESCA atomic O/C ratios, but also from curve resolution of the  $C_{1s}$  envelope.

The deconvoluted  $C_{1s}$  signal shows  $\overset{O}{\parallel} \underline{C} - O$ ,  $>\underline{C} = O$ ,  $\overset{O}{\parallel} \underline{C} - O$  and  $O - \overset{O}{\parallel} \underline{C} - O$  functionalities: peaks characteristic of graphitic carbon and shake up are also present. The oxidised carbon environments are considerably more abundant than in the  $C_{1s}$  spectrum of vitrinite. This trend is particularly noticeable for the carboxyl moiety.

A low level of organic nitrogen was present at a binding energy of 400.6eV; however sulphur was not detected. Silicon ( $Si_{2p}$  104.4eV) and aluminium ( $Al_{2p}$  75.5eV) were present in trace quantities, the combined intensity of the  $Si_{2p}$  and  $Al_{2p}$  signals amounting to less than 1% of the total  $C_{1s}$  peak intensity.

## 2.6 Conclusions

A recent report<sup>264</sup> into basic coal sciences research presents a critical survey of the present-day philosophy and methodology used in

the elucidation of the structure and characteristics of coals and coal-related materials. The report emphasizes the need for fundamental research using standard coal samples, of well-defined history, and urges the application and development of techniques new to the area.

As mentioned previously (Section 2.2), relatively little work has been published relating to ESCA studies of coal. The work presented in this chapter has shown that elemental analyses from ESCA data are in reasonable agreement with microanalytical results. Furthermore, the inadequacies of analytical determinations 'by difference' have been highlighted for the particular case of oxygen.

In addition, the technique of ESCA is well suited to the detection of the mineral phase associated with coals and kerogens. This is amply illustrated by the analyses of the untreated torbanite and the isolated torbanite kerogen. The ability of a method to monitor the mineral content of such materials is attractive since the presence of a mineral matrix is known to affect the burning characteristics of coal<sup>265</sup> and the pyrolysis of kerogens.<sup>236,266</sup>

The weathering and oxidation of coals and cokes also affects subsequent combustion.<sup>267</sup> ESCA is able to probe the outmost monolayers of a solid, with a minimum of preparation. The high sensitivity of the technique is such that changes in surface composition may be detected with ease.

The following chapter describes the use of ESCA to monitor the modifications in chemical functionalisation which occur when coal and kerogen are subjected to oxygen glow discharge treatments. Since the oxidation process may be readily controlled, it is hoped that such treatments may afford selective oxidation, thus providing an insight into the relative susceptibility of the materials to the reactive species present in the plasma.

Line shape analysis is capable of revealing information on the chemical environments within a sample, although the limitations of such deconvolutions must be realised.

The combined use of ESCA and nmr techniques offers considerable potential in structural studies of coal and coal related materials.

CHAPTER THREE

PLASMA TREATMENT OF A SERIES OF GEOCHEMICAL MATERIALS

AND POLYMER FILMS

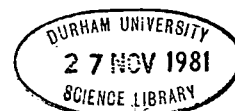
## CHAPTER THREE

### PLASMA TREATMENT OF A SERIES OF GEOCHEMICAL MATERIALS AND POLYMER FILMS

#### 3.1 Fundamental Aspects of Plasmas

The term *plasma* refers to a gaseous state comprising atoms, molecules, metastables and excited states of these species, and electrons such that the concentration of positively and negatively charged species is roughly equal. This state of matter can be generated through the action of either very high temperatures or strong electric or magnetic fields. De-excitation of excited states (electronic, vibrational and rotational) produces a wide range of electromagnetic radiation. The various plasmas which may be found in nature and in the laboratory, defined by their electron density and average electron energy, are summarised in Figure 3.1. The area which has proved to be of greatest interest to chemists is that associated with charge densities of  $\sim 10^{10} \text{ cm}^{-3}$  and average electron energies of  $\sim 1.0 \text{ eV}$ .

Plasmas produced by gaseous electrical discharges are to be considered here, and may be divided into two types. Firstly 'hot' or 'equilibrium' plasma, characterised by a high gas temperature and an approximate equality between the gas and electron temperatures. These plasmas are generally regarded as being of more interest to physicists, typical examples of 'hot' plasmas including arcs and plasma torches. The second type of plasma, with which this thesis is to be concerned, might be termed 'cool' and is of primary interest to chemists. Cool or nonequilibrium plasmas have the characteristic feature that the Boltzmann temperature of the ions and molecules is roughly ambient whilst that of the electrons is some two orders of magnitude greater.



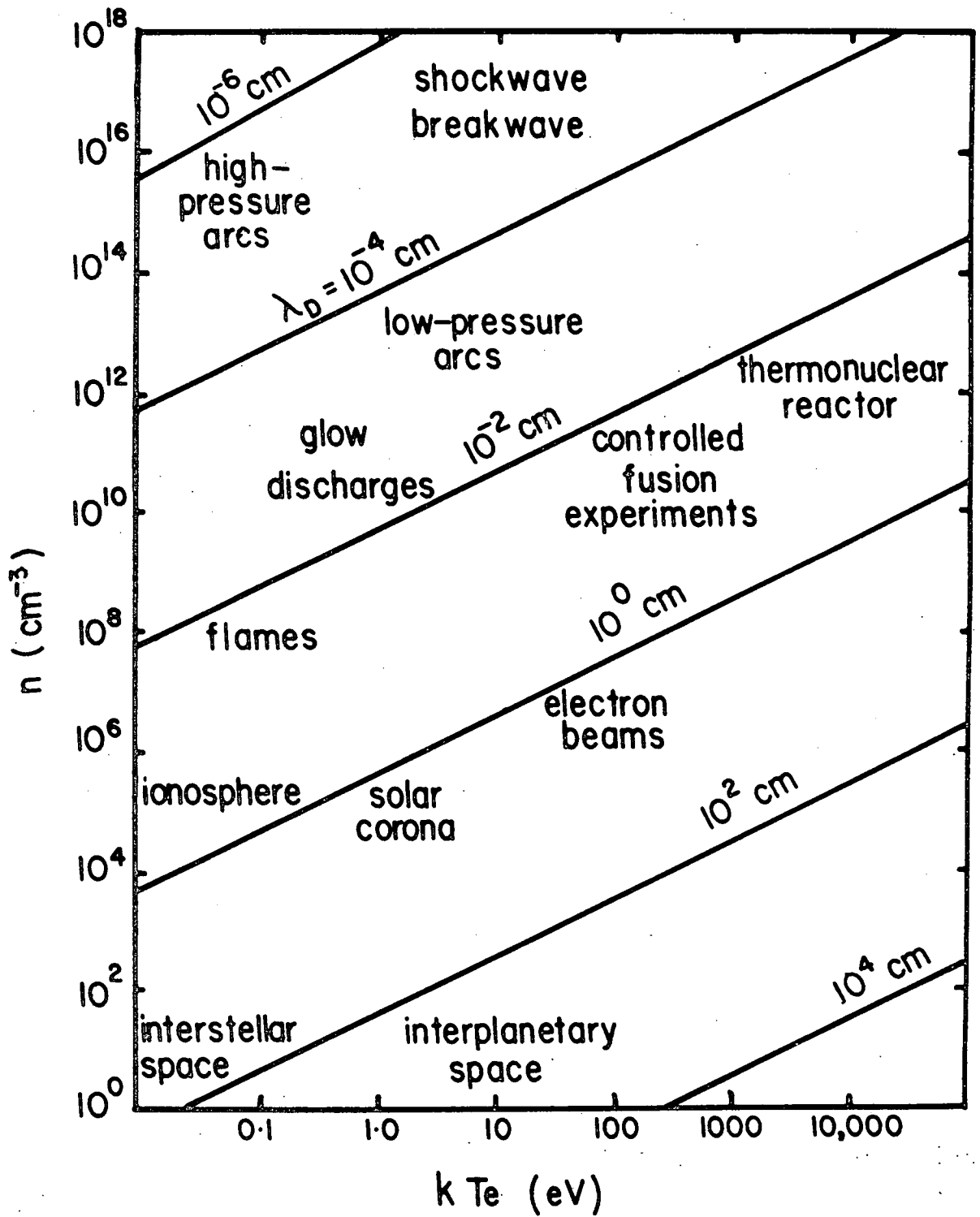


Figure 3.1 Plasmas characterised by their charge density and electron energy

The criterion of overall electrical neutrality is satisfied when the dimensions of the discharged gas column are significantly greater than the Debye length  $\lambda_D$ ,<sup>129</sup>

$$\lambda_D = \left[ \frac{\epsilon_0 k T_e}{n e^2} \right]^{\frac{1}{2}} \quad (3.1)$$

which defines the distance over which a charge imbalance may exist.

In equation 3.1  $\epsilon_0$  is the permittivity of free space,  $k$  is the Boltzmann constant,  $T_e$  is the electron temperature,  $n$  is the electron density and  $e$  is the charge on the electron.

Electrons within the plasma are accelerated by the electric field and produce further ionisation by collisions with other species. The collision process is shown schematically in Figure 3.2.

Although the interaction of radio frequency glow discharges with solids in general has been an active area of research in both industrial and academic laboratories, few attempts have been made to characterise the plasmas involved in terms of the energy distribution of electrons, ions and metastables. Expressions describing the electron energy distribution in reference to energy input, discharge dimensions and gas pressure lead to a Maxwellian distribution of electron energies, Figure 3.3. This relationship holds strictly for simple systems only, for example hydrogen, as depicted in Figure 3.4. For more complex systems, the average electron energies may be analysed by electrical probe measurements<sup>130-1</sup> and direct electron sampling.<sup>124</sup>

In general, plasmas generate a plentiful supply of electromagnetic radiation, through de-excitation of excited states, particularly in the U.V.

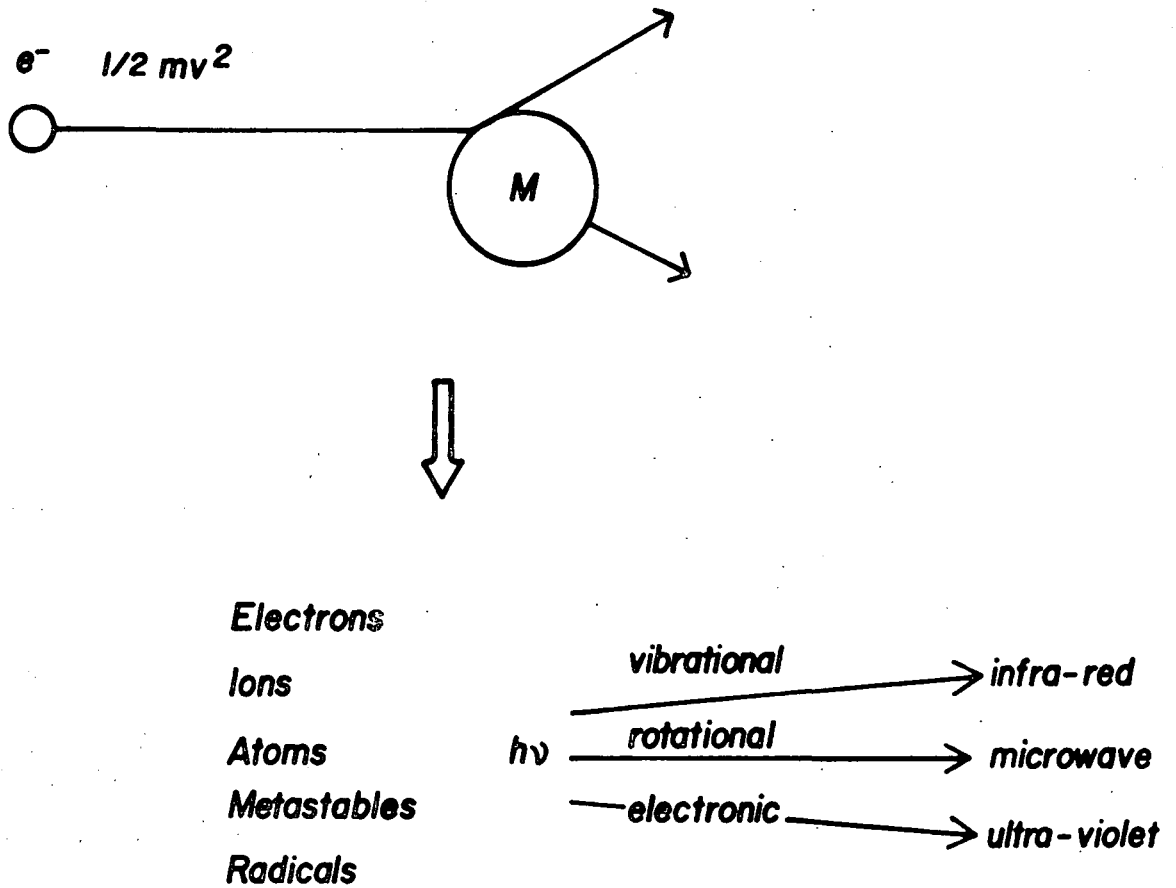


Figure 3.2 The collision process in a plasma

and vacuum U.V. and in fact plasmas are frequently used as sources in these regions. The relatively small output in the visible region is responsible for the characteristic colour for plasmas excited in a given system and hence the appellation 'glow discharge'.

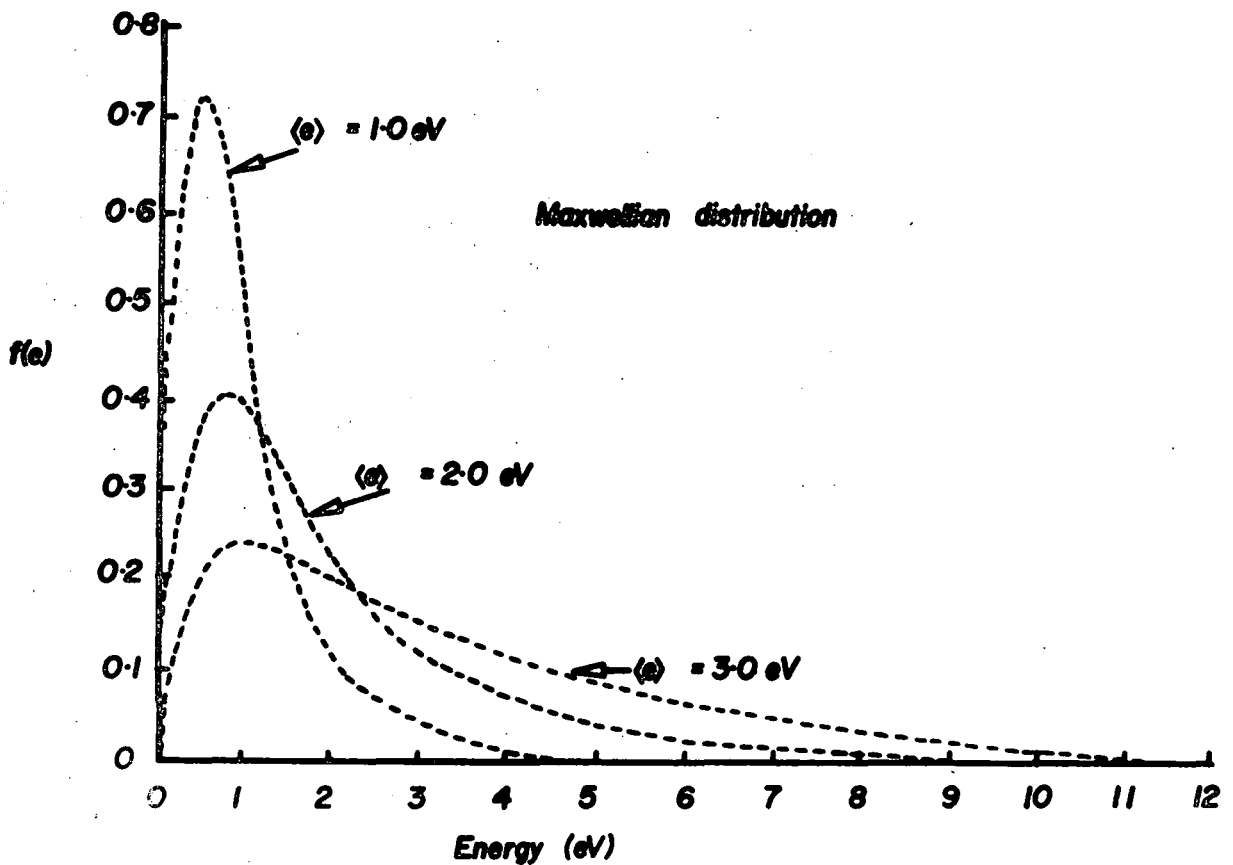


Figure 3.3 Maxwellian distribution function of electron energies

The production of a non-equilibrium glow discharge may be accomplished in several ways, the three principal variables being the source of electrical power to sustain the plasma, the coupling mechanism and what may be loosely termed the "plasma environment". The aspects of interest are outlined in Figure 3.5 : the combination selected for a given investigation depends on such factors as cost, ease of construction and convenience. Whilst most of the early work<sup>133-6</sup> involved A.C. and

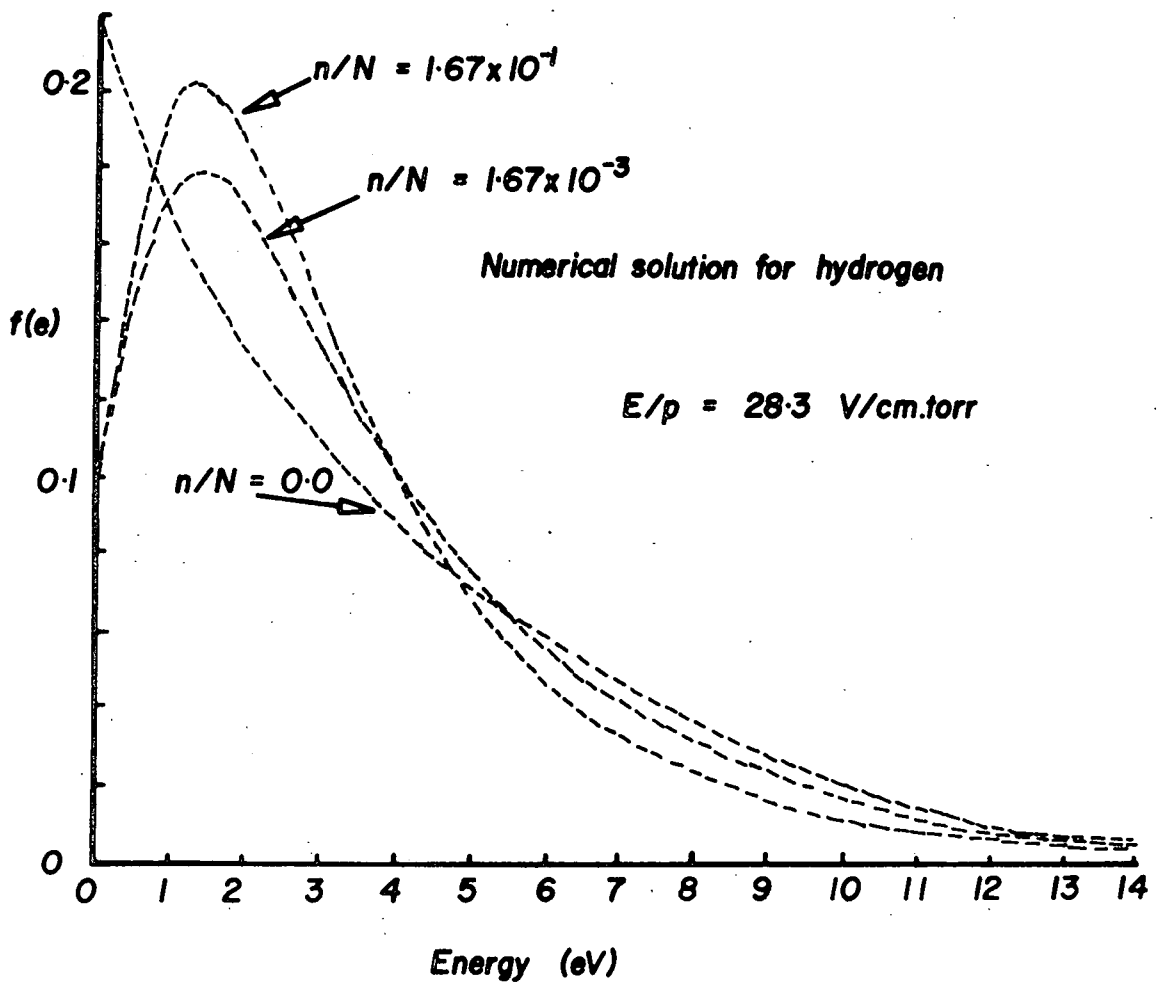


Figure 3.4 Numerical Solution for hydrogen

## Elements of a Glow Discharge Experiment

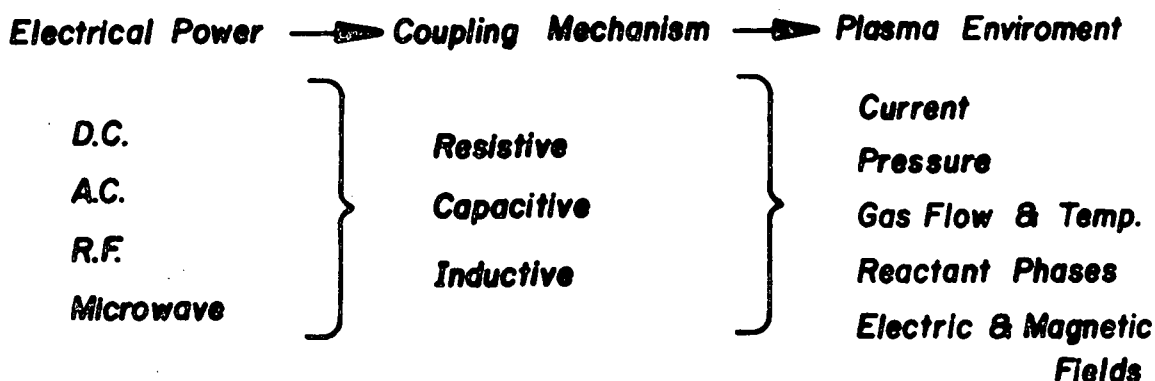


Figure 3.5 Elements of a glow discharge experiment

D.C. electrodeless discharges, the greater flexibility and closer control over operating parameters has, of recent years, shifted the emphasis towards the use of inductively coupled radio frequency and microwave plasmas.

Electrode discharges, in which electrodes are positioned in contact with the gas itself, may employ A.C., D.C. or R.F. power and are generally resistively coupled. These suffer from electrode contamination during usage. A more flexible set-up, particularly as far as in situ plasma treatments, employing a reactor attached to characterisation instrumentation and allowing for sample analysis without the risks of atmospheric contamination are concerned, involves the use of electrodeless R.F. discharges. Electrodeless R.F. discharges may be either capacitively

or inductively coupled, and are well-suited to flow systems with copper coils wound around the external surface of a typically cylindrical reactor. Electrodeless microwave discharges may also be excited inductively, using tuned cavities which can be in a demountable form to attach conveniently to a cylindrical reactor. <sup>137</sup>

The operating parameters of a glow discharge experiment are those of power input and operating pressure. Powers may range from 0.1W to a few kilowatts. Low frequency and D.C. discharges are generally characterised in terms of the voltage and current supplied to the electrodes. Typical operating voltages being in the range  $\sim 10 - 100$  V and  $\sim 1$  A current at pressures of  $\sim 1$  torr. For R.F. and microwave plasmas the situation is somewhat less straightforward, and the requisite instrumentation to measure the power in the plasma is relatively expensive. Operating pressures can range from  $\sim 0.01$  torr with R.F. and microwave discharges, and up to atmospheric pressure for D.C. discharges. An account of the fundamental processes which occur in glow discharge (D.C. and R.F.) has been presented by Lucas. <sup>138</sup>

Low power levels ( $< 1.0$  W) are generally difficult to sustain, but when using R.F. power this can be accomplished by pulsing the power input. Thus, with switching in the microsecond range it becomes possible to obtain stable plasmas operating at low average power loadings.

### 3.2 Reactive Species in Plasmas

Plasmas excited by electrical discharges contain a variety of species arising from collisions involving electrons accelerated by the electric field. Many of the species are sufficiently energetic to cause chemical reactions. A typical plasma may contain electrons, ions, metastables, neutral molecules and free radicals in ground and excited

states, and photons of various energies. The plasma is therefore a complex entity overall (Figure 3.6) and not surprisingly it is only for the simplest systems that any great attempt has been made to fully characterise a given system under standard operating conditions.<sup>230</sup>

**Energies associated with a glow discharge.**

	<u>eV</u>
<b>Electrons</b>	<b>0 - 20</b>
<b>Ions</b>	<b>0 - 2</b>
<b>Metastables</b>	<b>0 - 20</b>
<b>U.V./visible</b>	<b>3 - 40</b>

**bond energies:-**

<b>C—H</b>	<b>4.3</b>	<b>C=O</b>	<b>8.0</b>
<b>C—N</b>	<b>2.9</b>	<b>C—C</b>	<b>3.4</b>
<b>C—Cl</b>	<b>3.4</b>	<b>C=C</b>	<b>6.1</b>
<b>C—F</b>	<b>4.4</b>	<b>C≡C</b>	<b>8.4</b>

Figure 3.6 Energies associated with a glow discharge and some typical bond energies

The work in this thesis concentrates on treatments using plasmas excited in oxygen, although air<sup>139</sup> and hydrogen have also been employed to a lesser extent. A discharge pressure of 0.2 torr (as monitored by a Pirani vacuum gauge) was maintained in all the experimental runs.

3.2. 1) Oxygen Plasma.<sup>140</sup> Under the conditions of pressure and temperature used, the only ion likely to be present is  $O_2^+$ . Other species present will be atomic oxygen, singlet oxygen and ozone. Hydrated protons and  $OH^+$  are unlikely to be formed.

3.2. 2) Air Plasma.<sup>140</sup> The principal positive ion will be  $O_2^+$ , formed by the following reactions:



At 0.2 torr, NO and  $NO^+$  will also be present:



The peroxy isomer of  $NO_2^-$  has also been observed in oxygen plasmas containing nitrogen. Other species present will be atomic oxygen, atomic nitrogen, singlet oxygen and  $N_2^*$ . The existence of  $N_4^+$  is unlikely as are hydrated protons.

3.2. 3) Hydrogen Plasma.<sup>141</sup> At the low pressure employed in this work there is little evidence for the existence of hydrogen in reactive states other than atomic hydrogen. At higher

pressures (30 - 300 mm Hg) hydrogen atoms combining by three body collision processes appear to give rise to persistent, unstable molecules which retain the greater part of the energy of recombination and may survive up to  $10^8$  collisions in the gas phase. Thus chemical reactions of active hydrogen could be due to one or more of the following species: hydrogen atoms (H), excited hydrogen atoms ( $H^*$ ,  $H_2^+$  ions), excited hydrogen molecules ( $H_2^*$ ), protons ( $H^+$ ) or unstable complexes ( $H_x^*$ ).

Detailed coverage of the chemical aspects of electrical discharges are to be found in books by McTaggart, <sup>141</sup> and Hollahan and Bell. <sup>142</sup>

### 3.3 Applications of Plasma Chemistry

Recent years have witnessed a growing awareness of the great potential of the field of 'plasma chemistry' and especially its application to a wide range of topics of academic and technological importance. An indication of the areas in which glow discharges have been developed is given in Table 3.1 and will be summarised in the following discussion.

Table 3.1 Some applications of a radio frequency glow discharges

- |                                       |   |                                 |
|---------------------------------------|---|---------------------------------|
| i) Chemistry :                        | synthesis<br>rearrangement<br>degradation<br>polymerisation | (thick films<br>(thin coatings) |
| ii) Surface modification of polymers: | cross-linking<br>oxidation<br>grafting                      |                                 |
| iii) Ashing and Etching:              | trace analysis<br>Interface analysis                        |                                 |
| iv) Sputtering <sup>143</sup> :       | deposition<br>etching                                       |                                 |

### 3.3.1 Preparative Organic Plasma Chemistry <sup>144</sup>

Although equilibrium 'hot' plasmas have been used for a number of inorganic reactions, their use in organic chemistry is limited due to the low thermal stability of most organic substances. Research into organic aspects of plasma chemistry has focussed on the synthesis of new compounds and preparation of known substances via easier or more economic routes, using the 'cool' plasma as an alternative means by which energy may be transferred to molecules. Typical reactions occurring in glow discharges are:

- 1) Generation of atoms or radicals
- 2) Isomerisation
- 3) Elimination of atoms or small groups
- 4) Dimerisation and polymerisation
- 5) Reactions involving a complete scrambling or destruction of the starting material

All but the last type have shown results which are of value to preparative chemistry. Since the chemistry involved in these reactions is rather complex, it is not surprising that the study of mechanism of plasma reactions is fraught with difficulty: attempts to facilitate the investigation of mechanistic pathways have employed simple model compounds. <sup>240</sup> Similarities have been observed between the reaction products obtained from certain substances using the plasma as the reactive medium and those formed in systems activated by related methods such as pyrolysis <sup>241</sup> and photolysis, <sup>144</sup> for which mechanisms are somewhat better understood.

Preparative organic synthesis in glow discharges is still in the early stages of development. No doubt, with improved diagnostic techniques,

a better understanding of the basic processes involved will lead to improved selectivity of reaction, optimisation of yield and growth of the field as a whole.

### 3.3.2 The Application of Plasma Techniques to Polymers

There are basically three areas of polymer science in which plasmas have been utilised, namely plasma polymerisation, surface modification of polymers and polymer etching. Discussion of the latter will be given in Section 3.3.4; modification of the surfaces of a range of polymer systems forms part of the experimental work of this chapter and is introduced in Section 3.5.

### 3.3.3 Plasma Polymerisation

The glow discharge synthesis of polymers has been a particularly active area of research, especially in industrial laboratories.<sup>145</sup> The attractiveness of this approach stems from the capability of producing pore-free, uniform films of superior physical, chemical, electrical and mechanical properties.<sup>134</sup>

The basic experimental set-up comprises a means of introducing the 'monomer' into an appropriate reactor in which the plasma is excited, and a system to enable substrates to be introduced to interact with the plasma. (In this context the term 'monomer' describes the low molecular weight starting materials used in these studies. Due to the complexity of the processes taking place in the plasma it is often not possible to identify the true precursor to polymerisation.) With suitable vacuum line techniques and provision for heating or cooling sample reservoirs, it is possible to work with monomers encompassing a wide range of volatilities. The plasma polymerised film may be deposited either on an inert substrate or by direct interaction with, for example, a polymer,

as in the case of grafting.<sup>146-7</sup> Alternatively, plasmas excited in inert gases<sup>126</sup> may be employed to effect modification at the surface of a polymer via selective energy transfer (both direct and radiative) to yield a cross-linked surface network.

The principal advantages of glow discharge synthesis of polymer films are as follows:

- 1) The technique is applicable to batch or continuous processing
- 2) There is low initial capital outlay
- 3) It may be suitably applied to a wide range of systems
- 4) Close control may be exercised over experimental conditions.

It should also be noted however that such films cannot be produced to a specific formula; although the reproducibility of composition and surface characteristics of a polymer film produced by the glow discharge technique, under fixed experimental conditions, is high. Thick films tend to be rather brittle and discoloured.

A variety of analytical techniques have been used in the characterisation of plasma polymerised films.<sup>148-151</sup> These include both chemical and physical methods and may relate to either the bulk or surface properties of the film. It is of particular relevance to this thesis to note the important contribution which has been made by ESCA to the understanding of the complexities of the processes involved.<sup>152-3</sup>

A 'state of the art' account of plasma polymerisation will be given by AbRahaman.<sup>154</sup>

### 3.3.4 Plasma Ashing and Etching

Radio frequency glow discharges have found considerable applications in the area of chemical and physical analysis.<sup>155</sup>

The R.F. plasma has been employed successfully, in conjunction with other methods, to help resolve a number of analytical problems in wide-ranging disciplines.

Although oxygen plasmas have received the most attention in the realms of 'low temperature ashing', (LTA), as the technique has been named, the use of plasmas excited in hydrogen, a to date little explored medium, may be attractive where oxidising conditions are to be avoided.

The principal advantages of LTA, compared with chemical 'wet-ashing' or high temperature ashing using a muffle or combustion furnace operating at  $\sim 600-900^{\circ}\text{C}$ , lie in the fact that the process employs a dry gas at low temperatures, typically ranging from room temperature to  $250 - 300^{\circ}\text{C}$ . Thus the physical structure of the sample tends to be retained whilst chemical contamination, degradation and removal of readily volatilised elements is kept to a minimum, thereby facilitating trace analysis. 180-1, 183-4

In the plasma ashing experiment the sample to be treated is placed on a glass slide, dish or boat inside the reaction chamber. The plasma is initiated in a flowing gaseous environment at an operating pressure in the region of 0.5 - 1.5 torr. Samples may be in the form of powders, flat sheet, microtomed section, film, foam, microscopic specimens, or even liquids of low vapour pressure: the plasma ashing of whole mice has been reported. 181

The reaction mechanisms are very complex, especially for heterogeneous systems such as oxygen plasma interacting with coal 183 or biological tissue, and it is not possible to obtain detailed information on the precise mechanistic pathways by which these ashing processes occur. When oxidisable organic material is present, CO and CO<sub>2</sub> are formed most commonly and these products lend a blue tinge to the emitted visible

radiation from the plasma: pure oxygen is pink under discharge conditions. The colour change from blue to pink gives an indication of the completeness of ashing; change in weight may also be used. For thorough ashing of powder samples, it may be necessary to stir or redistribute the ash at intervals during plasma treatment so as to prevent the formation of a layer of ashed material which would otherwise inhibit further reaction.

The recovery of trace constituents from largely organic matrices on LTA through the plasma oxidation of the organic phase has been used in the analysis of trace elements present in a variety of biological specimens:<sup>180-1,183-</sup> The factors governing the retention of a given element during ashing have been investigated and include the nature of the plasma and the chemical environment in which the element is bound.<sup>156</sup>

Microscopic techniques have been used to study the structure of the residual ash.<sup>183-4, 186</sup> The preservation of the plasma ash pattern of biological specimens by subsequent coating with a plasma polymerised thin film has been reported.<sup>157</sup>

The fields of application of plasmas to inorganic materials analyses include geochemical, metallurgical, marine and soil sciences.<sup>155</sup> With the exception of coal, most of these materials have a high ratio of inorganic/organic phases and often it is desirable to remove the low level organic materials before analysis, to separate phases at low temperature without destroying their chemical or physical nature, and to minimize volatilisation and sintering.

The removal of the outermost layer of a sample by means of a plasma, plasma etching, has been applied to a wide range of materials, including organic polymers,<sup>158</sup> bio-organic materials, carbon and graphite, metals and other inorganic materials.<sup>155, 186</sup> Plasma etching has been used to reveal crystalline or multiphase fine structure, three dimensional ash

structures<sup>159</sup> and mineral distributions. Particular application of plasma etching is to be found in the removal of photoresist materials used in the semiconductor industry,<sup>160</sup> and in the study of interfaces such as those present in Langmuir multilayer based electronic devices comprising III-V semiconductors.<sup>161</sup> Selective etching<sup>143</sup> may be achieved by obtaining a favourable etch-rate ratio between the materials under consideration, and may be enhanced by using plasmas excited in gaseous mixtures,<sup>162</sup> and those containing fluorocarbon molecules.<sup>182</sup>

### 3.4 Geochemical Applications of Plasma Chemistry

The application of plasma chemistry to geochemical substances may be divided into two broad areas:

- 1) Plasma pyrolysis and gasification of fossil fuels.
- 2) Analysis of the mineral component of materials as a means of estimating the amount of organic oxygen present.

A recent account of the plasma chemistry of fossil fuels<sup>163</sup> reviews the areas of research currently underway which aim to develop the production of organic compounds from complex organic materials such as coal, shale and tar using plasma degradative techniques. This is likely to be of growing importance in the manufacture of acetylene and natural gas, the fossil fuel in shortest supply and greatest demand, and also provide new routes to the molecules which act as building blocks in large-scale organic chemical production. Various types of plasma have received attention, namely glow discharges,<sup>165</sup> microwave discharges,<sup>164</sup> electrical arcs and plasma jets.<sup>166, 187-8</sup> Hydrogen, nitrogen, argon, carbon dioxide and mixtures of these gases have been used as the exciting medium.<sup>163-4</sup> The review by Venugopalan et al also discusses the

application of lasers <sup>167</sup> and flash heating techniques, and the status of work on plasma desulphurisation of coal and petroleum.

The second area of application relates to the problems associated with oxygen stoichiometry in analyses of coal and related materials, a subject reviewed by Volborth <sup>168</sup> in some detail, and discussed in Chapter Two of this thesis. The determination of organic oxygen content is important for the classification, assessment and utilisation of coal. The method of determining oxygen content 'by difference' is unreliable; moreover it considers only the total oxygen found in the analysed sample and not the organic oxygen component. A knowledge of the original mineral composition of a coal is therefore necessary. This is especially so when the characteristic properties of a coal are being evaluated. Formulae have been proposed to give an estimate of the percentage mineral matter content from high temperature ashing. <sup>169,170</sup> Relationships between the mineral matter and inorganic oxygen content in the ash are available in the literature. <sup>171-2</sup>

The low temperature ashing procedure based on that described by Gluskoter <sup>173</sup> in 1965 has been used to analyse ash for its component minerals. Hamrin and co-workers <sup>174</sup> have emphasized the importance of subtracting the determined inorganic oxygen content in order to obtain a more accurate value for organic oxygen by the formula

$$O_{\text{org}} = O_{\text{tot}} - O_{\text{inorg}} \quad (3.2)$$

Even though LTA is far more gentle than the high temperature ashing method, during which alteration of the nature of the mineral matter is known to occur, the ash so formed does not contain all the mineral matter in the coal in its original state. Several research groups have pointed out the problems in the LTA determination: <sup>175-7</sup> some pyrite may be oxidised

to haematite and some organic sulphur may be fixed in the ash as sulphate, especially in sub-bituminous coals and lignites.

$\text{SO}_3$  fumes may form, partially decomposing the carbonates, and considerable nitrogen and unburned carbon may be present. These unwanted side reactions cannot be totally eliminated and it follows then that equation 3.2 is not strictly correct. However, Miller, Yarzab and Given<sup>177</sup> have described a new method for determining the mineral matter contents of coals, based on LTA, using an oxygen plasma in which these side reactions are minimized, thereby providing an accurate and rapid evaluation.

Studies of the plasma ashing of coal and other geochemical samples have concentrated on either kinetic aspects using weight loss measurements and analysis of the gaseous products evolved, or have focussed on the composition, both chemical and structural, of the residual ash. Analytical methods employed in the study of the ash have included infra-red spectroscopy,<sup>178</sup> X-ray diffraction,<sup>173</sup> chemical analyses<sup>173</sup> and more recently instrumental neutron activation analysis.<sup>179</sup>

The work to be presented in a later section of this chapter (Section 3.6) is concerned with the interaction of the species existing in 'cool' plasmas (for the most part those excited in oxygen) with the surface region of some materials of geochemical interest (a selection from those already encountered in Chapter Two). Emphasis is to be placed on the initial changes brought about by very mild plasma treatments, with the aim of introducing a certain selectivity to the attack in an attempt to probe the relative susceptibility of the materials to the reactive species. In such an investigation ESCA allows small changes in surface functionalisation to be monitored with ease, in the initial stages of reaction where bulk analytical techniques would detect no change.

### 3.5 Modification of polymer surfaces by oxygen plasmas

#### 3.5.1 Introduction

Complementary to the investigation of the changes, as detected by ESCA, affected by low power inductively coupled R.F. plasma, excited in oxygen on the coal, kerogen and bitumen samples analysed in Chapter Two, a selection of polymer samples were also treated under similar conditions.

The rationale behind this study is two-fold. Firstly, research in Durham <sup>126, 212-3</sup> has shown that 'cool' plasmas may be conveniently used to affect functionalisation at polymer surfaces in a controlled manner, both in terms of extent of reaction and the range over which functionalisation occurs. In the particular case of oxygen plasmas, <sup>213</sup> it has become evident that a variety of functionalities may be introduced and studies of polyethylene (high and low density), polypropylene and polystyrene indicate the surface sensitivity and selectivity of the process. Comparing and contrasting the extent of oxygen uptake during the initial stages of interaction of an oxygen plasma (0.2 torr and 0.4W) with polyethylene and polystyrene films reveals the greater susceptibility of polystyrene to the oxidation. Clark and Dilks found the relative order of reactivity of the three polymers towards the oxygen glow discharge to be polystyrene > polypropylene > polyethylene, which is entirely reasonable in terms of the relative reactivities of unsaturated versus saturated systems and of tertiary versus primary and secondary C-H bonds. The reaction is rapid and is essentially complete after approximately five seconds as far as the change in surface composition revealed by ESCA is concerned. Figures 3.7 and 3.8 show the core level spectra of polyethylene and polystyrene before treatment and after exposure to oxygen plasma respectively. The greater susceptibility of the unsaturated system is clearly evident.

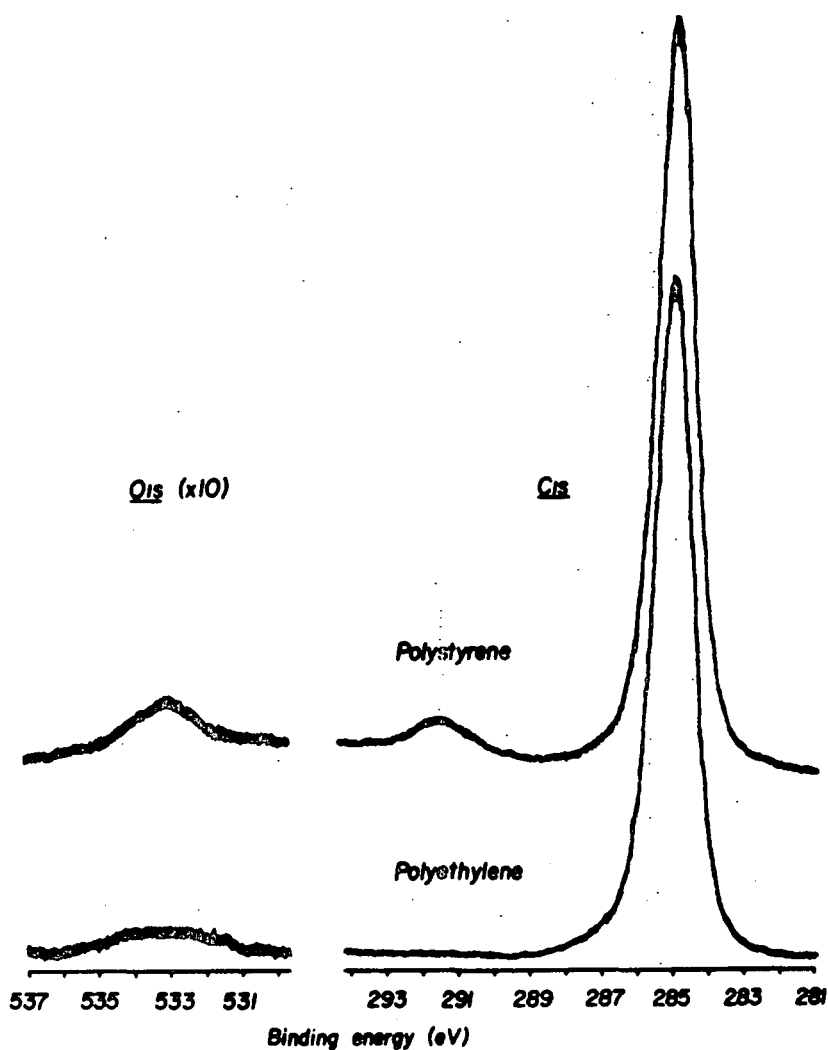


Figure 3.7 ESCA core level spectra of untreated samples of polyethylene and polystyrene films

On increasing the time of exposure to an oxygen plasma (0.2 torr, 0.1W) all the components of the  $C_{1s}$  spectra of treated polyethylene and polystyrene films were found to reach a constant intensity after approximately 16 seconds, by which time a high extent of surface oxidation had taken place. The relevant spectra for polyethylene are reproduced in Figure 3.9. The data presented by Clark and Dilks<sup>213</sup> demonstrate that the

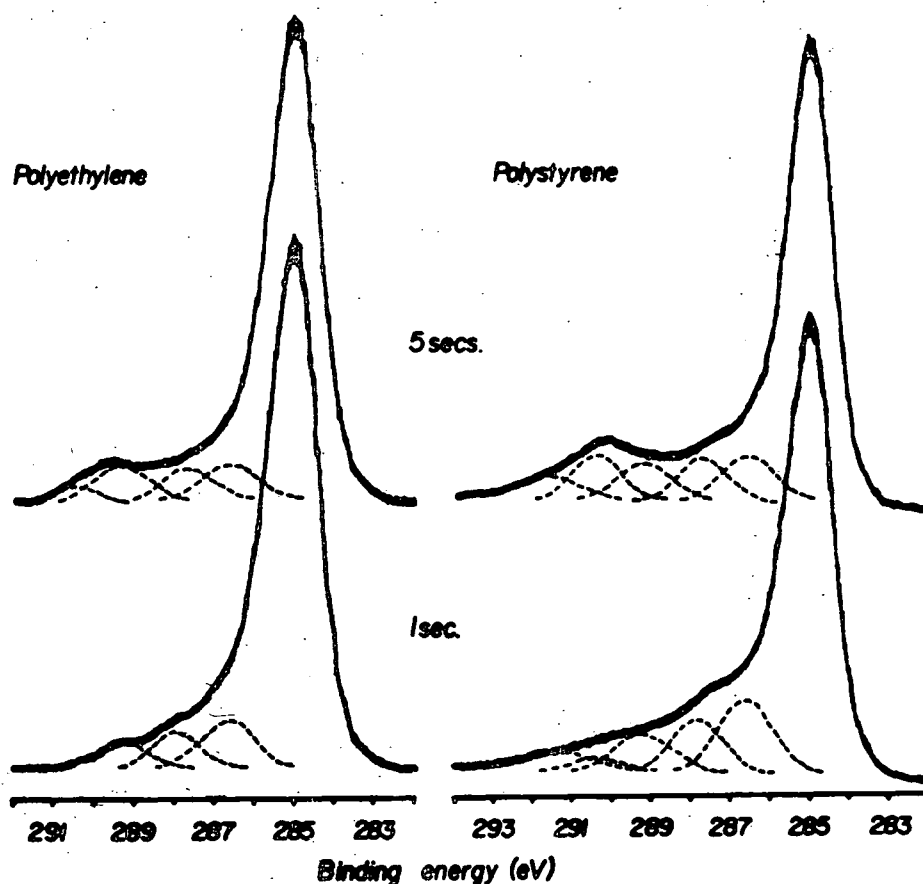


Figure 3.8 C<sub>1s</sub> spectra for examples exposed to an oxygen plasma (0.2 torr, 0.4W) for 1 and 5 sec

overall compositions of the oxidised polymers, when oxidations are carried out in pure oxygen plasmas at low power, are sensitive functions of the molecular structures of the starting materials. It follows that the use of polyethylene and polystyrene films as a means of monitoring the effects of the plasmas subsequently employed in reaction with materials of ill-defined composition should aid the development of a more thorough understanding of the complex processes involved. This approach has been extended to include a variety of polymer systems each having functionalities of particular interest.

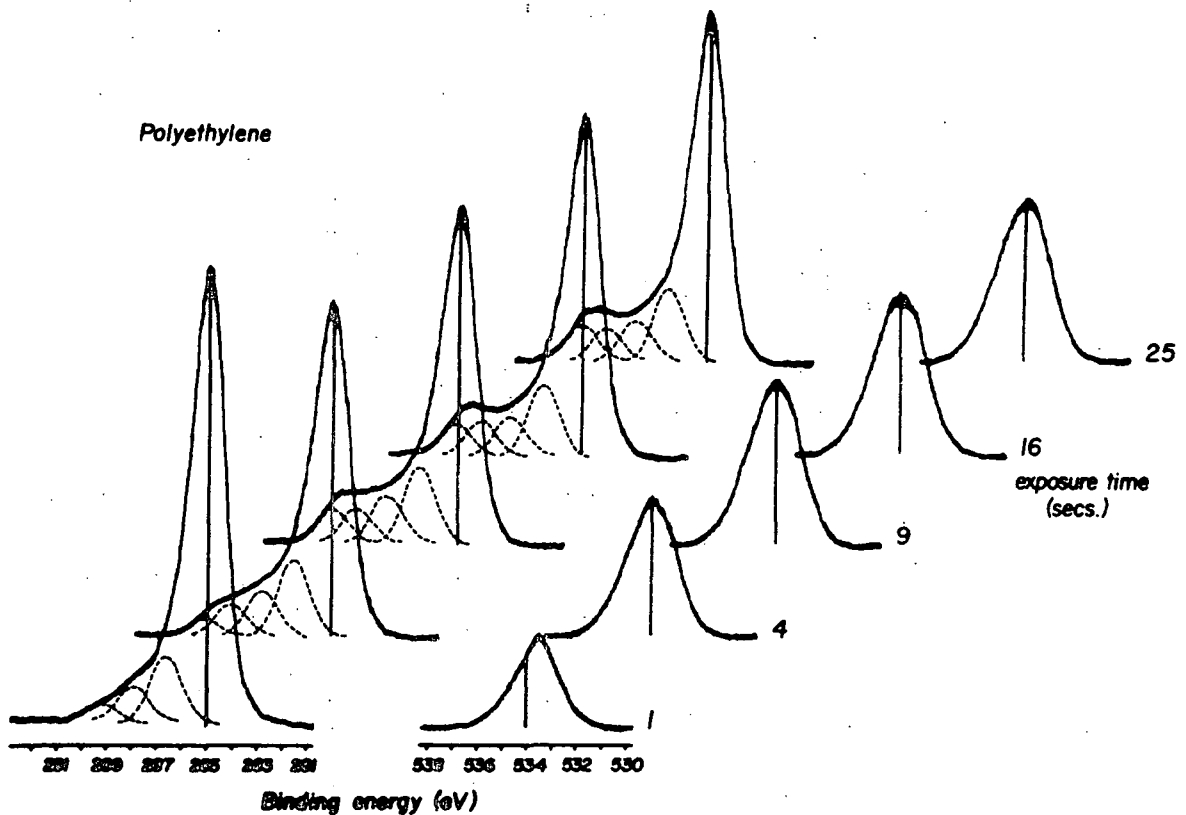


Figure 3.9 C<sub>1s</sub> and O<sub>1s</sub> spectra of polyethylene versus time of exposure to an oxygen plasma (0.2 torr, 0.1W)

Secondly, the surface modification of polymers, especially those in film form, is an area of considerable technological and industrial importance in its own right.<sup>214</sup> Electrical discharge (radio frequency, microwave and corona) excited in a variety of gases is a technique widely used as a method to increase the surface free energy and wettability of the material.<sup>215</sup> This procedure has the advantage over wet chemical processes in that the interaction occurs at the gas/solid interface.

It is a clean reaction which takes only seconds to achieve the required results and is therefore ideally suited to a flow-system. Whilst producing profound changes in the surface properties of the polymer (permeability, bondability, printability), the overall properties of the material, for which it was originally chosen, remain unchanged (electrical characteristics, tensile strength etc.).

The advent of surface sensitive forms of spectroscopy has, in recent years, allowed considerable progress to be made in the investigation of the surface chemistry brought about by a variety of surface treatments of polymers. This is particularly true in the case of glow discharge techniques where the thickness of the modified layer has been estimated to be in the range of 0 to 10 $\mu\text{m}$ ,<sup>133</sup> depending on the conditions of the discharge (pressure, power, gas and flow rate).

### 3.5.2 Experimental

#### 3.5.2a Polymer Samples

This investigation involved a total of seven different homopolymers (Figure 3.10) studied in the form of thin films. Details of the origins of the polymer samples are as follows:

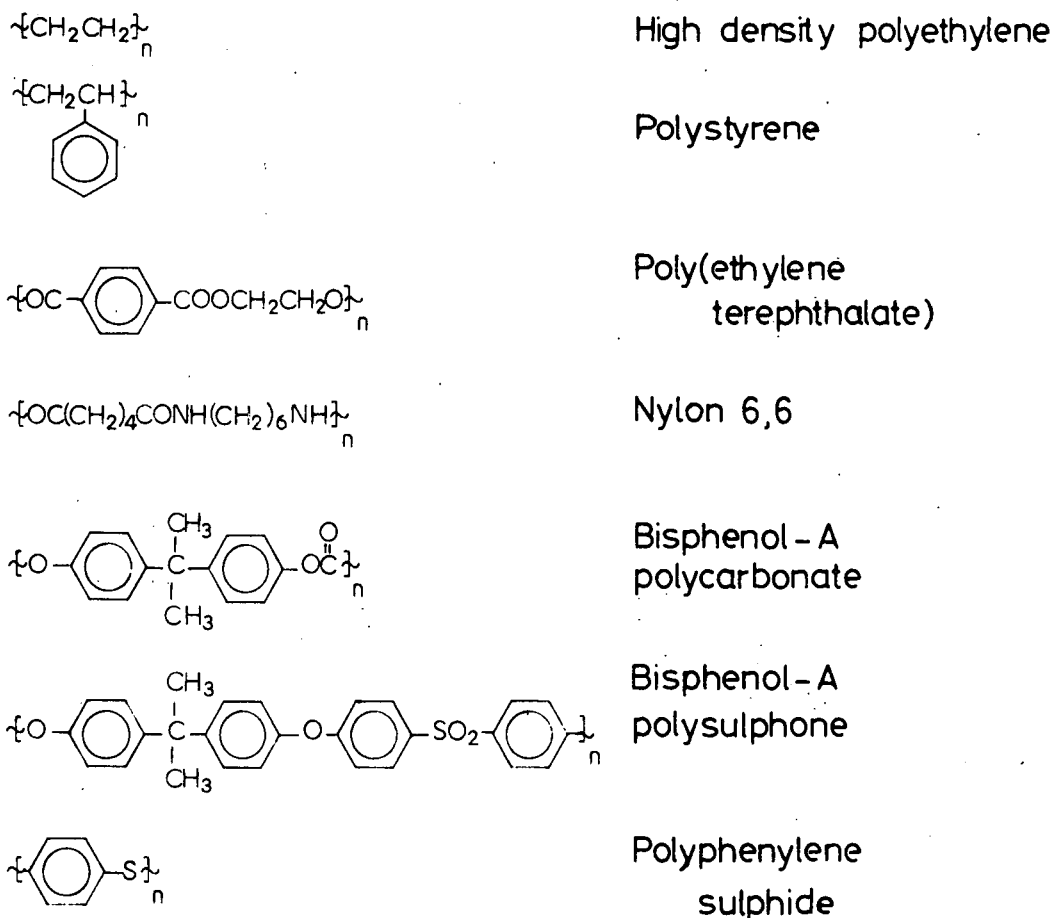


Figure 3.10 Polymers Investigated

- 1) High density polyethylene (HDPE) TFE 554 was supplied by the Metal Box Company and is known to contain the antioxidant Irganox 1076, [Octadecyl 3-(3,5-diterbutyl-4-hydroxyl phenyl) propionate] at the 0.016% level.
- 2) Polystyrene film was supplied by Dr A. Davis of the Ministry of Defence.
- 3) Poly(ethylene terephthalate), (PET), 'Mylar' film was supplied by Dr T. Kent of the Home Office (PSDB).
- 4) Nylon 6,6 was manufactured by Cellomer Associates.

- 5) Bisphenol-A polycarbonate film was cast onto glass from a 12% wt/vol solution in chloroform.
- 6) Bisphenol-A polysulphone film was prepared by Dr A. Davis, MOD.
- 7) Polyphenylene sulphide, 'Ryton' was manufactured by Phillips Chemical Company.

Also included in this study was a sample of ferrous sulphide (technical grade), representative of an inorganic sulphide.

#### 3.5.2b Sample Preparation

All films were used in their 'as received' forms without pretreatment. Prior to being subjected to plasma modification, samples were mounted on a spectrometer probe-tip composed of copper by means of double-sided adhesive 'Scotch' insulating tape. In the case of the ferrous sulphide sample, a small portion of the solid was crushed to a powder using a pestle and mortar. The powder was then pressed onto the tape with the aid of a metal spatula and the excess that had not adhered was tapped off.

#### 3.5.2c Plasma Instrumentation

Plasmas were excited in all cases using a Tegal Corporation radio frequency generator capable of delivering a power output from 0.05 - 100 watts, continuously variable and operating at a frequency of 13.56 MHz. (This is a frequency allotted by international communications authorities at which one can radiate a certain amount of energy without interfering with communications.) The system includes

a pulsing facility which may be employed on a microsecond time scale to give greater stability to the plasma at low average power loadings ( $< 1$  W). Tuning of the radio frequency power<sup>216</sup> was achieved by an L-C matching network in an inductively coupled mode and monitored by the standing wave ratio using a Heathkit HMI02 R.F. power meter.

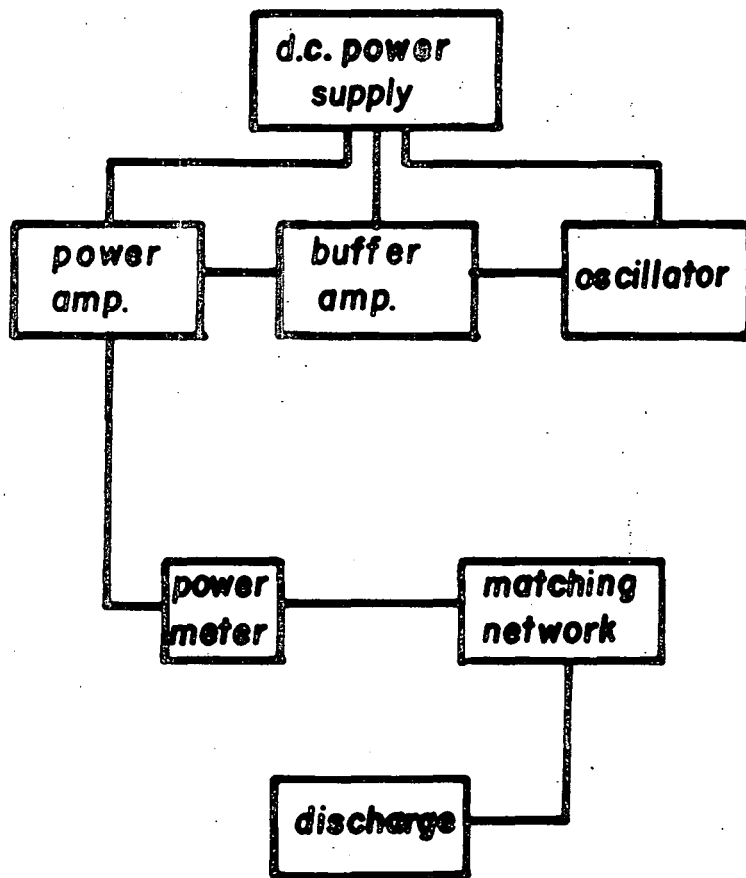


Figure 3.11 Schematic representation of the plasma rig electronics

The purpose of this network is to increase the power dissipation in the discharge and to protect the generator. A schematic of the electronics associated with the plasma rig is shown in Figure 3.11.

### 3.5.2d Plasma Configuration

The plasma reactor was mounted in a greaseless vacuum system, pumped by a two stage rotary pump with a pumping speed rating of  $50 \text{ l min}^{-1}$ . Pressures were monitored using a Pirani vacuum gauge for oxygen plasma work and the gas introduced via a leak valve.

The reactor consisted of 6cm diameter Pyrex tubing in an inverted 'T' shape configuration, as shown in Figure 3.12.

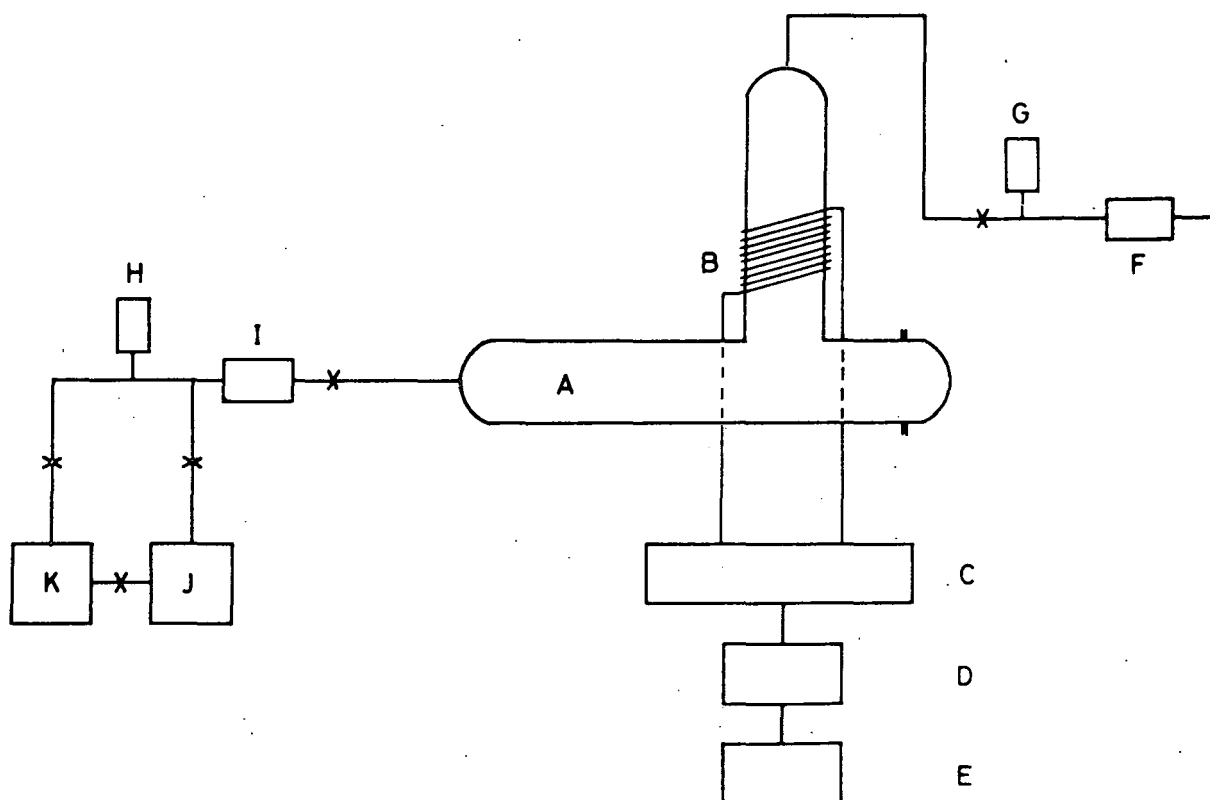


Figure 3.12 Schematic diagram of the inductively coupled R.F. plasma instrumentation: A, reactor; B, R.F. coil; C, matching unit; D, standing wave ratio bridge; E, R.F. source; F, leak valve; G, Pirani gauge; H, Penning gauge; I, cold trap; J, backing pump; K, diffusion pump; X, vacuum valve.

The overall dimensions were 37cm long and 30cm high, with inlet and outlet tubes 1/4" and 1/2" diameter respectively, the inlet tube being at the top. The discharge was excited in the vertical limb by a 9 turn 6 $\mu$ H copper coil electrode wound externally and centred 18cm from the inlet tube.

The premounted sample was positioned on a glass slide resting on the walls of the reactor such that the sample was positioned along the length of the reactor, its surface horizontal and facing uppermost and lying 1.5cm from the reactor floor at the centre of the 'T'. (Since there is a concentration profile of ions, radicals and neutral species extending through the glow region and into the region immediately outside of the reactor, the orientation of the sample in relation to the reactor geometry becomes important if processing under reproducible conditions is to be affected.) 132, 217

### 3.5.2e Experimental Procedure

The sample, mounted on the probe-tip, was positioned in the plasma reactor and the system evacuated to a pressure in the region of  $5 \times 10^{-2}$  torr. Oxygen gas from standard laboratory cylinders, obtained from the British Oxygen Corporation, was used without further purification. The vacuum line was flushed with oxygen gas, evacuated, and then let up to the required pressure (0.2 torr) via a leak valve. The system was purged for approximately 20 minutes before the glow discharge was initiated. In this way any residual nitrogen would be removed, and allowed an equilibrium flow to be established.

Chosen power settings for this investigation were 10 W and 0.4 W, the latter achieved by means of the pulsing facility described previously; a treatment time of 5 seconds was used throughout. The characteristic

electromagnetic output in the visible region gave a pale white tinge to the oxygen plasma and was sometimes very difficult to observe at the 0.4 W power setting. In all cases the glow region extended throughout the length of the vertical coil region and for a substantial distance on either side of the sample position in the horizontal portion of the reactor.

Once treated, the polymer was removed from the reactor, attached to the spectrometer probe and introduced into the spectrometer via the fast insertion lock. Typically, ESCA analysis began approximately three minutes after treatment and took 40 minutes to complete.

#### 3.5.2f ESCA Instrumentation

Spectra of the untreated and plasma modified samples were recorded on the A.E.I. ES200B spectrometer using  $MgK\alpha_{1,2}$  radiation as previously described. In all cases the measured binding energies are quoted with a precision of  $\pm 0.2$  eV and area ratios, determined by curve fitting procedures,  $\pm 5\%$  accuracy.

#### 3.5.3 Results and Discussion

It is convenient here to present an account of the comparisons which can be made from the effects of oxygen plasma treatment at 10 W and 0.4 W power settings at a pressure of 0.2 torr and treatment time 5 seconds on samples of polyethylene and polystyrene film. From the knowledge so obtained, together with preliminary data regarding the extent of reaction (as far as ESCA is concerned) of the geological materials at the higher power setting, and the more thorough study of gilsonite (Section 3.6.2a), the grounds on which the more gentle oxygen plasma was chosen for the major part of the work in this chapter will

become clear. Discussion of the changes occurring for each polymer system will be dealt with in turn, before summarising the conclusions which may be drawn regarding the surface effects of such oxygen plasma treatments on the polymer films as a whole.

### 3.5.3a Polyethylene, Polystyrene, Poly(ethylene terephthalate) and Bisphenol-A polycarbonate polymer films

The core level spectra for the untreated and plasma treated samples of polyethylene and polystyrene are displayed in Figures 3.13 and 3.14. The oxygen plasma treatments, at either power setting, clearly give rise to considerable oxidative functionalisation.

The information levels available from the ESCA experiment have been covered in Chapter One. However, the particular features of interest in this study arise from analyses of:

- 1) The integrated relative intensities of  $C_{1s}$  and  $O_{1s}$  core levels, particularly as a function of the electron take-off angle  $\theta$  (either  $30^\circ$  or  $70^\circ$  normal to the sample surface).<sup>†</sup>
- 2) The component peak analysis of the individual core level band profiles.

---

<sup>†</sup> The spectrometer configuration was such that the X-ray source and entrance slit to the analyser were at right angles to one another. A take-off angle of  $90^\circ$  therefore corresponds to grazing exit with respect to the sample surface (Figure 1.12). The ESCA sampling depth varies with take-off angle, spectra at  $\theta = 30^\circ$  and  $70^\circ$  relating to 'subsurface' and 'surface' composition respectively. Hence depth profiling may be achieved using angular dependence studies. This subject, and the angular dependence of absolute and relative peak intensities has been discussed elsewhere. 212

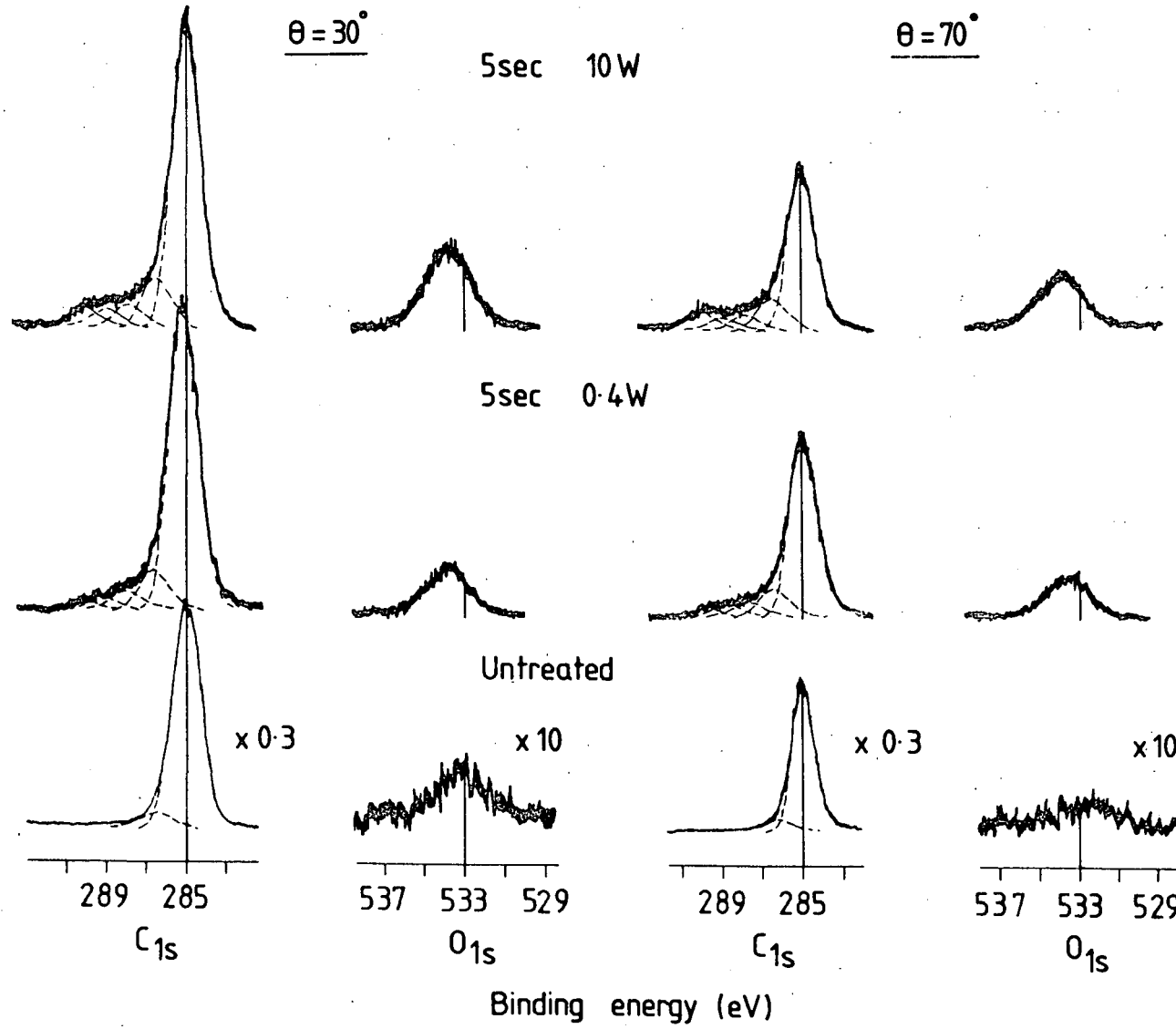


Figure 3.13  $C_{1s}$  and  $O_{1s}$  spectra of polyethylene before and after oxygen plasma treatment (0.2 torr)

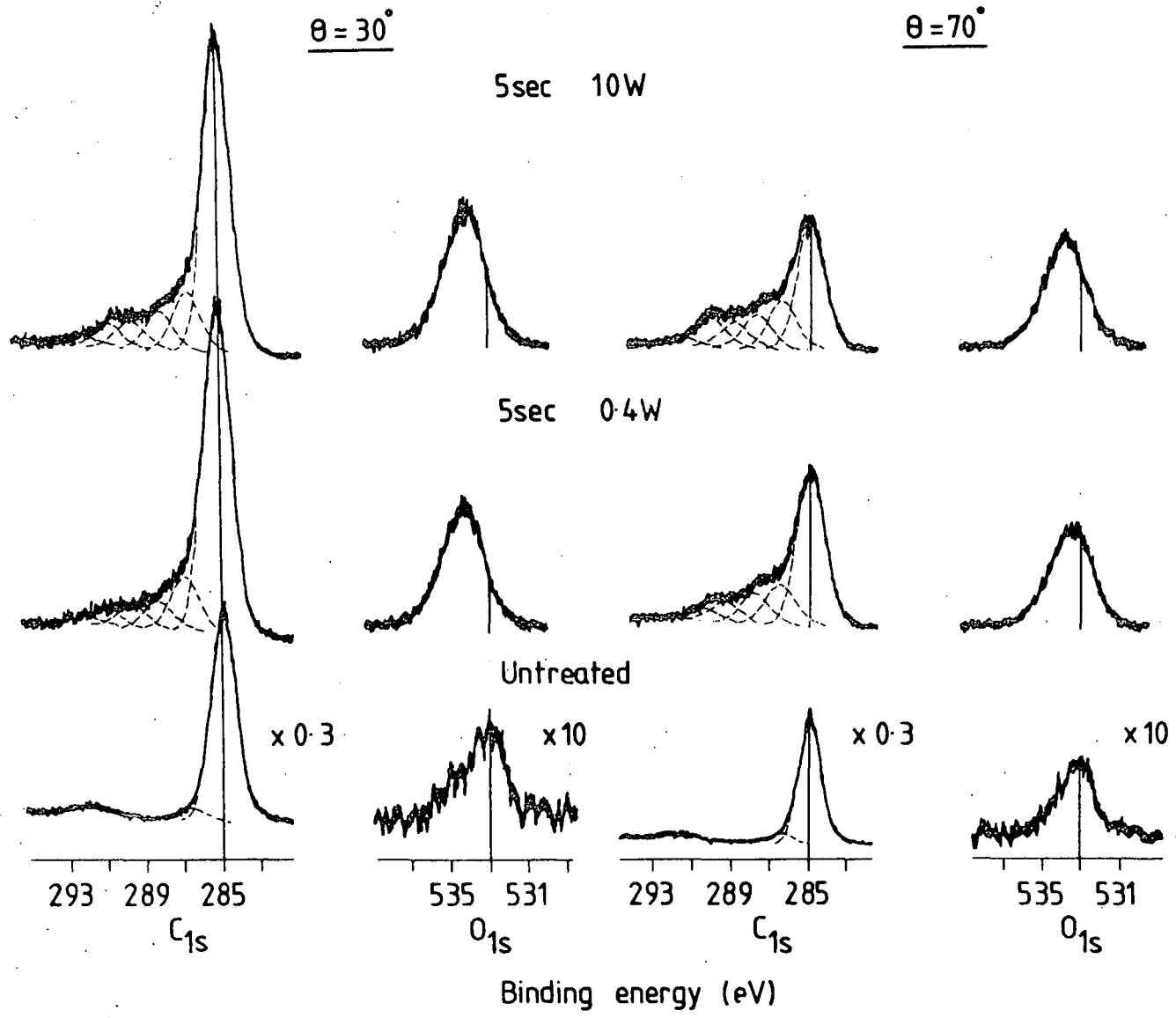


Figure 3.14  $C_{1s}$  and  $O_{1s}$  spectra of polystyrene before and after oxygen plasma treatment (0.2 torr)

This oxidative functionalisation is evident by the increased intensity of the  $O_{1s}$  core level signal and the development of a shoulder to the higher binding energy side of the  $C_{1s}$  photoelectron peak at 285 eV representative of  $(\underline{C}H_2)_n$  environments. Analysis of the  $C_{1s}$  levels of both polyethylene and polystyrene at the  $30^\circ$  and  $70^\circ$  take-off angles by standard line shape analysis shows that the oxidative functionalisation provides  $\underline{C} - O$ ,  $>\underline{C} = O$ ,

$$\begin{array}{c} O \\ || \\ \underline{C} - O \end{array} \text{ and } \begin{array}{c} O \\ || \\ - O - \underline{C} - O \end{array} \text{ structural features.}$$
 In the case of the plasma treated polystyrene films, there is a marked decrease in the  $C_{1s}$  component occurring in the region of 292 eV associated with low-energy  $\pi \rightarrow \pi^*$  shake-up transitions accompanying core ionisation.<sup>39</sup> This is indicative of oxidative attack on the aromatic ring.

In the case of polyethylene, whilst for the untreated material the low level of oxygen functionality (corresponding to  $\sim 1$  carbon in 150) is manifest in terms of a low intensity  $O_{1s}$  peak, corresponding to  $\sim 1\%$  of the intensity of the  $C_{1s}$  peak; for the oxygen plasma treated sample (0.4W, 5 sec) the  $O_{1s}$  levels correspond to  $\sim 19\%$  and  $27\%$  of the  $C_{1s}$  intensity at take-off angles of  $30^\circ$  and  $70^\circ$  respectively. A similar trend is apparent for polystyrene film, although the extent of reaction, as far as the level of oxygen uptake is concerned, is greater. The distinctive difference for the two take off angles confirms that reaction is confined to the outermost few monolayers and is therefore not detectable by IR or MATR for example. This suggests that the surface reaction is diffusion limited and the time scale of the experiment indicates that the reactive species in the plasma ( $O$ ,  $O_2^+$  etc.) react with low activation energy, even with saturated systems.

Comparing the spectra obtained from the stronger oxygen plasma of polyethylene and polystyrene with the spectra previously presented by Clark and Dilks,<sup>213</sup> it is apparent that the higher power treatment produces extensively oxidised surfaces for both polymers. For this reason the milder plasma treatment (0.4 W, 0.2 torr and 5 seconds) was used for the main part of the experimental work, so as to highlight any differences in modification which may occur.

The results of the deconvoluted spectra for the polymer systems, containing carbon and oxygen only, investigated under oxygen plasma are set out in tabular form (Table 3.2) and include those samples oxidised at the 10 W power setting. A convenient form by which 'at a glance' comparisons may be drawn between treated and untreated samples is presented in Figure 3.15.

Reasonable homogeneity exists between surface and subsurface for the untreated polymer samples as revealed by varying the take off angle. Slight contamination caused by the presence of silicon as silica ( $Si_{2p}$  at 102.1 eV binding energy detectable on the wide scan spectrum) accounts for ~ 74% of the oxygen signal at the surface of the polystyrene film. The untreated poly(ethylene terephthalate) shows a slightly more intense peak at 285 eV at  $70^\circ$  compared with the corresponding peak at  $30^\circ$  take-off angle. This points to a fine layer of hydrocarbon build-up on the film which would tend to mask the oxygen functionality at the very surface.

A feature which is common to all four polymers (and indeed is found in the other polymers containing nitrogen and sulphur functional groups) concerns the surface specificity of the modifications affected under the conditions of the oxygen plasma. The extent of oxidation is greater for the  $70^\circ$  take-off angle spectra. The aromatic polymer, polystyrene, is considerably more susceptible to oxygen plasma than the

Table 3.2 Oxygen plasma (0.2 torr) treatments of polymer films. Relative area intensities of C<sub>1s</sub> and O<sub>1s</sub> spectra at 30° and 70° take-off angles. (Total C<sub>1s</sub> peak taken as 100 units area)

	θ	Total C <sub>1s</sub> peak taken as 100 units area						O <sub>1s</sub>	C <sub>1s</sub> /O <sub>1s</sub>	
		C - H	C - O	>C = O	$\begin{array}{c} \text{O} \\    \\ \text{C} - \text{O} \end{array}$	$\begin{array}{c} \text{O} \\    \\ \text{O} - \text{C} - \text{O} \end{array}$	π → π*			
Polyethylene	Untreated	30°	95.2	4.8	-	-	-	-	1.1	90.9
		70°	94.0	5.5	0.5	-	-	-	1.1	90.9
	0.4 W, 5sec	30°	84.0	10.1	3.4	1.7	0.8	-	18.5	5.4
		70°	80.0	11.2	4.0	3.2	1.6	-	27.2	3.7
	10 W, 5sec	30°	76.3	11.5	5.3	3.1	3.8	-	30.5	3.3
		70°	69.9	13.3	6.3	3.5	7.0	-	35.7	2.8
Polystyrene	Untreated	30°	90.1	4.5	-	-	-	5.4	1.9	52.6
		70°	89.8	5.1	-	-	-	5.1	2.5	40.0
	0.4 W, 5sec	30°	73.5	11.8	5.9	3.7	2.9	2.2	39.7	2.5
		70°	61.3	15.3	11.0	7.4	4.3	0.6	65.0	1.5
	10 W, 5sec	30°	70.9	10.4	6.1	4.3	3.1	1.2	41.1	2.4
		70°	50.8	18.3	11.2	8.1	10.2	1.5	72.1	1.4

Table 3.2 (Continued)

	$\theta$	$\underline{\text{C}} - \text{H}$	$\underline{\text{C}} - \text{O}$	$= \underline{\text{C}} = \text{O}$	$\begin{array}{c} \text{O} \\ \parallel \\ \underline{\text{C}} - \text{O} \end{array}$	$\begin{array}{c} \text{O} \\ \parallel \\ \text{O} - \underline{\text{C}} - \text{O} \end{array}$	$\pi \rightarrow \pi^*$	$\text{O}_{1s}$	$\text{C}_{1s}/\text{O}_{1s}$	
Poly(ethylene terephthalate)	Untreated	30°	59.0	21.2	0.3	17.1	0.6	1.8	53.1	1.9
		70°	61.3	17.2	4.9	14.1	0.6	1.8	45.8	2.2
	0.4 W, 5sec	30°	52.4	25.7	-	19.9	1.6	0.5	66.7	1.5
		70°	53.2	16.0	11.2	17.0	2.7	-	67.8	1.5
Bisphenol-A polycarbonate	Untreated	30°	78.1	13.3	-	-	6.3	2.3	23.2	4.3
		70°	78.4	13.5	-	-	6.1	2.0	24.3	4.1
	0.4 W, 5sec	30°	66.7	16.7	5.3	4.0	5.3	2.0	38.8	2.6
		70°	64.0	19.2	5.9	5.0	5.0	0.8	46.0	2.2

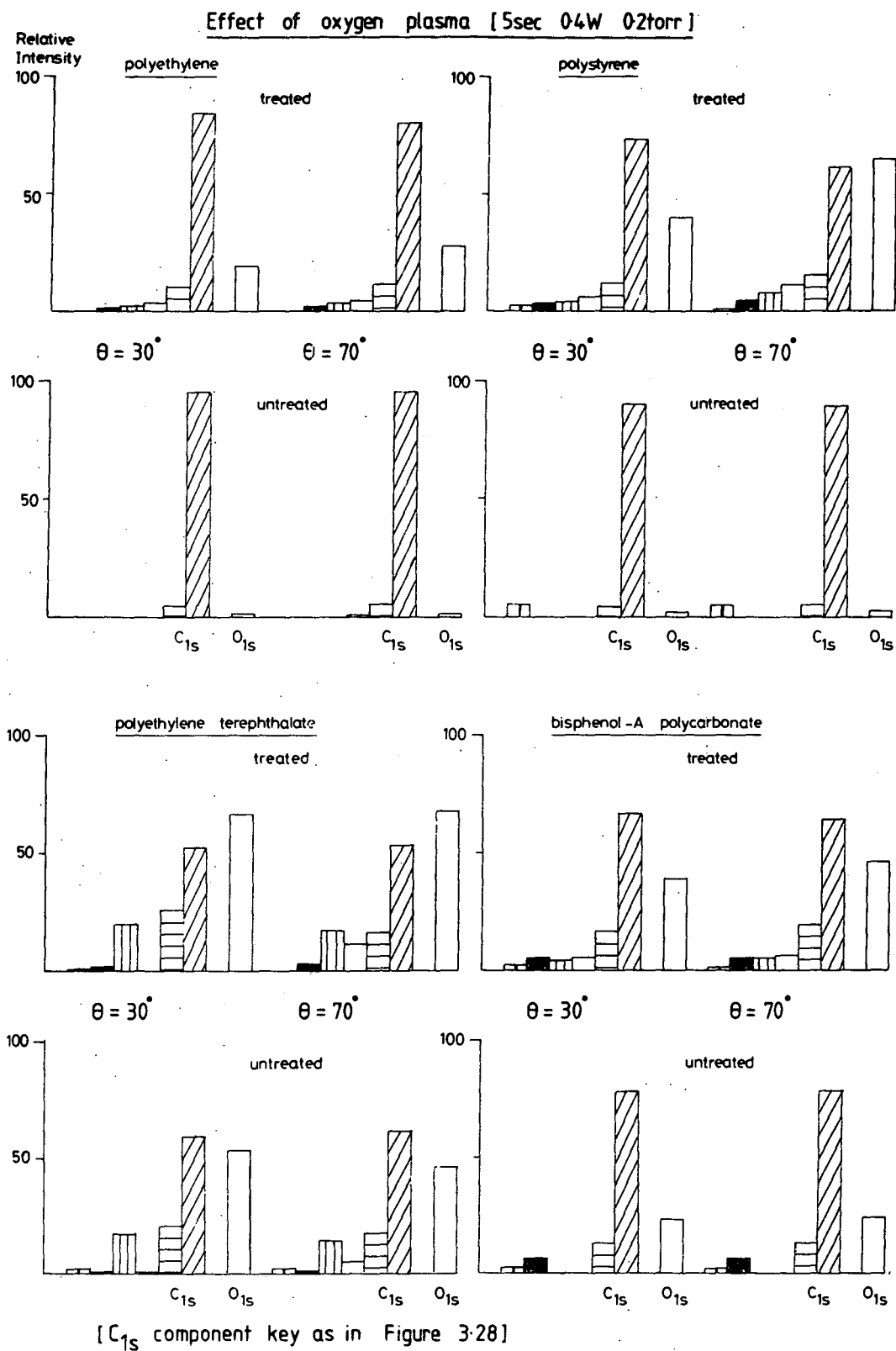


Figure 3.15 Effect of oxygen plasma treatment (0.2 torr) on polyethylene, polystyrene, poly(ethylene terephthalate) and bisphenol-A polycarbonate polymer films

saturated polymer high density polyethylene under identical conditions. The oxidation of polystyrene is accompanied by a substantial drop in aromatic surface composition. This is revealed by the decrease in the intensity of the shake-up satellite, arising from  $\pi \rightarrow \pi^*$  excitations accompanying core ionisation. A similar situation is found to exist for the other systems containing aromatic rings as part of the polymer chain backbone (in contrast to the pendant aromatic rings in polystyrene). The trend to become apparent is that the greatest decrease in aromatic character manifests itself at the outermost surface of the film.

### 3.5.3b Nylon 6,6, Polyphenylene sulphide, Bisphenol-A polysulphone and Ferrous sulphide

Turning now to consider the changes occurring when the polymer films of nylon 6,6, polyphenylene sulphide and bisphenol-A polysulphone are subjected to oxygen plasma treatment, it is convenient to consider the core level photoelectron spectra themselves, together with figures relating to the changes in overall elemental composition as revealed in the ESCA experiment. The pertinent spectra and data are to be found in Figures 3.16 - 18 and Table 3.3 respectively.

It is interesting to note that nylon 6,6 experiences a comparatively small oxygen uptake and very little change in nitrogen levels as far as chemical nature and concentration are concerned. Analysis of the  $C_{1s}$  envelope reveals low level hydroxyl formation (286.6 eV) accompanied by growth of a peak in the region of 289.5 eV binding energy which indicates the existence of  $\overset{O}{\underset{||}{C}} - O$  structural features present either as the free acid or ester functionalities. The former may be underestimated due to the proximity of the predominant  $\underline{C} - H$  peak (285 eV) and  $\underline{C} - N$  signal (286.1 eV).



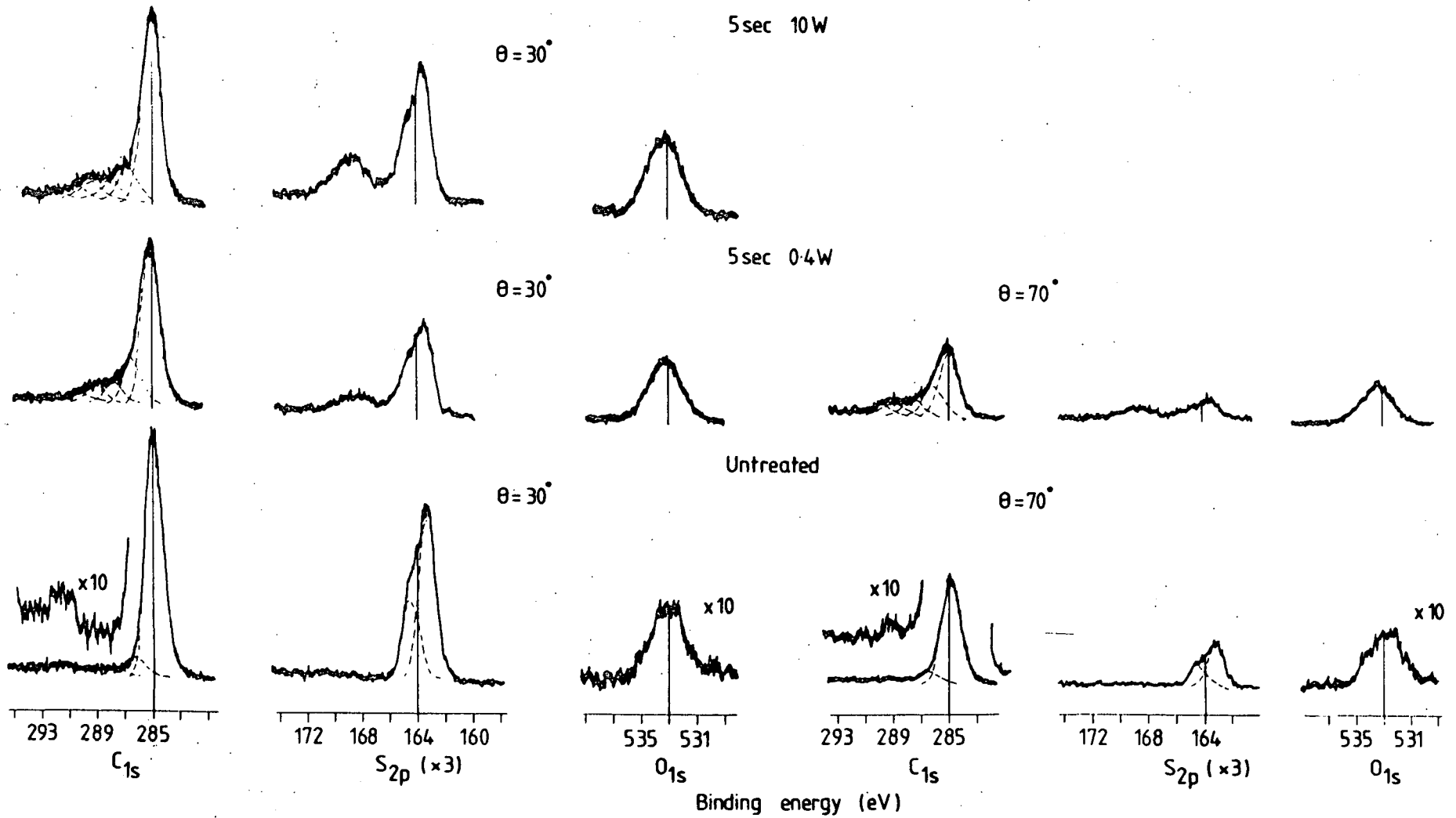


Figure 3.17 Effect of oxygen plasma on the core level spectra of polyphenylene sulphide

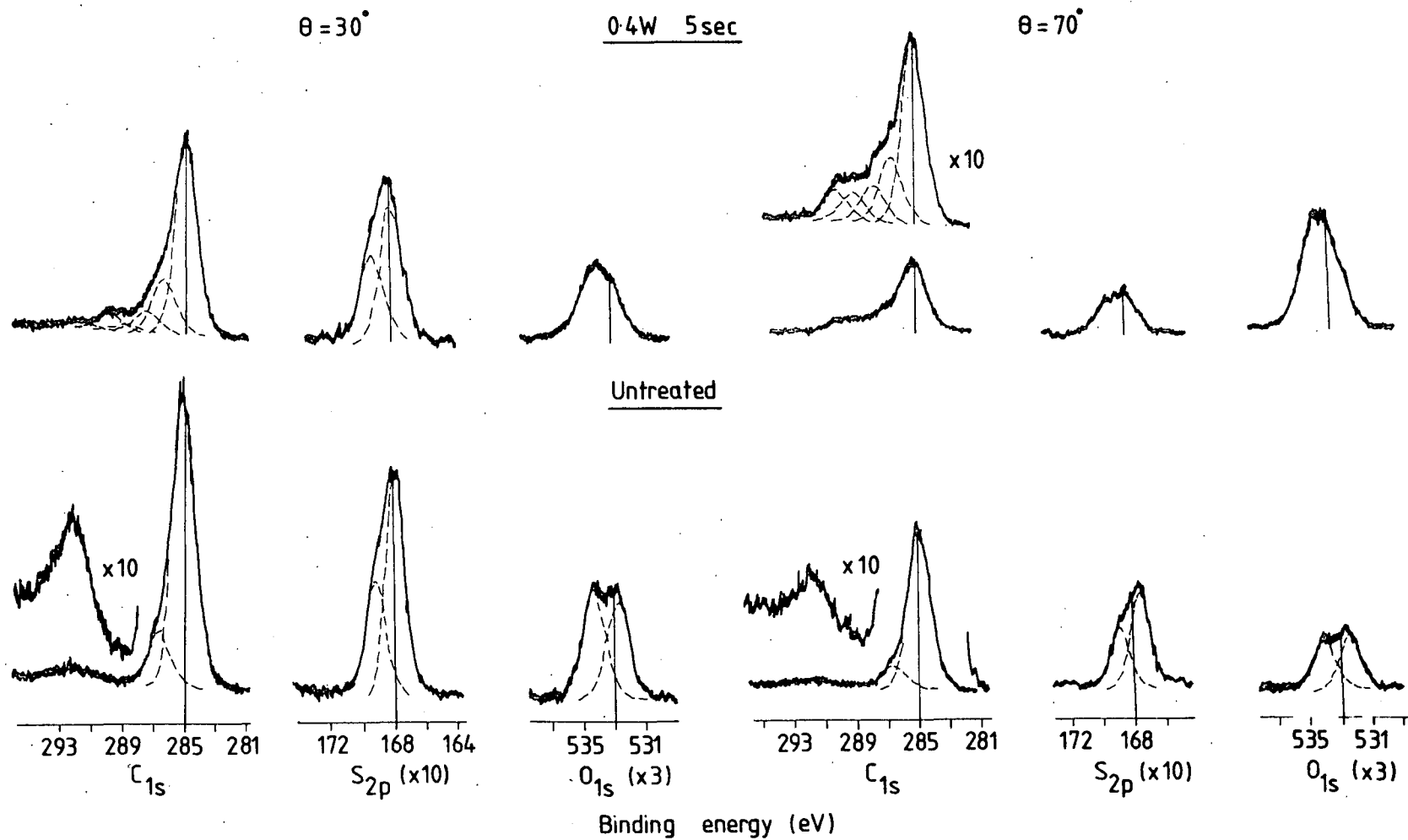


Figure 3.18 Effect of oxygen plasma on the core level spectra of bisphenol-A polysulphone

Table 3.3 Relative intensities of the core level spectra of Nylon 6,6, Polyphenylene sulphide and Bisphenol-A polysulphone before and after oxygen plasma treatment

		$\theta$	$C_{1s}$	$N_{1s}$	$O_{1s}$	$S_{2p}$	
Nylon 6.6	Untreated	$(30^\circ)$	100	16.1	20.3	-	
		$(70^\circ)$	100	15.8	22.1	-	
	Plasma (0.4 W 5 sec)	$(30^\circ)$	100	16.9	29.8	-	
		$(70^\circ)$	100	15.7	39.0	-	
	Polyphenylene sulphide	Untreated	$(30^\circ)$	100	-	5.1	29.7
			$(70^\circ)$	100	-	8.6	15.5
Plasma (.4 W 5 sec)		$(30^\circ)$	100	-	48.0	23.0	
		$(70^\circ)$	100	-	57.6	13.8	
		(10 W 5 sec)	$30^\circ$	100	-	56.6	30.0
Bisphenol-A polysulphone		Untreated	$(30^\circ)$	100	-	19.1	7.8
	$(70^\circ)$		100	-	17.2	6.8	
	Plasma (0.4 W 5 sec)	$(30^\circ)$	100	-	42.5	7.8	
		$(70^\circ)$	100	-	58.2	5.8	

Although the surface stoichiometry of the sample of polyphenylene sulphide, as determined using the 70° take-off data, is not representative of the elemental composition expected for the pure material, and a low level of oxygen also exists, the material does serve as a model for organic sulphide groups in an aromatic chain. Indeed, on exposure to oxygen plasma, the well-resolved doublet of the S<sub>2p</sub> peak (caused by spin orbit splitting, Section 1.4.2) is attacked. The oxidised sulphur moiety gives rise to a broad band centred at a binding energy of 168.6 eV; a signal correspondingly reduced in intensity from unoxidised sulphide is found at 164.2 eV. Oxidation of the organic carbon also occurs and is shown by the formation of a broad shoulder on the C<sub>1s</sub> peak. The oxidised

carbon is present as  $\underline{\text{C}} - \text{O}$ ,  $>\underline{\text{C}} = \text{O}$ ,  $\underline{\text{C}} - \text{O}$  and  $-\text{O} - \underline{\text{C}} \div \text{O}$  functionalities. Use of an oxygen plasma at 10W power for 5 seconds produces more extensive oxidation of the sulphide groups, but has surprisingly little effect on the C<sub>1s</sub> envelope (Figure 3.17).

As an example of an inorganic sulphide, ferrous sulphide (FeS<sub>2</sub>), which occurs naturally as pyrite and is recognised as being a component of the mineral matter present in coal<sup>208</sup> and kerogen,<sup>228</sup> was included in the series of materials of well defined composition. Technical grade pellets of the sulphide were ground to a powder before use. Spectra of untreated and plasma treated samples are shown in Figure 3.19. Whilst little oxidation is evident at the low power oxygen plasma (.4 W), a marked change in S<sub>2p</sub> line shape becomes noticeable using a 10 W oxygen plasma over a period of 5 seconds.

Bisphenol-A polysulphone which contains the sulphone linkage

$$\begin{array}{c} \text{O} \\ \parallel \\ (-\text{S}-) \\ \parallel \\ \text{O} \end{array}$$
 shows oxidative functionalities under the carbon envelope on

exposure to oxygen plasma (Figure 3.18). The nature and concentration of the sulphur present at the surface of the film remains unchanged.

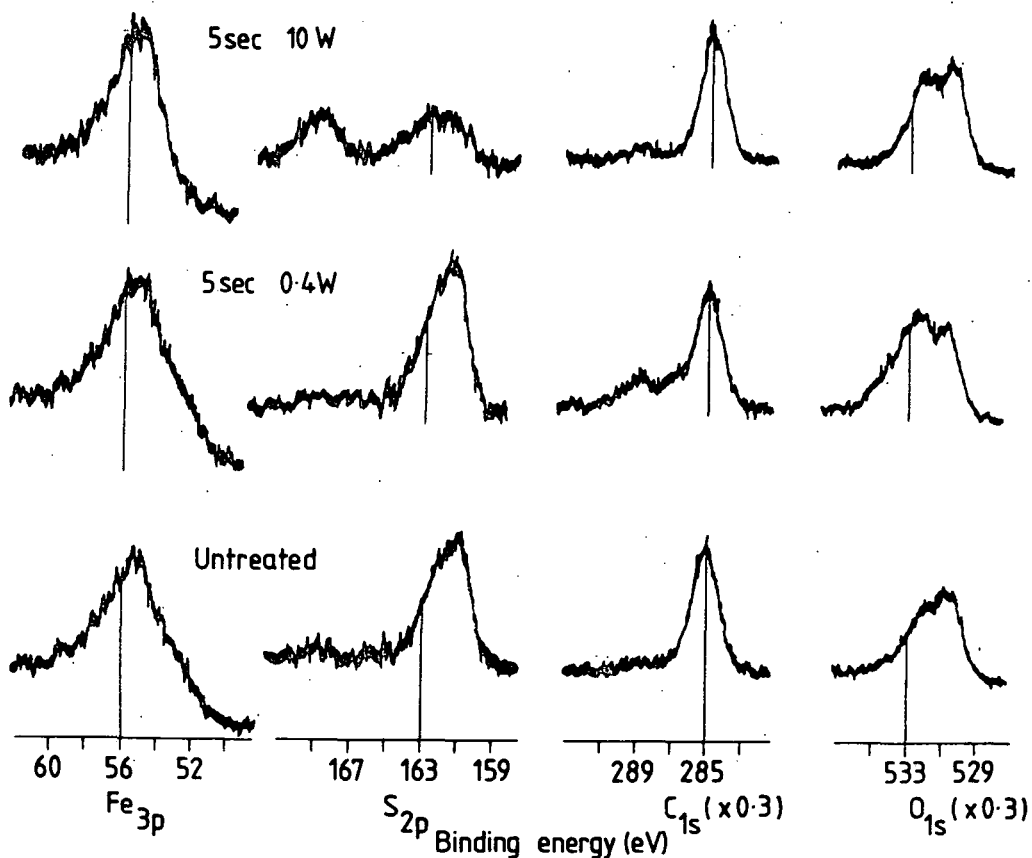


Figure 3.19 Effect of oxygen plasma on the core level spectra of ferrous sulphide

In conclusion to the work on surface modification of polymer films by oxygen plasma, the power setting of 0.4 W at 0.2 torr for a period of 5 seconds has been seen to offer a suitable dosage to provide a means of probing the surface sensitivity and selectivity of the treatment employing ESCA as the analytical technique.

### 3.6 Modification of a series of geochemical materials by oxygen plasma treatments

The plasma treatments of the series of polymer samples discussed in the previous section suggest that extensive oxygen functionalisation as detected by the ESCA experiment may occur for the samples of geochemical interest considered in Chapter Two, even after very gentle plasma treatment. This section investigates the degree of modification which does occur for a selection of coal, kerogen and bitumen samples subjected to glow discharge excited in oxygen principally at the same dosages already encountered. Special attention is paid to a study of the oxidation of gilsonite as a function of treatment time and plasma power.

#### 3.6.1 Experimental

The experimental details are basically the same as those relating to the previous section. Samples were used as powders and mounted on a spectrometer probe-tip by means of double-sided Scotch insulating tape before treatment. In the case of the treatment of gilsonite at 50 W power setting, for a total period of 80 minutes, the powder sample was placed in a small pyrex watch-glass and positioned on the glass slide inside the plasma reactor. At intervals during treatment, the watch-glass was removed and the contents reground so as to aid the uniform ashing of the sample. After treatment the sample was powdered and mounted on a probe-tip ready for ESCA analysis.

All ESCA analyses were carried out using the ES 200B spectrometer and the spectra were deconvoluted in the usual manner.

### 3.6.2 Results and Discussion

#### 3.6.2a Plasma treatment of Gilsonite

Figure 3.20 shows the  $C_{1s}$ ,  $O_{1s}$ ,  $N_{1s}$  and  $S_{2p}$  core level spectra for samples of gilsonite treated in an oxygen plasma (0.4 W, 0.2 torr) for varying treatment times. Progressive uptake of oxygen is evident as treatment time increases, with little variation in nitrogen level and functionality. The low level of sulphur, as monitored by the  $S_{2p}$  peak, remains after 10 seconds treatment and shows a broadening of the band to higher binding energy. This may be explained by oxidation of the sulphur components present in the bitumen. The intensity of the sulphur peak is hard to determine with a high degree of accuracy due to the level of background noise and weak nature of the signal. There appears to be little observable change in sulphur concentration.

Changes in abundance of oxygen and nitrogen, relative to the core level spectrum for the untreated sample, as a function of treatment time, together with the change in hydrocarbon to functionalised carbon ratio are presented in Figure 3.21. The relative intensity of the  $O_{1s}$  signal is plotted against treatment time in Figure 3.22. Also indicated in Figure 3.22 are the changes in  $C_{1s}$  envelope shape with oxygen uptake. It may be seen from Figures 3.21 and 3.22 that the surface composition tends to a steady value after less than 10 seconds. This equilibrium value corresponds to a stoichiometry at the surface region of  $C_{100} N_3 O_{27} S_{0.26}$ ; compared with a stoichiometry of  $C_{100} N_3 O_2 S_{0.17}$  for the starting material as detected by ESCA.

Deconvolution of the  $C_{1s}$  envelopes into their component peaks allows analysis of the types of carbon-oxygen functionality introduced at the surface. This information is presented in tabular form (Table 3.4)

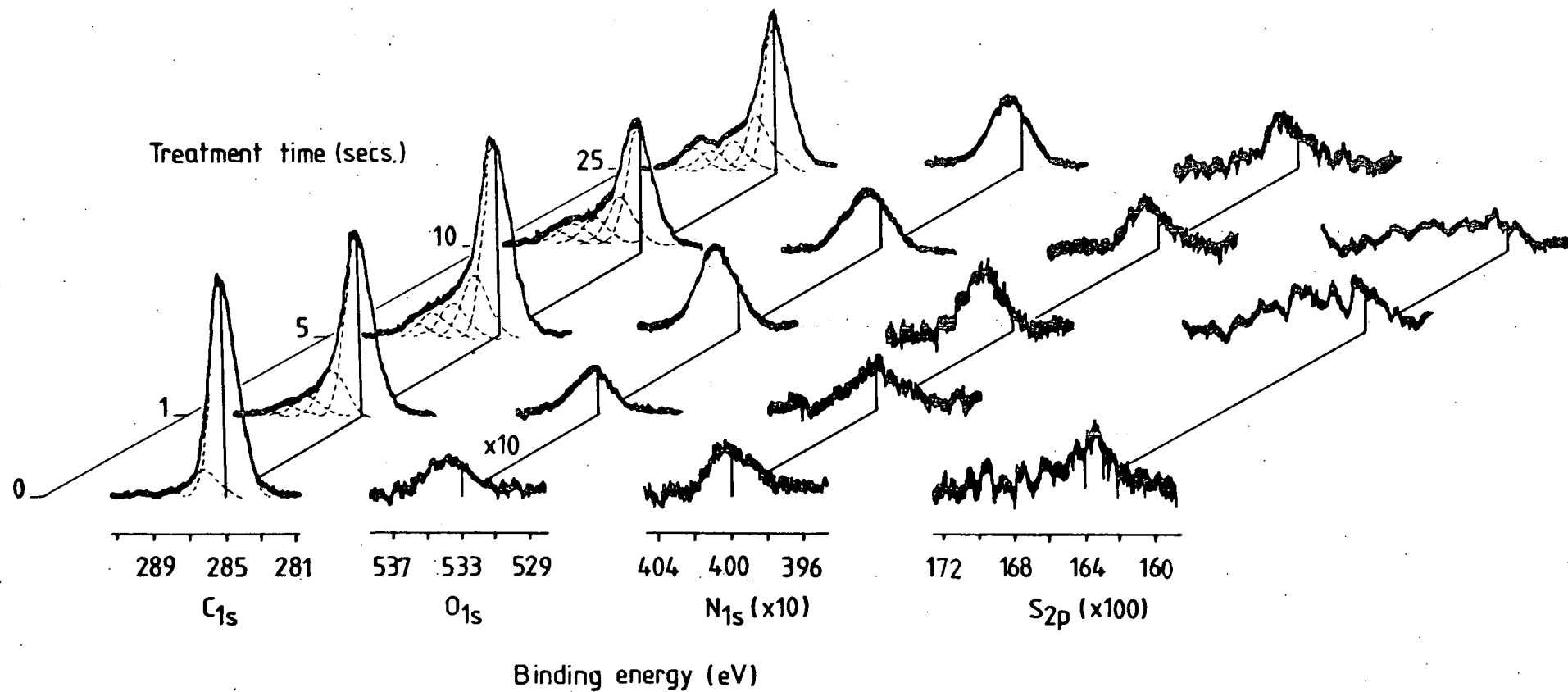


Figure 3.20 Core level spectra of gilsonite versus time of exposure to an oxygen plasma (0.4 W, 0.2 torr)

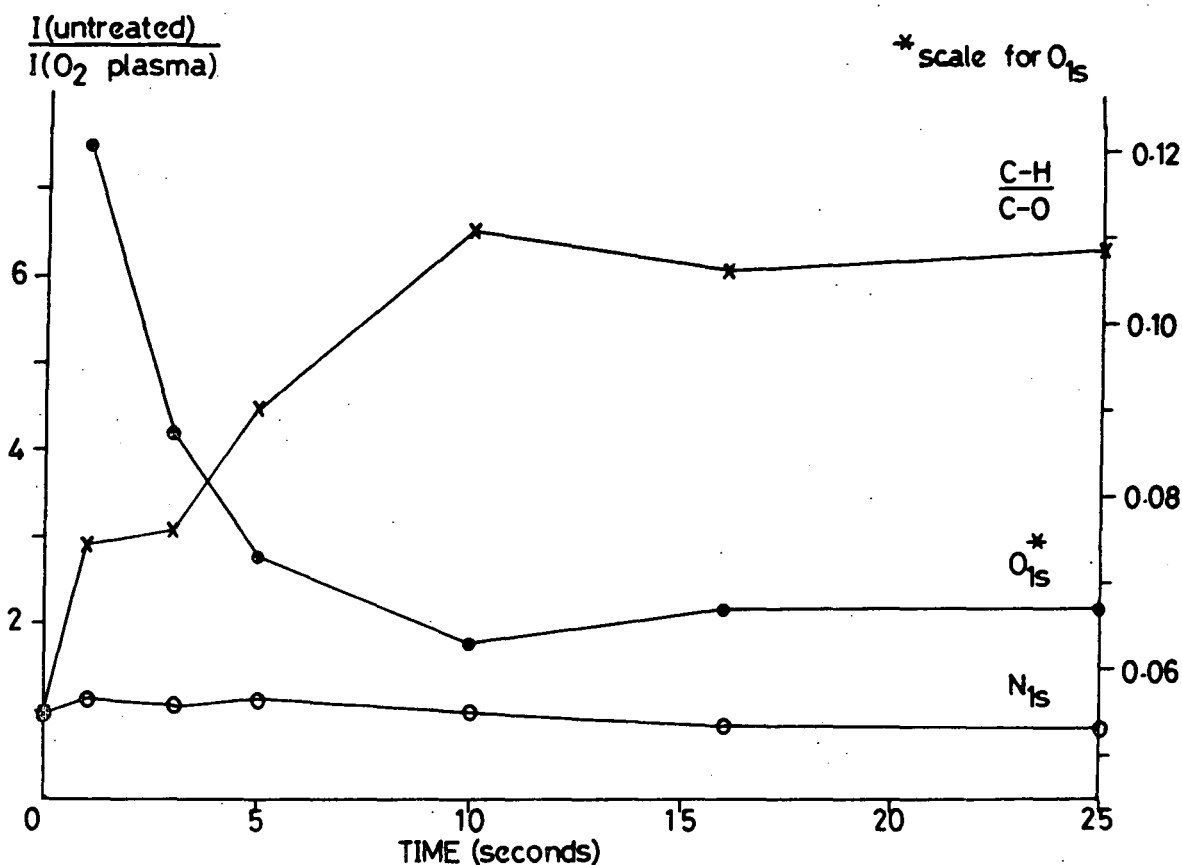


Figure 3.21 Changes in  $O_{1s}$  and  $N_{1s}$  intensities and hydrocarbon to functionalised carbon ratio, relative to the untreated sample for gilsonite versus time of exposure to an oxygen plasma (0.4 W, 0.2 torr).

and a graphical representation is offered in Figure 3.23. The untreated gilsonite spectra show a very low level of oxygen functionalisation. Comparison of the peak at 286.3 eV binding energy under the carbon envelope with the integrated  $C_{1s}/O_{1s}$  intensity data suggests that the carbon singly bonded to oxygen corresponds almost exclusively to ether linkages, rather than free hydroxyl groups. Interaction of the plasma

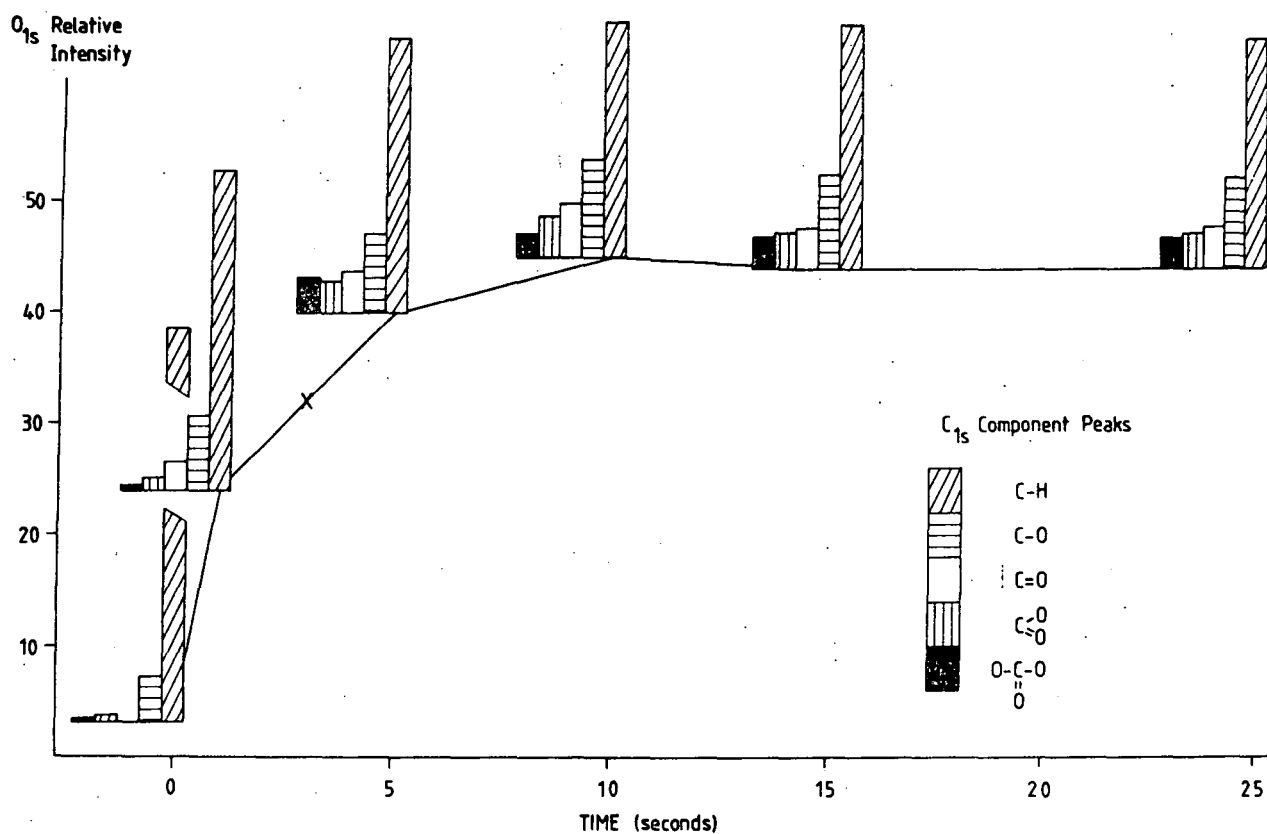


Figure 3.22 Relative intensity of  $O_{1s}$  signal as a function of oxygen plasma (0.4 W, 0.2 torr) exposure time, showing accompanying changes in shape of  $C_{1s}$ -envelope

Table 3.4

Gilsonite exposed to an Oxygen Plasma (0.4 W, 0.2 torr)

Relative area intensities of core electron signals, figures in brackets indicate binding energies (eV)

Treatment time (secs)	Total C <sub>1s</sub>	<u>C</u> - H	<u>C</u> - O	> <u>C</u> = O	<u>C</u> - O	- O - <u>C</u> - O	O <sub>1s</sub>	N <sub>1s</sub>
0	100	88.1	10.6	-	0.9	0.4	2.9	3.4
			(286.3)		(288.5)	(290.1)	(534.0)	(400.0)
1	100	72.2	17.3	6.5	2.9	0.4	24.5	3.0
			(286.6)	(288.2)	(289.6)	(290.6)	(533.5)	(400.2)
3	100	70.7	15.5	8.5	4.9	0.4	31.8	3.3
			(286.5)	(288.2)	(289.5)	(290.5)	(533.6)	(400.1)
5	100	62.1	18.6	9.3	6.8	8.1	39.1	3.0
			(286.5)	(287.8)	(288.9)	(290.1)	(534.1)	(400.9)
10	100	53.1	22.3	11.7	8.5	4.5	45.1	3.4
			(286.2)	(287.6)	(288.9)	(290.1)	(533.8)	(400.3)
16	100	54.9	20.3	9.3	8.2	7.1	44.0	4.0
			(286.3)	(287.7)	(288.9)	(290.1)	(533.7)	(400.6)
25	100	53.8	21.0	10.8	7.0	7.5	44.1	4.1
			(286.3)	(287.7)	(289.0)	(290.1)	(533.9)	(400.7)

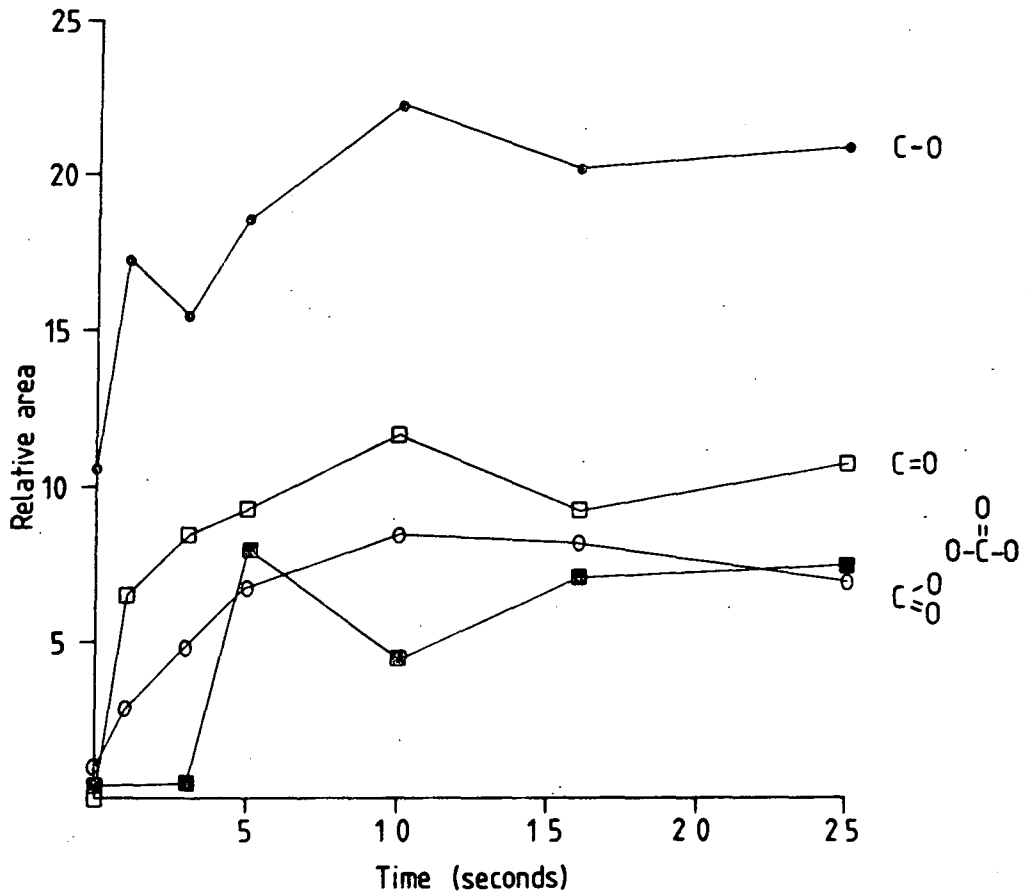


Figure 3.23 Intensities of the individual oxidised carbon component peaks (expressed as % of total  $C_{1s}$  band intensity) plotted against treatment time

with the material results in extensive oxygen uptake in the very early stages of reaction (after 1 second treatment time), during which

$\overset{\text{O}}{\parallel}$   
 $\underline{\text{C}} - \text{O}$ ,  $>\underline{\text{C}} = \text{O}$  and  $\underline{\text{C}} - \text{O}$  structural features become notably more apparent.  
 Build-up of carbonate groups on the material, as sampled by ESCA,

Increases after about the third second of treatment and reaches a steady value after a period of 16 seconds treatment. This latter trend is common to the other functional groups present, although a steady growth rate is shown to apply.

Certain similarities are found to exist between the development of the various components of the  $C_{1s}$  spectrum for polyethylene as a function of time of exposure to an oxygen plasma (0.1 W, 0.2 torr) as reported by Clark and Dilks,<sup>213</sup> and the plot for gilsonite treated in a 0.4 W oxygen plasma (Figure 3.23).

An important point to note relates to the extent of reaction which has taken place after 5 seconds treatment of gilsonite. The interaction with the oxygen plasma, although well advanced, has not reached its limiting value, as far as oxygen uptake or change in carbon functionality are concerned. It has been assumed that a similar situation is likely to exist for the other materials to be considered here when subjected to oxygen plasma under identical conditions.

In order to gain some feeling for the strength of the oxygen plasma initiated at 0.4 W, samples of gilsonite were exposed to a 10 W plasma for 5 seconds, a 50 W plasma for 5 seconds, and a far longer treatment comprising four 20 minute consecutive periods at 50 W power. The sample for the latter experiment was placed, in powder form, on a watch-glass as described in the experimental section (Section 3.6.1) and reground between 'ashing' periods. Core level spectra for the  $C_{1s}$ ,  $O_{1s}$ ,  $N_{1s}$  and  $S_{2p}$  components are shown in Figure 3.24.

As might be anticipated, more extensive oxidation occurs after 5 seconds at 10 W than is present using a 0.4 W oxygen plasma for the same length of time. This higher degree of oxidation is also exhibited in the sulphur functional groups. Substantial oxidation is also introduced at

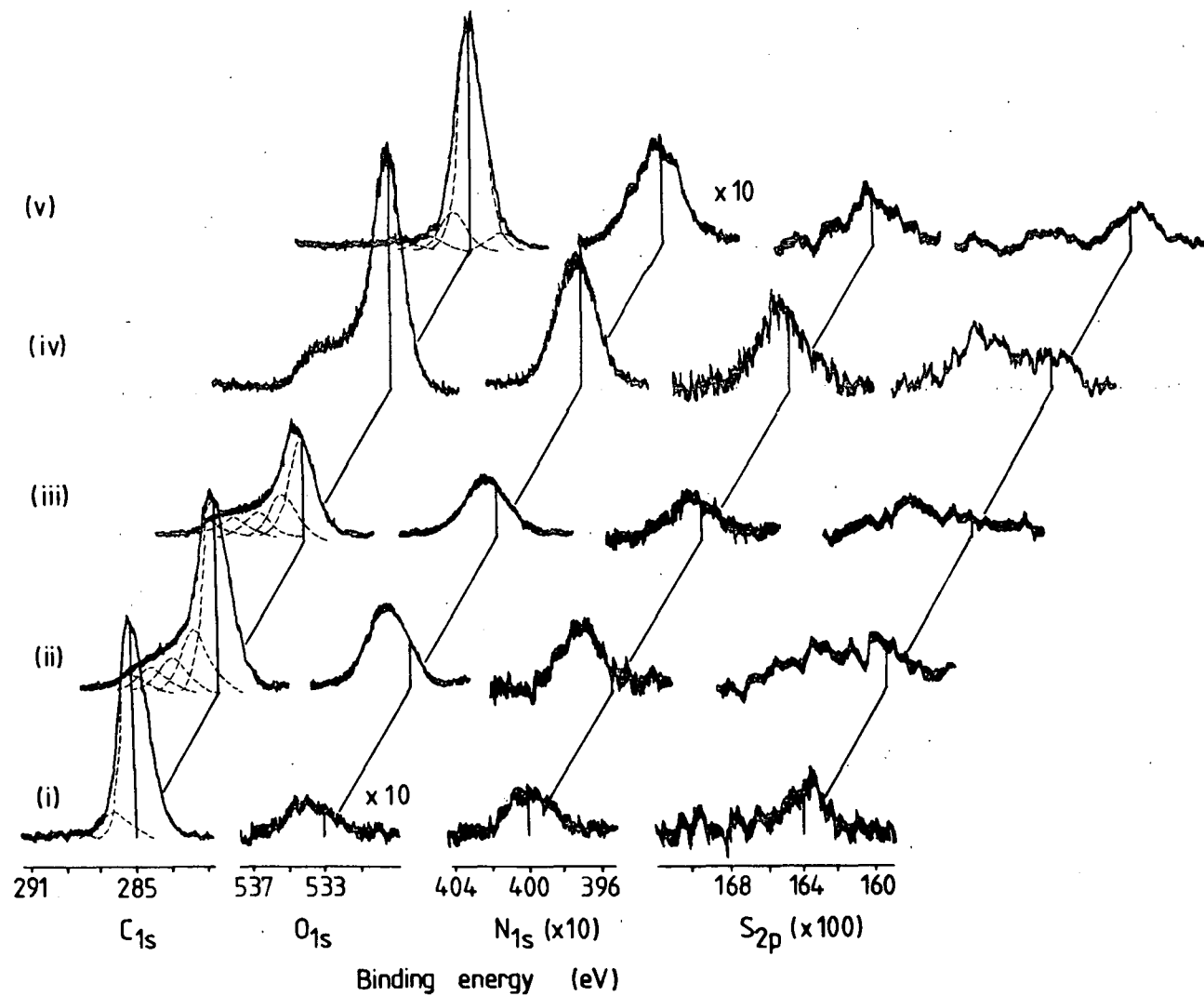


Figure 3.24 Core level spectra of gilsonite to show the effect of oxygen plasma treatments (0.2 torr) at different powers. (i) untreated; (ii) 5 sec at 0.4W; (iii) 5 sec at 10W; (iv) 5 sec at 50W; (v) 4 x 20 mins at 50W.

a power of 50 W. The residue obtained from prolonged plasma treatment was noticeably a darker shade of brown than untreated gilsonite and was also more char-like in texture.

The ESCA core level spectra for the gilsonite sample exposed to a 50 W plasma for a total time of 80 minutes, and prepared for analysis as previously described, offer close resemblance to those for untreated gilsonite. The oxygen concentration shows approximately a 2.5 fold increase compared to the considerably greater increases in surface oxidation experienced under the other conditions of treatment and analysis. The carbon envelopes for the untreated sample and treated sample ground prior to analysis are closely similar. The spectrum of the latter sample includes a slightly greater carbon singly bonded to oxygen peak than for the untreated material: the component at 283.2 eV binding energy is representative of graphitic carbon. The sulphur band of the 'pre-ground' sample shows a comparatively large component of unoxidised sulphur; again a similarity to the untreated spectrum is evident.

Little difference is found between the microanalysis data (wt. %) for the untreated and plasma treated samples:

	C	H	N	S	Ni	V	Sn
Untreated	84.25*	12.38*	2.84*	0.61*	0.02	<0.01	<0.01
Plasma treated	84.07	10.93	2.96	0.60	0.04	<0.01	<0.01

\* denotes an averaged value.

The inaccuracies encountered when determining oxygen analyses 'by difference' have already been discussed. It can be seen that the microanalysis figures for the untreated powder account for 100.1 wt. % of the sample and 98.6 wt. % of the plasma treated gilsonite. Infra-red

spectroscopy employing samples prepared as KBr discs showed no apparent differences between plasma treated and untreated gilsonite.

It is clear from the data obtained using bulk characterisation techniques and the data obtained from the ESCA spectra of the powder ground after plasma treatment that the chemical modification effects of plasma oxidation do not penetrate the bulk of the solid to any significant extent.

Throughout the experimental results on gilsonite the nitrogen levels of the plasma treated samples remain little affected. Vanderborgh and co-workers<sup>167</sup> in their study of the laser pyrolysis of carbonaceous rocks monitored by gas chromatography - mass spectrometric analysis of the gaseous products, include a sample of gilsonite. They note that their analysis shows little evidence of nitrogen compounds, even though it is known that gilsonite contains significant porphyrin (condensed pyrroles) content. It is suggested the pyrrole nitrogen is left behind in the graphitic char. A similar situation was found in the case of a sample of high volatile bituminous coal.

Preliminary work on the action of hydrogen plasma on gilsonite is reported in Section 3.7.

### 3.6.2b Oxygen plasma treatment of a series of coal, kerogen and bitumen samples

The results presented in this discussion relate to the effects of oxygen plasma treatment, at 10W and 0.4W power settings at a pressure of 0.2 torr and treatment time 5 seconds, on a series of samples already encountered in Chapter Two.

Table 3.5 shows information pertaining to the relative intensities of the core level signals of the elements carbon, oxygen, nitrogen and

sulphur for samples before and after treatment. It may be seen that a striking feature, common to all the materials, is the increase in the relative intensity of the  $O_{1s}$  signal upon interaction with the oxygen plasma. This increase in surface oxidation is greater for the stronger (IOW) treatment. Analysis of the shape and location on the binding energy scale of the core level envelopes reveals that the additional oxygen is present, for the most part, in the form of oxidised carbon functionalities (Figure 3.25).

There is also a tendency for the centroid of the  $S_{2p}$  peak to move to higher binding energy which may indicate the oxidation of the sulphide-type sulphur species. This inference should not be taken as being the general case since elimination of organic sulphur moieties from the solid cannot be ruled out. If such reaction were to take place, whilst the oxidised sulphur component remained unaffected, then there would be a relative increase in the proportion of oxidised sulphur present.

As far as the reaction of inorganic sulphide with the oxygen plasma is concerned, in the case of ferrous sulphide ( $FeS_2$ ), which is known to be present in the mineral phase of both coal<sup>208</sup> and kerogen,<sup>228</sup> no significant loss of sulphur is found to occur. The spectra illustrated in Figure 3.19 show the formation of a peak at 168.9eV binding energy after treatment of  $FeS_2$  in a IOW oxygen plasma (0.2 torr) for 5 seconds. The growth of this peak corresponds to the creation of sulphate environments. The relative intensities of the total sulphur band with respect to the  $Fe_{3p}$  peak intensity for the treated and untreated samples do not differ to any significant extent.

Kimmeridge kerogen has the highest sulphur content of the geochemical samples in this investigation. The behaviour of the distinct doublet of the  $S_{2p}$  core level, indicative of the presence of both sulphide and oxidised sulphur functionalities, when subjected to oxygen plasma, was monitored with interest.

Table 3.5 Effect of oxygen plasma (0.2 torr, 5 seconds) at 0.4W and 10W power. Relative area intensities of core electron signals, total C<sub>1s</sub> area taken as 100 units, figures in brackets indicate binding energies (eV)

	<u>C-H</u>	<u>C-O</u>	<u>&gt;C=O</u>	<u>C=O</u> 0	<u>O-C=O</u> 0	<u>O<sub>1s</sub></u>	<u>N<sub>1s</sub></u>	<u>S<sub>2p</sub></u>
Gilsonite		(286.3)		(288.5)	(290.1)	(534.1)	(400.0)	(163.6)
Untreated	88.1	10.6	-	0.9	0.4	2.9	3.4	0.32
0.4W		(286.5)	(287.8)	(288.9)	(290.1)	(534.1)	(401.9)	
	62.1	18.6	9.3	6.8	8.1	39.1	3.0	0.32
10W		(286.2)	(287.6)	(289.0)	(290.2)	(533.8)	(400.8)	(167.6)
	51.5	22.7	11.9	8.8	5.2	52.6	3.9	0.29
Weathered Gilsonite		(286.3)	(287.9)	(289.1)	(290.5)	(533.0)	(399.5)	
Untreated	83.3	13.3	1.7	0.8	0.8	6.3	3.5	0.64
0.4W		(286.2)	(287.4)	(288.7)	(289.8)	(290.9)	(533.9)	(400.6)
	53.5	22.5	11.2	6.4	5.3	1.1	44.9	3.5
10W		(286.6)	(287.9)	(288.9)	(289.8)	(533.7)	(400.8)	
	62.9	16.4	5.5	4.2	4.2	55.3	2.6	0.20

Continued overleaf.....

Table 3.5 (Continued)

		<u>C-H</u>	<u>C-O</u>	<u>&gt;C=O</u>	$\begin{array}{c} \text{O} \\ \parallel \\ \text{C-O} \end{array}$	$\begin{array}{c} \text{O} \\ \parallel \\ \text{O-C-O} \end{array}$	$\text{O}_{1s}$	$\text{N}_{1s}$	$\text{S}_{2p}$	$\text{S}_{ox}$	$\text{S}_{sulphide}$	
Untreated Torbanite	(283.5)		(286.3)	(287.6)	(289.4)	(290.0)	(292.0)	(534.1)	(401.2)			
Untreated	6.5	46.7	34.6	10.3	4.2	1.4	0.9	162.6	1.5	-		
0.4W	(283.4)		(286.2)	(287.8)	(289.4)	(290.6)	(292.2)	(533.9)	(401.7)			
	5.5	34.4	30.9	14.4	8.9	4.5	1.4	216.5	2.5			
Demineralised Torbanite												
Untreated		69.9	(286.3)	(287.9)	(289.4)	(290.1)		(533.7)	(400.5)			
			19.6	5.6	3.5	1.4		11.4	2.1	0.7		
0.4W		55.5	(286.3)	(287.5)	(288.5)	(289.6)	(291.0)	(533.8)	(400.6)			
			18.3	10.6	6.7	7.8	1.1	52.2	2.4	0.7		
Kimmeridge Kerogen												
Untreated		76.8	(286.3)	(287.5)	(288.8)	(290.2)		(532.8)	(400.5)			
			16.2	4.0	2.0	1		16.1	3.1	9.4	(168.8)	(163.5)
0.4W		65.2	(286.5)	(287.8)	(289.2)	(290.1)		(533.6)	(400.7)			
			13.3	7.6	5.7	2.4		41.3	2.9	5.4	(168.7)	(163.3)
10W		52.9	(286.4)	(287.7)	(289.0)	(290.0)		(533.7)	(401.0)			
			18.5	11.6	9.5	7.4		68.8	4.5	6.8	(168.9)	(163.9)

Continued overleaf.....

Table 3.5 (Continued)

	<u>C-H</u>	<u>C-O</u>	> <u>C=O</u>	$\begin{array}{c} \text{O} \\ \parallel \\ \text{C-O} \end{array}$	$\begin{array}{c} \text{O} \\ \parallel \\ \text{O-C-O} \end{array}$		$\text{O}_{1s}$	$\text{N}_{1s}$	$\text{S}_{2p}$	
Vitrinite										
Untreated	69.0	(286.4) 20.7	(288.0) 5.1	(289.1) 0.7	(290.2) 2.1	(291.6) 1.4	(533.2) 19.8	(399.9) 3.0	(164.4) 0.8	
0.4W	49.8	(286.5) 18.9	(287.6) 10.4	(288.6) 9.5	(289.8) 10.0	(291.8) 1.5	(533.6) 57.7	(400.2) 4.0	1.4	
10W	44.2	(286.4) 17.3	(287.6) 14.6	(289.0) 13.7	(290.1) 8.8	(291.9) 1.3	(533.9) 77.0	(400.8) 3.0	0.25	
Brown Coal										
Untreated	(283.8) 5.9	52.5	(286.2) 23.8	(287.6) 9.9	(288.9) 4.0	(290.0) 3.0	(291.6) 1.0	(533.3) 46.5	(400.6) 1.5	-
0.4W	(283.9) 5.8	44.8	(286.4) 22.0	(287.7) 9.9	(288.9) 11.2	(290.1) 5.4	(291.6) 0.9	(534.1) 79.4	(400.3) 1.4	-
10W	(283.6) 1.7	42.4	(286.4) 20.8	(287.6) 14.0	(289.0) 11.9	(290.1) 8.1	(291.9) 1.3	(534.3) 85.6	(401.2) 2.4	0.3

Table 3.5a Effect of oxygen plasma (0.2 torr, 5 seconds) at 0.4W and 10W power

	<u>Relative Intensities</u>				<u>Intensity Ratio</u>				<u>(Untreated)</u>
	C-H	O <sub>1s</sub>	N <sub>1s</sub>	S <sub>2p</sub>	<u>C-H</u> <u>C-O</u>	O <sub>1s</sub>	N <sub>1s</sub>	S <sub>2p</sub>	<u>(Plasma treated)</u>
Gilsonite									
Untreated	88.1	2.9	3.4	0.32					
0.4W	62.1	39.1	3.0	0.32	4.5	0.07	1.1	1.0	
10W	51.5	52.6	3.9	0.29	7.0	0.06	0.9	1.1	
Weathered Gilsonite									
Untreated	83.1	6.3	3.5	0.64					
0.4W	53.5	44.9	3.5	0.47	4.3	0.14	1.0	1.4	
10W	62.9	55.3	2.6	0.20	2.9	0.11	1.4	3.2	
Untreated Torbanite									
Untreated	46.7	162.6	1.5	-					
0.4W	34.4	216.5	2.5	-	1.7	0.75	0.6	-	
Demineralised Torbanite									
Untreated	69.9	11.4	2.1	0.7					
0.4W	55.5	52.2	2.4	0.7	1.9	0.22	0.9	1.0	

Continued overleaf.....

Table 3.5 (Continued)

	<u>Relative Intensities</u>				<u>Intensity ratio</u> $\frac{\text{(Untreated)}}{\text{(Plasma treated)}}$				$S_{\text{ox}}$	$S_{\text{sulphide}}$
	C-H	$O_{1s}$	$N_{1s}$	$S_{2p}$	$\frac{C-H}{C-O}$	$O_{1s}$	$N_{1s}$	$S_{2p}$		
Kimberidge Kerogen										
Untreated	76.8	16.1	3.1	9.4						
0.4W	65.2	41.3	2.9	5.4	1.8	0.4	1.1	1.7	1.1	2.7
10W	52.9	68.8	4.5	6.8	2.9	0.2	0.7	1.4	0.8	2.3
Vitrinite										
Untreated	69.0	19.8	3.0	0.8						
0.4W	49.8	57.7	4.0	1.4	2.2	0.34	0.8	0.6		
10W	44.2	77.0	3.0	0.3	2.8	0.26	1.0	2.7		
Brown Coal										
Untreated	52.5	46.5	1.5	-						
0.4W	44.8	79.4	1.4	-	1.4	0.6	1.1	-		
10W	42.4	85.6	2.4	0.3	1.5	0.5	0.6	-		

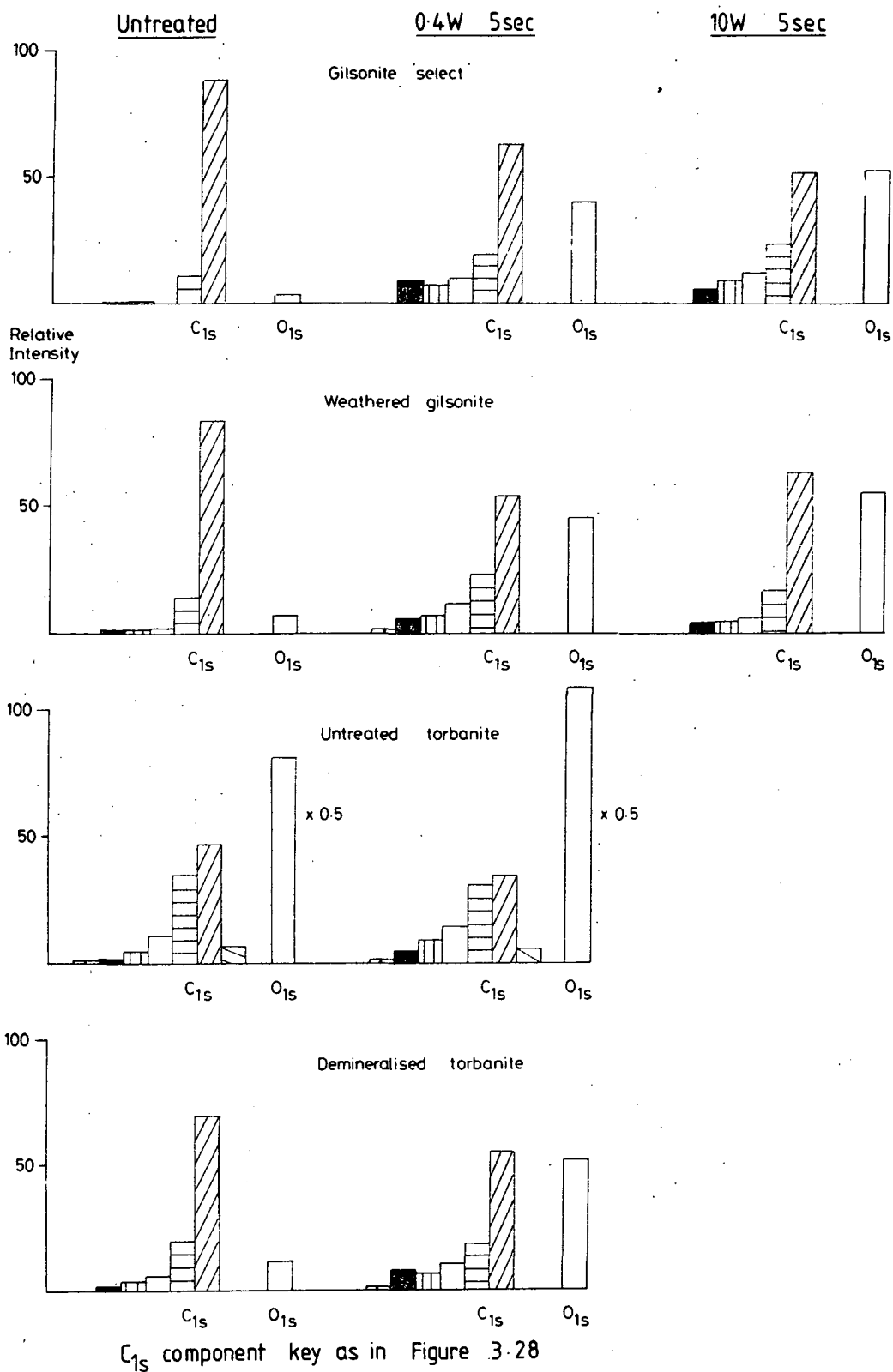


Figure 3.25 Effect of oxygen plasma treatment (0.2 torr) on the geochemical materials

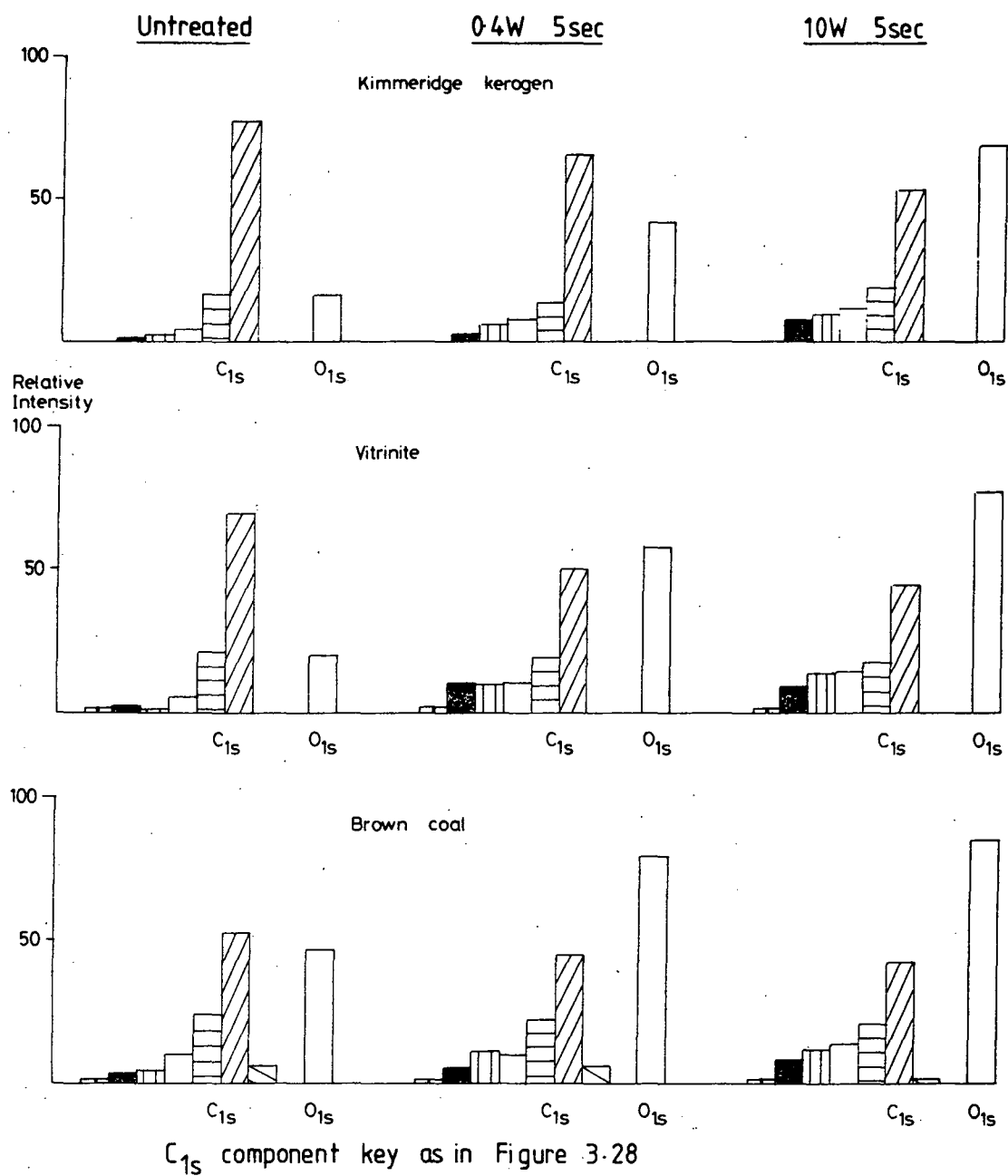


Figure 3.25a Effect of oxygen plasma treatment (0.2 torr) on the geochemical materials.

Relative intensity measurements show that there is an overall decrease in sulphur level after plasma treatment (Table 3.5). From a comparison of the shape of the  $S_{2p}$  envelopes before and after treatment (Figure 3.26), it is evident that the higher binding energy component of the doublet structure becomes more predominant upon exposure to oxygen plasma.

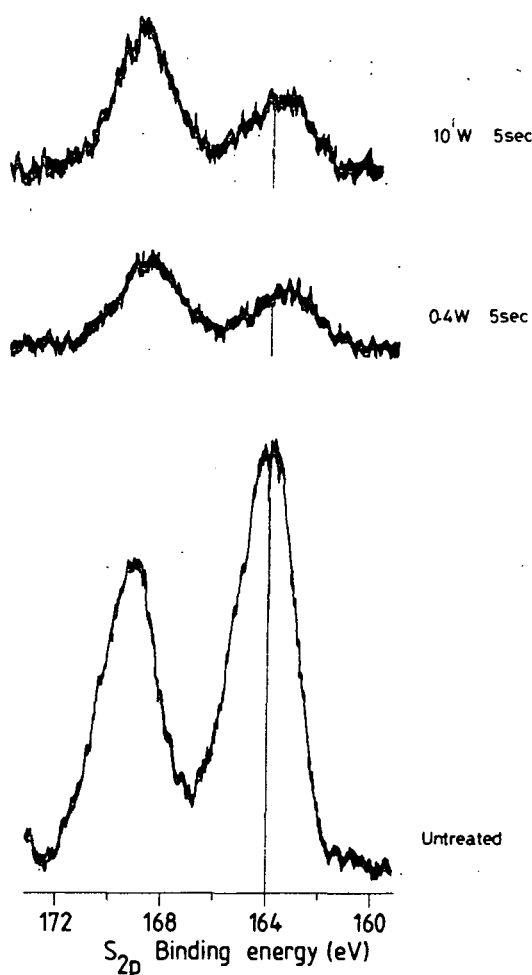


Figure 3.26  $S_{2p}$  core level spectra for Kimmeridge kerogen before and after oxygen plasma treatment

These observations would seem to indicate that the low binding energy sulphur peak includes a component other than inorganic pyrite, presumably organic sulphide. The sulphide functionalities in polyphenylene

sulphide have been shown to be susceptible to oxidative attack even at the 0.4W treatment level (Figure 3.17), resulting in the growth of an oxidised sulphur component.

An additional process which is likely to accompany the surface oxidation phenomena concerns the elimination of organic fragments from the material as a whole. Indeed, this is the basis of low temperature plasma ashing (Sections 3.34 and 3.4) although far stronger plasma treatments are employed in such processes. Recently, Suhr and coworkers<sup>272</sup> have investigated the desulphuration by plasma technique of a series of thioethers as model compounds for sulphur functionalities present in crude oil. It was found that while aliphatic, as well as aromatic thioethers and thiophene react easily, benzothiophenes are hard to desulphurise. The addition of oxygen to the plasma system greatly improved the desulphurisation reactions.

It is quite plausible, therefore, that it is the elimination of organic sulphide, rather than the increase of oxidised sulphur moieties, which is the overriding factor behind the observed changes in  $S_{2p}$  envelope shape.

As was found to be the case for gilsonite, oxygen plasma treatment has comparatively little effect on the position of the  $N_{1s}$  signal. In particular, no evidence was found for the presence of oxidised nitrogen functionalities.

The nature of the silicon and aluminium components of the mineral phase of the 'raw' torbanite sample before and after treatment was also studied. No change in binding energy of either the  $Si_{2p}$  or  $Al_{2p}$  peak was found. The intensities of both peaks, relative to the total carbon intensity, were increased, the respective intensity ratios of the silicon and aluminium 2p signals for untreated : plasma treated (0.4W) being 100 : 120 and 100 : 116.

This could be due to either removal of the organic phase at the surface of the material, leaving a greater proportion of mineral component exposed, or, the inhomogeneous nature of the torbanite itself.

Figure 3.27 shows the change in oxygen level, relative to the oxygen level in the untreated sample, plotted against the relative intensity

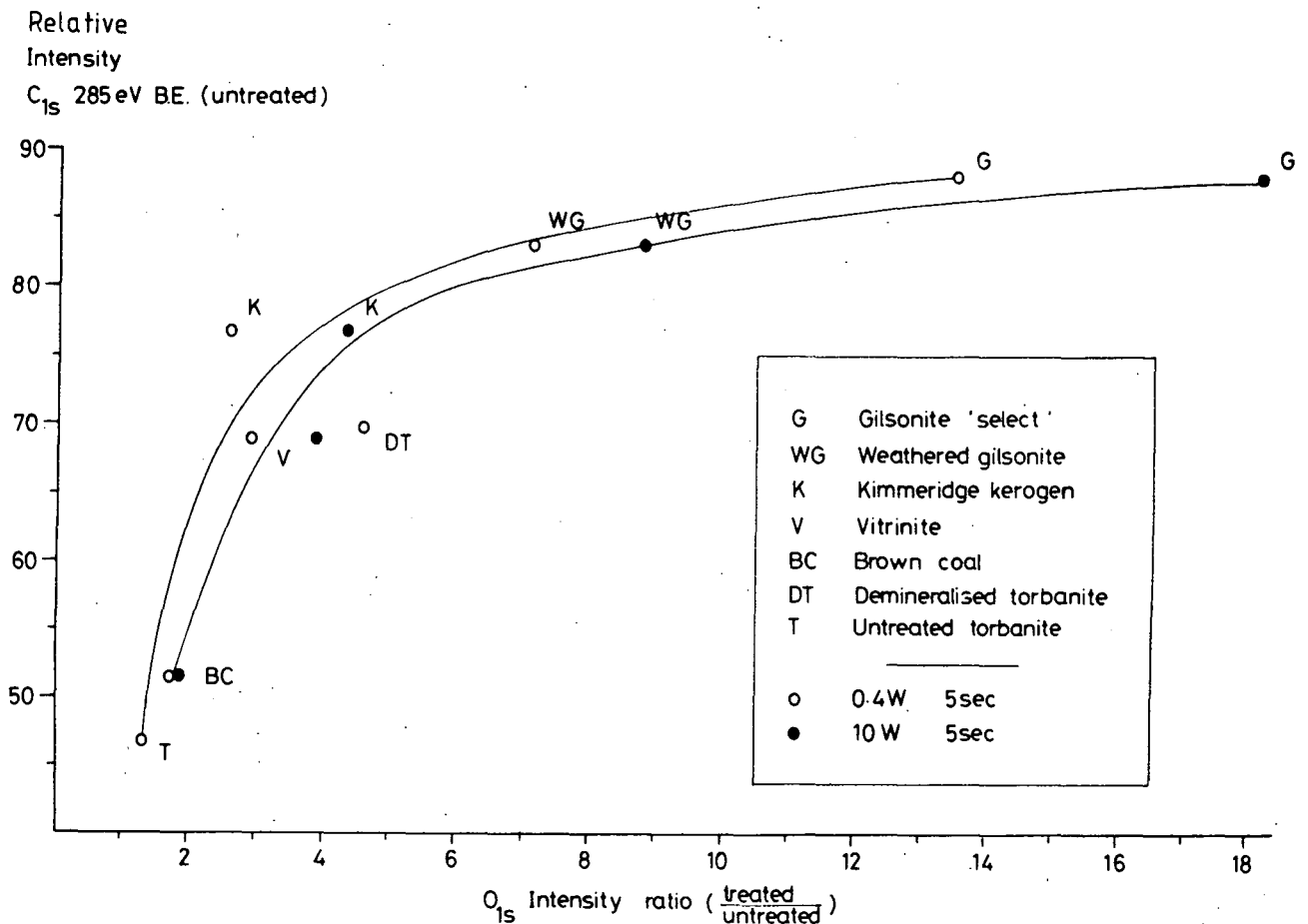


Figure 3.27 A measure of the oxygen uptake of a series of materials exposed to oxygen plasma (0.2 torr, 5 secs).

of the unoxidised carbon component (at 285eV binding energy) of the untreated material, for the samples examined. Results at both plasma powers are included. The trend to emerge from this diagram is that the greater the proportion of unoxidised carbon in the untreated sample, the greater will be the change in oxygen level, relative to the oxygen level in the untreated

sample, on exposure to oxygen plasma. This is quite reasonable since there will be more available sites at which reaction could occur for a material such as gilsonite, with predominantly hydrocarbon character, than for brown coal or a material already containing a substantial proportion of oxidised carbon prior to oxygen plasma treatment.

In the case of two materials each having the same initial elemental stoichiometry, the more reactive material, with respect to interaction with an oxygen plasma, would be expected to show a higher extent of oxygen uptake. The work of Clark and Dilks<sup>213</sup> on the relative reactivity of polystyrene, polypropylene and polyethylene has already been cited (Section 3.5.1) as demonstrating the greater susceptibility of unsaturated systems, as opposed to saturated systems, towards oxygen plasma. It is also expected that the more reactive material will exhibit less variation in oxygen uptake when a gentle or a more powerful plasma is employed. Analysis of the experimental data presented in Table 3.2 for polyethylene and polystyrene films exposed to oxygen plasma at 0.4W and 10W power does in fact exemplify these ideas.

Comparison of the overall oxygen uptake which occurs for gilsonite with the corresponding values for polystyrene and polyethylene films (at  $\theta = 30^\circ$ ) is as follows:

	Untreated	0.4W	10W
Gilsonite	2.9	39.1	52.6
Polyethylene	1.1	18.5	30.5
Polystyrene	1.9	39.7	41.1

It would appear that the reactivity of gilsonite towards oxygen plasma bears more resemblance to that of the aromatic film, polystyrene, than to polyethylene.

At the time of writing this account, it is not possible to draw firm conclusions as to the relative reactivities of the coal, kerogen and bitumen samples. Additional characterisation of the behaviour of the individual samples when exposed to oxygen plasma, as functions of treatment time and plasma power, are needed, along with similar data for model systems. This work is currently underway.

### 3.7 Hydrogen plasma treatments of gilsonite and brown coal

The oxidising properties of the plasma excited in oxygen has been discussed in previous sections. Here the potential use of hydrogen plasma in the *reduction* of oxidised species present in samples of gilsonite and brown coal is investigated.

#### 3.7.1 Experimental

The experimental plasma rig has already been described in Section 3.5.2d and depicted in Figure 3.12. Care was taken to remove atmospheric oxygen from the plasma environment. To this end the reactor was pumped down to a pressure of  $\sim 10^{-4}$  torr by means of a diffusion pump for a period of approximately 30 minutes before leaking in hydrogen gas (supplied by British Oxygen Corporation and used without further purification) to a pressure of 0.2 torr, as monitored by a Pirani pressure gauge. The system was allowed to equilibrate before the plasma was initiated. The characteristic electromagnetic radiation in the visible region gave rise to a lilac glow.

#### 3.7.2 Results and Discussion

The materials chosen for use in this study were brown coal and gilsonite, both of which were found to undergo changes during hydrogen plasma treatment. The results are shown in Table 3.6 and the core level spectra for carbon and oxygen are represented in Figures 3.28 and 3.29

##### 3.7.2a Brown coal

Hydrogen plasma treatment of brown coal clearly gives rise to a decrease of oxygen functionalisation in the surface regions as sampled by ESCA. Indeed the surface stoichiometry (as far as carbon and oxygen

Table 3.6 Treatments involving the use of plasmas excited in hydrogen. Relative area intensities, figures in brackets indicate binding energies (eV)

	Total C <sub>1s</sub>		<u>C</u> - H	<u>C</u> - O	> <u>C</u> = O	<u>C</u> = O	O - <u>C</u> - O	O <sub>1s</sub>	N <sub>1s</sub>	
<u>Brown Coal</u>		(283.5)		(286.2)	(287.6)	(288.9)	(290.0)	(291.6)		
Untreated	100	5.9	52.5	23.8	9.9	4.0	3.0	1.0	46.5	1.5
Hydrogen Plasma 10 W, 30 sec	100	-	70.4	(286.7) 22.5	(287.8) 4.9	(289.8) 2.1	-	-	35.2	2.0
<u>Gilsonite</u>				(286.5)	(288.1)					
Hydrogen Plasma 10 W, 30 sec	100	-	92.6	6.5	0.9	-	-	-	5.6	2.5
Untreated	100	-	88.1	(286.3) 10.6	-	(288.5) 0.9	(290.1) 0.4	-	2.9	3.4
Oxygen Plasma 0.4 W, 25 sec	100	-	53.8	(286.3) 21.0	(287.7) 10.8	(289.0) 7.0	(290.1) 7.5	-	44.1	4.1
Oxygen Plasma ) 0.4 W, 25 sec ) + ) )	100	-	69.4	(286.5) 19.4	(287.9) 6.3	(289.4) 4.2	(290.4) 0.7	-	34.7	
Hydrogen Plasma ) 10 W, 30 sec )										

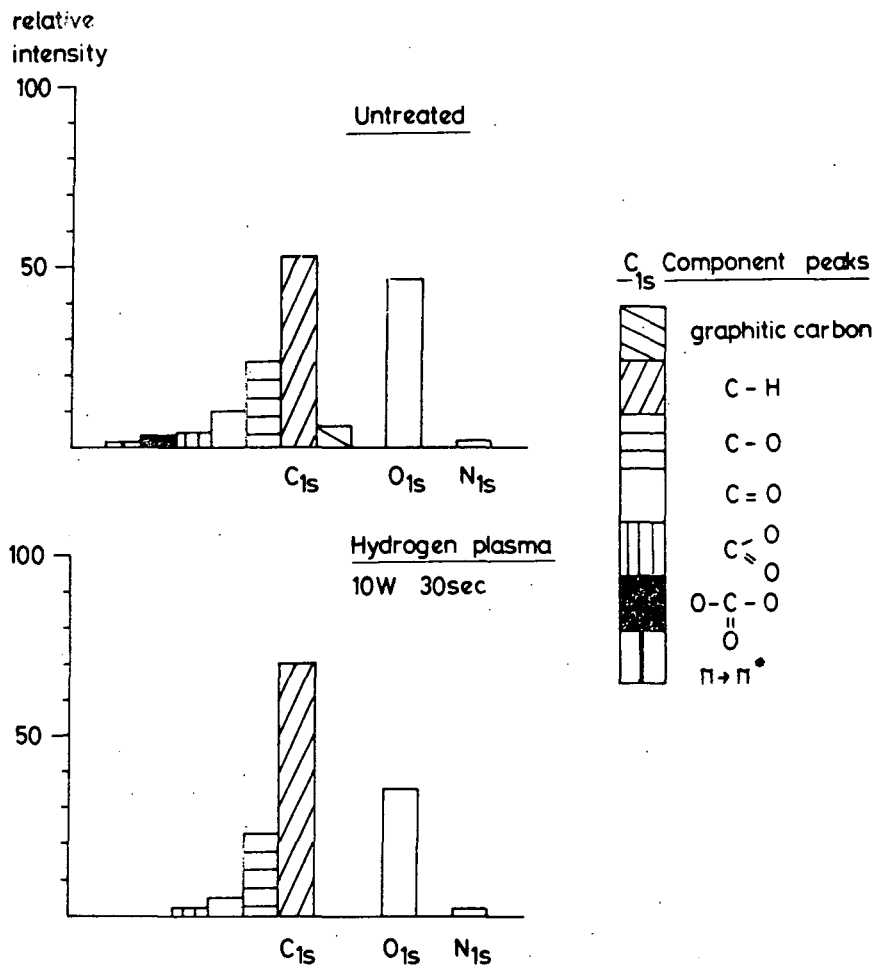


Figure 3.28 Effect of hydrogen plasma on brown coal

are concerned) is shown to change from  $C_{100} : O_{28}$  in the untreated sample, to  $C_{100} : O_{21}$  after hydrogen plasma treatment. As is to be expected, this modification is reflected not only in overall  $C_{1s} : O_{1s}$  intensity ratios, but also in the nature of the component peaks within the carbon photoionisation envelope itself. The broader nature of the  $C_{1s}$  signal from the untreated sample is suggestive of the presence of a graphitic carbon component to the lower binding energy side of the main peak at 285 eV, representative of the hydrocarbon component. On treatment with hydrogen plasma, the hydrocarbon peak is increased by 34% of its area compared with its value in the untreated specimen, and the component from graphitic carbon structure is no longer in evidence. Whilst C - O

structural features remain essentially unchanged, carbonyl, carboxyl and carbonate functionalities are substantially decreased, as is the peak at 291.6 eV which is due to shake-up transitions occurring in conjugated systems.

### 3.7.2b Gilsonite

Comparison of the spectra from hydrogen plasma treated gilsonite and untreated material (Figure 3.29) again shows an increase in the

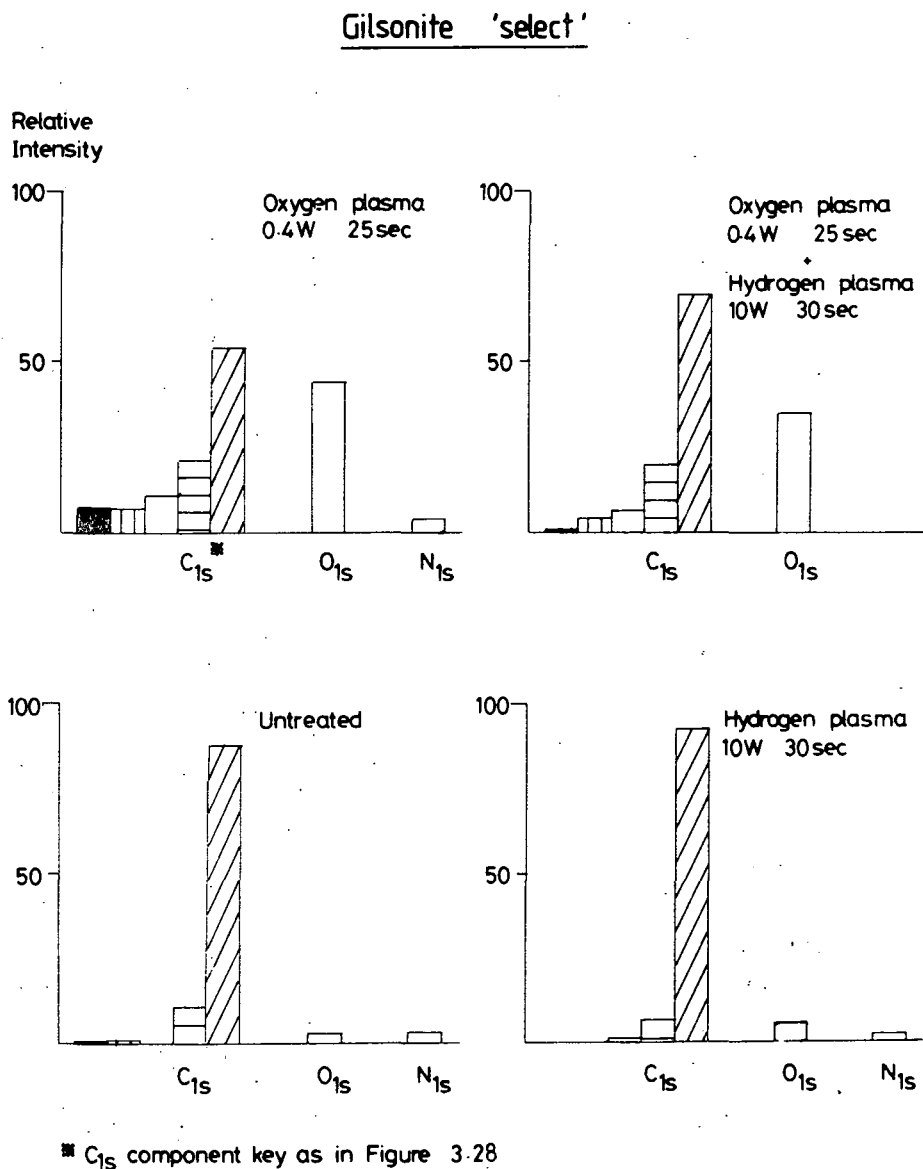


Figure 3.29 A comparison of the effects of oxygen and hydrogen plasmas on gilsonite

285 eV carbon signal after treatment. In contrast to brown coal the  $\underline{C} - O$  component in gilsonite decreases in intensity on exposure to hydrogen plasma.

Observation of the  $O_{1s}$  core electron signal after hydrogen plasma modification does in fact indicate that oxygen has been introduced at the surface region. This apparent uptake is relatively small compared with the oxidative effects of glow discharges excited in pure oxygen (or air). A most likely explanation accounting for this finding concerns reaction of residual oxygen absorbed in the solid sample itself which is not completely outgassed before the plasma is initiated. Reaction between the treated surface and the atmosphere, whilst transferring the sample to the spectrometer for analysis, although it cannot be ruled out completely, is thought to be of secondary importance in view of the low reactivity of the species likely to be present. High density polyethylene, when subjected to a mild hydrogen plasma (0.4 W, 10 sec, 0.2 torr), has been shown to yield a surface containing a level of oxygen functionality slightly higher than for the untreated sample, according to ESCA measurements.<sup>229</sup> Laser Raman spectroscopy was unable to detect any increase in oxygen content, confirming that reaction is confined to the outermost few monolayers of material.

The surface specificity of reaction is also demonstrated by the sequential treatment of a sample of gilsonite with oxygen and hydrogen plasmas. The carbon : oxygen stoichiometry changes from  $C_{100} : O_{27}$  in the oxygen plasma treated sample to  $C_{100} : O_{21}$  for a sample exposed to both oxygen plasma and hydrogen plasma in a sequential function : the stoichiometry of the untreated gilsonite is  $C_{100} : O_{1.7}$ . Treatment of the plasma oxidised surface with hydrogen plasma increases the hydrocarbon peak under the  $C_{1s}$  envelope, the  $\underline{C} - O$  component is little affected,

whilst the carbonyl, carboxyl and carbonate functionalities undergo reduction, the latter component decreasing by the most substantial amount.

A systematic investigation of the effects of sequential treatments using oxygen and hydrogen plasmas on the surface composition of a series of well-defined polymer systems has been carried out<sup>229</sup> a detailed account is beyond the scope of this thesis.

References

1. D.T. Clark, 'Chemical Aspects of ESCA' in 'Electron Emission Spectroscopy', Eds. W. Dekeyser and D. Riedel, D. Riedel Publishing Co., Dordrecht, Holland, 373 (1973).
2. M. de Broglie, Compt. Rend., 158, 1493 (1914).
3. M. de Broglie, Compt. Rend., 163, 87, 353 (1916).
4. H. Robinson and W.I. Rawlinson, Phil. Mag., 28, 277 (1914).
5. H. Robinson, Proc. Roy. Soc., A104, 455 (1923).
6. H. Robinson, Phil. Mag., 50, 241 (1925).
7. K. Siegbahn and K. Edvarson, Nucl. Phys., 1, 137 (1956).
8. K. Siegbahn, 'Alpha, Beta and Gamma Ray Spectroscopy', Chapter 3, Ed. K. Siegbahn, North Holland Publishing Co., Amsterdam (1965).
9. K. Siegbahn, C. Nordling, A. Fahlman, R. Nordberg, K. Hamrin, J. Hedman, G. Johansson, T. Berkmark, S.E. Karlsson, I. Lidgren and B. Lindberg, 'ESCA, Atomic, Molecular and Solid State Structure Studied by means of Electron Spectroscopy', Almqvist and Wiksell's, Uppsala (1967).
10. K. Siegbahn, C. Nordling, G. Johansson, J. Hedman, P.F. Heden, K. Hamrin, U. Gelius, T. Bergmark, L.D. Werme, R. Manne and Y. Baer, 'ESCA Applied to Free Molecules', North Holland Publishing Co. (1969).
11. J.G. Jenkin, R.C.G. Leckey and J. Liesegang, J. Electron Spectrosc. Rel. Phenom., 12, 1 (1977); 14, 477 (1978).
12. D.W. Turner, C. Baker, A.D. Baker and C.R. Brundle, 'Molecular Photoelectron Spectroscopy', J. Wiley and Sons Ltd. (1970).

13. D.T. Clark, 'Structure and Bonding in Polymers as Revealed by ESCA', in 'Electron Structure of Polymers and Molecular Crystals', Eds. J. Lodik and J.M. Andre, Plenum Press, New York (1975).
14. L.S. Cederbaum and W. Domcke, *J. Electron Spectrosc. Rel. Phenom.*, 13, 161 (1978).
15. H.B. Cullen, *Handbook of Physics*, Section 8, Chapter 2, McGraw-Hill (1967).
16. A. Rosen and I. Lindgen, *Phys. Rev.*, 176, 114 (1968).
17. P.S. Bagus, *Phys. Rev. A.*, 139, 619 (1965).
18. D.A. Shirley, *Advances in Chem. Phys.*, 23, 85, Eds. I. Prigogini and S.A. Rice, J. Wiley and Sons Ltd., New York (1973).
19. U. Gelius and K. Siegbahn, *Faraday Discuss. Chem. Soc.*, 54, 257 (1972).
20. L.C. Snyder, *J. Chem. Phys.*, 55, 95 (1971).
21. D.B. Adams and D.T. Clark, *Theoret. Chim. Act.*, 31, 171 (1973).
22. M.F. Guest, I.H. Hillier, V.R. Saunders and M.W. Wood, *Proc. Roy. Soc.*, A333, 201 (1973).
23. D.T. Clark, I.W. Scanlan and J. Müller, *Theoret. Chim. Act.*, 35, 341 (1974).
24. D.T. Clark and I.W. Scanlan, *J. Chem. Soc. Farad. Trans. II*, 70, 1222 (1974).
25. C.D. Wagner and P. Bilden, *Surface Sci.*, 35, 82 (1973).
26. U. Gelius, *Phys. Scr.*, 9, 133 (1974).
27. H. Basch, *J. Electron Spectrosc. Rel. Phenom.*, 5, 463 (1974).
28. M.E. Schwarz, in *M.T.P. Internat. Rev. Sci., Phys. Chem. Ser. 2*, Vol. 1 (Theoret. Chem.), Eds. A.D. Buckingham and C.A. Coulson, Butterworths, London, 189 (1975).

29. T.A. Koopmans, *Physica*, 1, 104 (1933).
30. R. Manne and T. Åberg, *Chem. Phys. Lett.*, 7, 282 (1970).
31. S. Pignatoro and G. Distofaro, *Z. Naturforsch. A.* 30a, 815 (1975).
32. T. Ohta, T. Fukitawa and H. Furoda, *Chem. Phys. Lett.*, 32, 369 (1975).
33. L. Yin, I. Adler, T. Tsang, L.J. Matienzo and S.O. Grim, *Chem. Phys. Lett.*, 24, 81 (1974).
34. T. Robert and G. Offergeid, *Chem. Phys. Lett.*, 29, 606 (1974).
35. P. Burroughs, A. Hamnett, A.F. Orchard and G. Thornton, *J. Chem. Soc. Dalton Trans.*, 1686 (1976).
36. D.C. Frost, C.A. McDowell and A. Ishitani, *Mol. Phys.*, 24, 861 (1972).
37. D.T. Clark, D.B. Adams, A. Dilks, J. Peeling and H.R. Thomas, *J. Electron Spectrosc. Rel. Phenom.*, 8, 51 (1976).
38. D.T. Clark and A. Dilks, *J. Polym. Sci. Polym. Chem. Edn.*, 14, 533 (1976).
39. D.T. Clark and A. Dilks, *J. Polym. Sci. Polym. Chem. Edn.*, 15, 15 (1977).
40. M.A. Brisk and A.D. Baker, *J. Electron. Spectrosc. Rel. Phenom.*, 7, 197 (1977).
41. A.E. Sandstrom in 'Handbook of Physics', Vol. XXX, 'X-Rays', 164, Ed. S.F. Flugge, Springer-Verlag (1957).
42. P. Auger, *J. Phys. Radium*, 6, 205 (1925).
43. P. Auger, *Compt. Rend.*, 65, 180 (1925).
44. J.J. Lander, *Phys. Rev.*, 91, 1382 (1953).
45. cf. T.A. Carlson, 'Photoelectron and Auger Spectroscopy', Plenum Press, New York (1975).
46. D. Coster and R. de L. Kronig, *Physica*, 2, 13 (1935).

47. E.H.S. Burhop, 'The Auger Effect and Other Radiationless Transitions', Cambridge University Press (1952).
48. C.C. Chang, *Surface Sci.*, 25, 53 (1971).
49. J.P. Coad, M. Gettings and J.G. Riviere, *Faraday Discuss. Chem. Soc.*, 60, 269 (1975).
50. cf. C.D. Wagner, *Discuss. Faraday Soc.*, 60, 291 (1975).
51. S.P. Kowalczyk, R.A. Pollak, F.R. McFeely, L. Ley and D.A. Shirley, *Phys. Rev.*, B8, 3583 (1973).
52. L. Ley, S.P. Kowalczyk, F.R. McFeely, R.A. Pollak and D.A. Shirley, *Phys. Rev.*, B8, 2392 (1973).
53. S.P. Kowalczyk, R.A. Pollak, F.R. McFeely, L. Ley and D.A. Shirley, *Phys. Rev.*, B8, 2387 (1973).
54. S.P. Kowalczyk, L. Ley, F.R. McFeely, R.A. Pollak and D.A. Shirley, *Phys. Rev.*, B9, 381 (1974).
55. C.D. Wagner, *Faraday Discuss. Chem. Soc.*, 60, 291 (1975).
56. C.D. Wagner, L.H. Gale and R.H. Raymond, *Anal. Chem.*, 51, 466 (1979).
57. W.L. Jolly and D.N. Hendrickson, *J. Amer. Chem. Soc.*, 92, 1863 (1970).
58. D.T. Clark, B.J. Cromarty and A. Dilks, *J. Polym. Sci. Polym. Chem. Edn.*, 16, 3173 (1978).
59. D.T. Clark and A. Harrison, *J. Polym. Sci. Polym. Chem. Edn.*,  
in press.
60. J.N. Murrell and B.J. Ralston, *J. Chem. Soc. Faraday Trans. II*,  
68, 1393 (1972).
61. M.E. Schwartz, *Chem. Phys. Lett.*, 6, 631 (1970).
62. D.A. Shirley, *Chem. Phys. Lett.*, 15, 325 (1972).
63. C.S. Fadley, 'Basic Concepts of X-ray Photoelectron Spectroscopy',  
in 'Electron Spectroscopy, Theory, Techniques and Applications',  
Vol. 2, 1, Eds. C.R. Brundle and A.D. Baker, Academic Press (1978).

64. R.E. Watson and A.J. Freeman in 'Hyperfine Interactions', Eds.  
A.J. Freeman and R.B. Frankel, Academic Press, New York (1967).
65. C.S. Fadley, D.A. Shirley, A.J. Freeman, P.S. Bagus and J.V. Mallow,  
Phys. Rev. Lett., 23, 1397 (1969).
66. J.H. van Vleck, Phys. Rev. Lett., 45, 405 (1934).
67. C.S. Fadley in 'Electron Spectroscopy', Ed. D.A. Shirley, 781,  
North Holland Publishing Co. (1972).
68. T. Novakov, ref. 26 of C.S. Fadley in 'Electron Spectroscopy',  
Ed. D.A. Shirley, North Holland Publishing Co. (1972).
69. G.M. Bancroft, I. Adams, H. Lampe and T.K. Sham, Chem. Phys. Lett.,  
32, 173 (1975).
70. R.P. Gupta and S.K. Sen, Phys. Rev. Lett., 28, 1311 (1972).
71. T. Novakov and J.M. Hollander, Bull. Amer. Phys. Soc., 14, 524 (1969).
72. T. Novakov and J.M. Hollander, Phys. Rev. Lett., 21, 1133 (1968).
73. G.K. Wertheim, 'Mössbauer Effect : Principles and Applications',  
Academic Press, New York (1964).
74. M.F. Ebel and H. Ebel, J. Electron Spectrosc. Rel. Phenom., 3,  
169 (1974).
75. A.F. Orchard, Electron Structure Magn. Inorg. Comp., 3 (1974).
76. J.F. McGilp and I.G. Main, J. Electron. Spectrosc. Rel. Phenom.,  
6, 397 (1975).
77. G. Johansson, J. Hedman, A. Berndtsson, M. Klasson and R. Nilsson,  
J. Electron. Spectrosc. Rel. Phenom., 2, 295 (1973).
78. D.T. Clark in 'Advances in Polymer Science', Springer-Verlag,  
24, 125 (1977).
79. T.A. Carlson and G.E. McGuire, J. Electron. Spectrosc. Rel. Phenom.,  
1, 161 (1972).

80. C.S. Fadley, R.J. Baird, W. Siekhaus, T. Novakov and S.A.L. Burgstrom, *J. Electron. Spectrosc. Rel. Phenom.*, 4, 93 (1974).
81. J.H. Scofield, Lawrence Livermore Laboratory Report UCRL, 51326, Jan (1973).
82. J.H. Scofield, *J. Electron. Spectrosc. Rel. Phenom.*, 8, 129 (1976).
83. D.T. Clark and H.R. Thomas, *J. Polym. Sci. Polym. Chem. Edn.*, 15, 2843 (1977).
84. D.T. Clark and D. Shuttleworth, *J. Polym. Sci. Polym. Chem. Edn.*, 16, 1093 (1977).
85. D.R. Penn, *J. Electron Spectrosc.*, 9, 29 (1976).
86. D.T. Clark and H.R. Thomas, *J. Polym. Sci. Polym. Chem. Edn.*, 16, 791 (1978).
87. cf. N. Beatham and A.F. Orchard, *J. Electron Spectrosc. Rel. Phenom.*, 9, 129 (1976).
88. A.F. Carley and R.W. Joyner, *J. Electron Spectrosc. and Rel. Phenom.*, 16, 1 (1979).
89. R.M. Eisenberg in 'Fundamentals of Modern Physics', Chapter 14, J. Wiley and Sons, New York (1961).
90. J.E. Castle, L.B. Hazell and R.D. Whitehead, *J. Electron Spectrosc. Rel. Phenom.*, 9, 247 (1976).
91. C.D. Wagner, *J. Electron Spectrosc.*, 10, 305 (1977).
92. C.D. Wagner, L.H. Gale and R.H. Raymond, *J. Vac. Sci. Tech.*, 15, 518 (1978).
93. B.L. Henke, *Adv. X-ray Analysis*, 13, 1 (1969).
94. C.D. Wagner, *Faraday Discuss. Chem. Soc.*, 60, 306 (1975).
95. K. Yates, A. Barrie and F.J. Street, *J. Phys.*, E6, 130 (1973).
96. K. Siegbahn, D. Hammond, H. Fellner-Feldegg and E.F. Barnett, *Science*, 176, 245 (1972).

97. D.T. Clark and P.J. Stephenson, Explosives and Propellants, (Proc. Waltham Abbey conf. 1980), Ed. T.J. Lewis, Plenum Press, In press.
98. I.H. Munro, Chem. in Brit., 15, 330 (1979).
99. M.L. Perlman, E.M. Rowe and R.E. Watson, Phys. Today, 27, 30 (1974).
100. E.M. Purcell, Phys. Rev., 54, 818 (1938).
101. J.C. Helmer and N.H. Welchert, Appl. Phys. Lett., 13, 268 (1968)
102. K. Siegbahn, J. Electron Spectrosc. Rel. Phenom., 5, 3 (1974).
103. J.J. Huang, J.W. Rabalais and F.O. Ellison, J. Electron Spectrosc. Rel. Phenom., 6, 85 (1975).
104. D.C. Frost, C.A. McDowell and B. Wallbank, Chem. Phys. Lett., 40, 189 (1976).
105. C.D. Wagner, W.M. Riggs, L.E. Davis, J.F. Moulder and G.E. Muilenberg (Editor), 'Handbook of X-ray Photoelectron Spectroscopy', Perkin Elmer Corporation, Physical Electronic Division (1979).
106. A.D. Baker and C.R. Brundle, 'An Introduction to Electron Spectroscopy', in 'Electron Spectroscopy, Theory, Techniques and Applications' Vol. 1, Eds. C.R. Brundle and A.D. Baker, 1, Academic Press, London (1977).
107. T.N. Rhodin and J.W. Gadzuk, 'Electron Spectroscopy and Surface Chemical Bonding', in 'The Nature of the Surface Chemical Bond', Eds. T.N. Rhodin and G. Ertl, 112, North Holland Publishing Co., Amsterdam (1979).
108. C.D. Wagner, Anal. Chem., 44, 1050 (1972).
109. N. Berthou and C.J. Jorgensen, Anal. Chem., 47, 482 (1975).
110. V.I. Nefedov, N.P. Sergushin, I.M. Band and M.B. Trzhaskovskaya, J. Electron Spectrosc. Rel. Phenom., 2, 383 (1973); 7, 175 (1975).

111. R.S. Swingle II, *Anal. Chem.*, 47, 21 (1975).
112. F.M. Chapman and L.L. Lohr, *J. Amer. Chem. Soc.*, 96, 4731 (1974).
113. J.T.J. Huang and J.W. Rabalais, 'X-ray Photoelectron Cross-sections and Angular Distributions' in 'Electron Spectroscopy, Theory, Techniques and Applications', Vol. 2, 225. Eds. C.R. Brundle and A.D. Baker, Academic Press, London (1978).
114. D.M. Wyatt, J.C. Carver and D.M. Hercules, *Anal. Chem.*, 47, 1297 (1975).
115. K.T. Ng and D.M. Hercules, *J. Electron Spectrosc. Rel. Phenom.*, 7, 257 (1975).
116. L.E. Cox and D.M. Hercules, *J. Electron Spectrosc. Rel. Phenom.*, 1, 193 (1972/73).
117. T.E. Madey, C.D. Wagner and A. Joshi, *J. Electron Spectrosc. Rel. Phenom.*, 10, 359 (1977).
118. cf. H. Siegbahn, L. Asplund, P. Kelfve and K. Siegbahn, *J. Electron Spectrosc. Rel. Phenom.*, 7, 411 (1975) and references therein.
119. O. Keski-Rahkonen and M.I. Krause, *At. Data Nucl. Data Tables*, 14, 139 (1974).
120. D.A. Huchital and R.T. McKeon, *Appl. Phys. Lett.*, 20, 158 (1972).
121. J.S. Brinnen, *Acc. Chem. Res.*, 9, 86 (1976).
122. D.T. Clark, H.R. Thomas and A. Dilks (unpublished data).
123. D.T. Clark, H.R. Thomas and A. Dilks, *J. Polym. Sci., Polym. Chem. Ed.*, 16, 1461 (1978).
124. D.T. Clark and A. Dilks, A.C.S. Centennial Meeting, New York, April 1976, 'International Symposium on Advances in Characterisation of Polymer Surfaces', 101, Ed. L.H. Lee, Academic Press, New York, (1976).

125. D.T. Clark and A. Dilks, *J. Polym. Sci. Polym. Chem. Ed.*, 16, 791 (1978).
126. D.T. Clark and A. Dilks, *J. Polym. Sci. Polym. Chem. Ed.*, 16, 911 (1978).
127. D.T. Clark and A. Dilks, *J. Electron Spectrosc. Rel. Phenom.*, 11, 225 (1977).
128. S. Evans, J.M. Adams and J.M. Thomas, *Phil., Trans. Roy. Soc. London Series A*, 292, 59 (1979).
129. A.T. Bell, 'Fundamentals of Plasma Chemistry' in 'Techniques and Applications of Plasma Chemistry', Eds. J.R. Hollahan and A.T. Bell, J. Wiley and Sons, New York (1974).
130. E.O. Johnson and L. Malter, *Phys. Rev.*, 80, 58 (1950).
131. J.D. Swift and M.J.R. Schwar, 'Electrical Probes for Plasma Diagnostics', Hiffe Books Ltd., London (1970) and references therein.
132. D.W. Rice and D.F. O'Kane, *J. Electrochem. Soc.*, 123, 1308 (1976).
133. M. Hudis, 'Plasma Treatment of Solid Materials' in 'Techniques and Applications of Plasma Chemistry', Eds. J.R. Hollahan and A.T. Bell, J. Wiley and Sons, New York (1974).
134. A.N. Mearns, *Thin Solid Films*, 3, 201 (1969).
135. V.M. Kolotyrkin, A.B. Gil'man and A.K. Tsapuk, *Russ. Chem. Phys.*, 36, 579 (1967).
136. 'Plasma Chemistry of Polymers', Ed. M. Shen, Dekker, New York (1976).
137. R.M. Fredericks and J. Asmussen Jr., *J. Appl. Phys.*, 42, 3647 (1971).
138. J. Lucas, *I.E.E. Proc.*, 128A, 313 (1981).
139. D.T. Clark and R. Wilson, unpublished results.
140. M.M. Shahin in 'Chemical Reactions in Electrical Discharges', Amer. Chem. Soc. Publications (1969).

141. F.K. McTaggart, 'Plasma Chemistry in Electrical Discharges', Elsevier Publishing Co., Amsterdam (1967).
142. J.R. Hollahan and A. Bell (Eds.), 'Techniques and Applications of Plasma Chemistry', J. Wiley and Sons, New York (1974).
143. B. Chapman, 'Glow Discharge Processes - Sputtering and Plasma Etching', J. Wiley and Sons (1980).
144. H. Suhr, 'Applications of Non-Equilibrium Plasmas to Organic Chemistry', In 'Techniques and Applications of Plasma Chemistry', Eds. J.R. Hollahan and A. Bell, J. Wiley and Sons, New York (1974).
145. H. Yasuda, 'Formation of Polymeric Materials by a Nonpolymerization Process : Glow Discharge Polymerization', in 'Contemporary Topics in Polymer Science', Ed. M. Shen, 103, Plenum Publishing Corp. (1979).
146. A. Pavlath and K.S. Lee, J. Macromol. Sci. Chem. A, 10, 579 (1976).
147. M.M. Millard and A.E. Pavlath, J. Macromol. Sci. Chem. A, 10, 619 (1976).
148. M.M. Millard, 'Synthesis of Organic Polymer Films in Plasmas', in 'Techniques and Applications of Plasma Chemistry', Eds. J.R. Hollahan and A. Bell, J. Wiley and Sons, New York (1974).
149. H. Yasuda, J. Macromol. Sci. Chem. A, 10, 383 (1976).
150. 'Plasma Polymerization', Eds. M. Shen and A.T. Bell, in Amer. Chem. Soc. Symp. Ser., 108 (1979).
151. M. Venugopalan, I. Sioun Lin and M.S. Grenda, J. Polym. Sci. Polym. Chem. Edn., 18, 2731 (1980).
152. D.T. Clark and D. Shuttleworth, J. Polym. Sci. Polym. Chem. Edn., 18, 407 (1980).
153. D.T. Clark and M.Z. AbRahaman, J. Polym. Sci. Polym. Chem. Edn., in press (1981).

154. M.Z. AbRahaman, Ph.D. Thesis, University of Durham, to be submitted (1981).
155. J.R. Hollahan, 'Applications of Low Temperature Plasmas to Chemical and Physical Analysis', in 'Techniques and Applications of Plasma Chemistry', Eds. J.R. Hollahan and A. Bell, J. Wiley and Sons, New York (1974).
156. S. Imai, Bunseki Kag., 27, 611 (1978).
157. O. Tsuji, T. Wydeven and K. Hozumi, Microchemical Journal, 22, 229 (1977).
158. J. Friedrich, H. Wittrich and J. Gähde, Acta Polymerica, 31, 59 (1980), and references therein.
159. W.J. Humphreys and W.G. Henk, J. Microscopy, 116, 255 (1979).
160. P.N. Crabtree, G. Gorin and R.S. Thomas, Scanning Electron Microscopy, Vol. 1, 543 (1978).
161. D.T. Clark and T. Fok, Thin Solid Films, 78, 271 (1981).
162. A. Goldman, 'Plasma Chemistry', NATO Advanced Study Institute, 'Electrical Breakdown and Discharges in Gases', Les Arcs, France (1981), Plenum Publishing Corp., in press.
163. M. Venugopalan, U.K. Roychowdhury, K. Chan and M.L. Pool, 'Plasma Chemistry of Fossil Fuels', in 'Topics in Current Chemistry', 90, 'Plasma Chemistry II', Ed. S. Veprék and M. Venugopalan, Springer-Verlag (1980).
164. Y.C. Fu, B.D. Blaustein and I. Wender, Chem. Eng. Prog. Symp. Ser., 67, 47 (1971).
165. T.W. Scott and M. Venugopalan, Nature, 262, 48 (1976).
166. S.C. Chakravartty, D. Dulta and A. Lahiri, Fuel, 55, 43 (1976).
167. N.E. Vanderborgh, M.A. Fletcher and C.E.R. Jones, J. Analytical and Appl. Pyrolysis, 1, 177 (1979).

168. A. Volborth, 'Problems in Oxygen Stoichiometry in Analyses of Coal and Related Materials', Chapter 55 in 'Analytical Methods for Coal and Coal Products', Vol. III, 543, Ed. C. Karr Jr., Academic Press, London (1979).
169. S.W. Parr, 'The Analysis of Fuel, Gas, Water and Lubricants', McGraw-Hill, New York (1932).
170. J.G. King, M.B. Maries and H.E.J. Crossley, J. Soc. Chem. Ind. London, 55, 277 (1936).
171. N.A. Brown, C.B. Belcher and T.G. Callcott, J. Inst. Fuel, 38, 198 (1965).
172. K. Kinson and C.B. Belcher, Fuel, 54, 205 (1975).
173. H.J. Gluskoter, Fuel, 44, 285 (1965).
174. C.E. Hamrin, P.S. Maa, L.L. Chyi and W.D. Ehmman, Fuel, 54, 70 (1975).
175. F.W. Frazer and C.B. Belcher, Fuel, 52, 41 (1973).
176. P.H. Given and R.F. Yarzab, 'Problems and Solutions in the Use of Coal Analyses', Tech. Rep. FE-0390-a, Pennsylvania State Univ.
177. R.N. Miller, R.F. Yarzab and P.H. Given, Fuel, 58, 5 (1979).
178. P.A. Estep, J.J. Kovach and C. Karr Jr., Anal. Chem., 40, 358 (1978).
179. C.E. Hamrin Jr., A.H. Johannes, W.D. James Jr., G.H. Sun and W.D. Ehman, Fuel, 58, 48 (1979).
180. C.E. Gleit and W.D. Holland, Anal. Chem., 34, 1454 (1962).
181. C.E. Gleit, Amer. J. Medical Electronics, 2, 112 (1963).
182. R. Kumar, C. Ladas and G. Hudson, Solid State Tech., p. 54, Oct (1976).
183. G.W. Meyer and W. Stewart, Scanning Electron Microscopy, 1, 341 (1977).
184. T.W. Davies and A.J. Morgan, J. Microscopy, 107, 47 (1976).
185. P. Valenta, H. Rützel, H.W. Nürnberg and M. Stoeppler, Z. Anal. Chem., 285, 25 (1977).

186. R.S. Thomas, 'Use of chemically reactive gaseous plasmas in preparation of specimens for microscopy', in 'Techniques and Applications of Plasma Chemistry', Eds. J.R. Hollahan and A. Bell, J. Wiley and Sons, New York (1974).
187. Y. Kawana, Chem. Econ. Engin. Rev., 4, 13 (1972).
188. R. Nicholson and K. Littlewood, Nature, 236, 397 (1972).
189. G.M. Bancroft, J.R. Brown and W.S. Fyfe, Chem. Geol., 25, 227 (1979).
190. D.C. Frost, B. Wallbank and W.R. Leeder, 'X-ray Photoelectron Spectroscopy of Coal and Coal Related Problems', Chapter II In 'Analytical Methods for Coal and Coal Products', Vol. 1, Ed. C. Karr Jr., Academic Press (1978).
191. J.M. Adams, S. Evans, P.I. Reid, J.M. Thomas and M.J. Walters, Anal. Chem., 49, 2001 (1977).
192. J.M. Adams and S. Evans, Clays and Clay Minerals, 27, 248 (1979).
193. D.C. Frost, W.R. Leeder and R.L. Tapping, Fuel, 53, 206 (1974).
194. W.J. Montgomery, 'Standard Laboratory Test Methods for Coal and Coke', Chapter 6 in 'Analytical Methods for Coal and Coal Products', Vol. 1, Ed. C. Karr Jr., Academic Press (1978).
195. D.C. Frost, W.R. Leeder, R.L. Tapping and B. Wallbank, Fuel, 56, 277 (1977).
196. C. Simeons, 'Coal - Its Role In Tomorrow's Technology', Pergamon Press (1978).
197. H. Harker and P.M.A. Sherwood, Phil. Mag., 27, 1241 (1973).
198. L.J. Dunne and H. Harker, Phil. Mag., 30, 1313 (1974).
199. N.L. Craig, A.B. Harker and T. Novakov, Atmos. Environm., 8, 15 (1974).
200. H. Marsh, P.M.A. Sherwood and D. Augustyn, Fuel, 55, 97 (1976).

201. W.D. Schneider and C.A. Luengo, *Energy Research*, 2, 123 (1978).
202. G. Eglinton and M.T.J. Murphy, in '*Organic Geochemistry*', Chapter 1, Eds. G. Eglinton and M.T.J. Murphy, Springer-Verlag (1969).
203. I.A. Breger, '*Origin and Classification of Naturally Occurring Carbonaceous Substances*', Chapter 3, in '*Organic Geochemistry*', Ed. L.A. Breger, Pergamon Press (1963).
204. B. Durand, '*Sedimentary Organic Matter and Kerogen. Definition and Quantitative Importance of Kerogen*', in '*Kerogen : Insoluble Organic Matter from Sedimentary Rocks*', Ed. B. Durand, Technip, Paris (1980).
205. J.M. Hunt, '*Petroleum Geochemistry and Geology*', W.H. Freeman and Company, San Francisco (1979).
206. B.P. Tissot and D.H. Welte, '*Petroleum Formation and Occurrence*', Springer-Verlag (1978).
207. E. Stach, M.-Th. Mackowsky, M. Teichmüller, G.H. Taylor, D. Chandra and R. Teichmüller, '*Stach's Textbook of Coal Petrology*', 2nd Edn., Gebrüder Borntraeger, Berlin (1975).
208. L. Petrakis and D.W. Grandy, *J. Chem. Educ.*, 57, 689 (1980).
209. H. Morita, *J. Chem. Educ.*, 57, 695 (1980).
210. W. Francis and M.C. Peters, '*Fuels and Fuel Technology*', 2nd Edn., Pergamon Press (1980).
211. M.C. Stopes, *Fuel*, 14, 4 (1935).
212. D.T. Clark and A. Dilks, *J. Polym. Sci. Polym. Chem. Edn.*, 15, 2321 (1977).
213. D.T. Clark and A. Dilks, *J. Polym. Sci. Polym. Chem. Edn.*, 17, 957 (1979).
214. S.H. Pinner and W.G. Simpson, '*Plastics : Surfaces and Finish*', Butterworths (1971).

215. C.B. Jones, Soc. Plast. Eng., 25, 724 (1979).
216. D. De Maw and B. Shriner, QST, p. 22, February (1980).
217. H. Yasuda, M.O. Burngarner, H.C. Marsh and N. Morosoff,  
J. Polym. Sci. Polym. Chem. Edn., 14, 195 (1976).
218. K. Bell and J.M. Hunt, 'Native Bitumens Associated with Oil Shales',  
Chapter 8 in 'Organic Geochemistry', Ed. I.A. Breger,  
Pergamon Press (1963).
219. J.M. Hunt, F. Stewart and P.A. Dickey, Am. Assoc. Pet. Geol. Bull.,  
38, 1671 (1954).
220. H. Abraham, 'Asphalts and Allied Substances', D. Van Nostrand  
Company, New York (1945).
221. A.T. Cross and G.T. Wood, Brigham Young University Geology Studies,  
22, 157 (1976).
222. J.M. Hunt, 'Composition and origin of the Uinta Basin bitumens', in  
'Oil and gas possibilities of Utah, re-evaluated', Ed. A.L. Crawford,  
Utah Geological and Mineralogical Survey, Bull. 54, Paper 24,  
249 (1963).
223. American Gilsonite Company, 'Another Milestone for American Gilsonite  
Company', (1979).
224. G.D. Hobson, 'Oil and Gas Accumulations, and Some Allied Deposits',  
Chapter I in 'Fundamental Aspects of Petroleum Geochemistry',  
Eds. B. Nagy and U. Colombo, Elsevier Publishing Company,  
New York (1967).
225. H.F. Kretchman, 'The Story of Gilsonite', American Gilsonite  
Company (1957).
226. P.J. Grantham and A.G. Douglas, in 'Advances in Organic Geochemistry  
1975', Eds. R. Campos and J.G. Enadimsa, 193, Technips (1977).

227. A.G. Douglas and P.J. Grantham, in 'Advances in Organic Geochemistry 1973', Eds. B. Tissot and F. Bienner, 261, Technips (1974).
228. B. Durand and J.C. Monin, 'Elemental Analysis of Kerogens', Chapter 4 in 'Kerogen : Insoluble Organic Matter from Sedimentary Rocks', Ed. B. Durand, Technip, Paris (1980).
229. D.T. Clark and R. Wilson, in preparation.
230. H. Helm, T.D. Märk and W. Lindinger, Pure and Appl. Chem., 52, 1739 (1980).
231. J.M. Hunt, Am. Assoc. Pet. Geol. Bull., 56, 2273 (1972).
232. B. Chappe, W. Michaelis and P. Albrecht, in 'Advances in Organic Geochemistry 1979', Eds. A.G. Douglas, J.R. Maxwell, Pergamon Press (1980).
233. D. Van de Meent, S.C. Brown, R.P. Philp and B.R.T. Simoneit, Geochim. et Cosmochim. Acta, 44, 999 (1980).
234. B. Durand (Ed.), 'Kerogen : Insoluble organic matter from sedimentary rocks', Technip, Paris (1980).
235. W.E. Robinson, 'Isolation procedures for kerogens and associated soluble organic materials', in 'Organic Geochemistry, Methods and Results', Eds. G. Eglinton and M.J. Murphy, Springer-Verlag (1969).
236. B. Horsfield and A.G. Douglas, Geochim. et Cosmochim. Acta, 44, 1119 (1980).
237. J. Unterzaucher, Ber. Deut. Chem. Ges., 73B, 391 (1940).
238. B. Durand and G. Nicaise, 'Procedures for kerogen isolation', in 'Kerogen : Insoluble organic matter from sedimentary rocks', Ed. B. Durand, Technip, Paris (1980).
240. H. Suhr and U. Künzel, Liebig's Ann. Chem. 2057 (1979).
241. A.G. Loudon, A. Maccoll and S.K. Wong, J. Chem. Soc. B, 1733 (1970).
239. D. Vitorovic in ref. 234.

242. A. Marchand and J. Conard, 'Electronparamagnetic resonance in kerogen studies', in 'Kerogen : Insoluble organic matter from sedimentary rocks'. Ed. B. Durand, Technip, Paris (1980).
243. H. Solli, S.R. Larter and A.G. Douglas, *J. Anal. and Appl. Pyrol.*, 1, 231 (1980).
244. R. Alexander, M.D. Gray, R.I. Kagi and G.W. Woodhouse, *Chem. Geol.*, 30, 1 (1980).
245. R.D. Sydansk, *Fuel*, 57, 66 (1978).
246. Y. Maekawa, T. Yoshida and Y. Yoshida, *Fuel*, 58, 864 (1979).
247. D. Vucelic, N. Juranic and D. Vitorovic, *Fuel*, 58, 759 (1979).
248. M.T. Melchior, K.D. Rose and F.P. Mikins, *Fuel*, 59, 594 (1980).
249. F.P. Miknis, V.J. Bartuska and G.E. Maciel, *Internat. Lab.*, p. 9, Jan/Feb (1980).
250. P.G. Rouxhet, P.L. Robin and G. Nicaise, 'Characterisation of kerogens and of their evolution by infrared spectroscopy', in 'Kerogen : Insoluble organic matter from sedimentary rocks', Ed. B. Durand, Technip, Paris (1980).
251. P.C. Painter and M.M. Coleman, *Internat. Lab.*, p. 17, April (1980).
252. B. Tissot, B. Durand, J. Espitalié and A. Combaz, *Am. Assoc. Pet. Geol. Bull.*, 58, 499 (1974).
253. T.F. Yen, 'Structural investigations on Green River oil shale kerogen', in 'Science and Technology of Oil Shale', Ed. T.F. Yen, Ann Arbor Science (1976).
254. D.W. van Krevelen, 'Coal', Elsevier Publishing Company, Amsterdam (1961).
255. B. Nagy and U. Colombo (Eds.), 'Fundamental aspects of petroleum geochemistry', Elsevier Publishing Company, Amsterdam (1969).
256. I.A. Breger (Ed.), 'Organic Geochemistry', Pergamon Press (1963).

257. G. Eglinton and M.T.J. Murphy (Eds.), 'Organic Geochemistry', Springer-Verlag (1969).
258. B. Budesinsky, *Anal. Chem.*, 37, 1159 (1965).
259. G. Khavari-Khorasani, H.E. Blayden and D.G. Murchison, *J. Microscopy*, 116, 337 (1979).
260. G.W. Hodgson, B.L. Baker and E. Peake, 'Geochemistry of Porphyrins', in 'Fundamental Aspects of Petroleum Geochemistry', Eds. B. Nagy and U. Colombo, Elsevier Publishing Co. (1967).
261. J.M.E. Quirke, G. Eglinton and J.R. Maxwell, *J. Am. Chem. Soc.*, 101, 7693 (1979).
262. S.K. Hajibrahim, J.M.E. Quirke and G. Eglinton, *Chem. Geol.*, 32, 173 (1981).
263. E.W. Baker, T.F. Yen, J.P. Dickie, R.E. Rhodes and L.F. Clark, *J. Am. Chem. Soc.*, 89, 3631 (1967).
264. Basic Coal Sciences Project Advisory Committee Report, Gas Research Institute, Chicago, Illinois, U.S.A. July (1980).
265. R. Cypres and C. Soudan-Moinet, *Fuel*, 59, 48 (1980).
266. J. Espitalié, M. Madec and B. Tissot, *Am. Assoc. Pet. Geol. Bull.*, 64, 59 (1980).
267. J.C. Crelling, R.H. Schrader and L.G. Benedict, *Fuel*, 58, 542 (1979).
268. D.W. van Krevelen, 'Geochemistry of Coal', in 'Organic Geochemistry', I.A. Breger (Ed.), Pergamon Press (1963).
269. B.S. Cooper and D.G. Murchison, 'Organic Geochemistry of Coal', in 'Organic Geochemistry', G. Eglinton and M.T.J. Murphy (Eds.), Springer-Verlag (1969).
270. D.T. Clark in 'Molecular Spectroscopy', A.R. West (Ed.), Heyden (1976).
271. C.E. Zobell, 'Organic Geochemistry of Sulphur', in 'Organic Geochemistry', I.A. Breger (Ed.), Pergamon Press (1963).
272. H. Suhr, P. Henne, D. Iacocca and M.J. Roper, *Liebigs Ann. Chem.*, p. 441 (1980).